From the

Comprehensive Pneumology Center (CPC), Helmholtz Center Munich

And the

Medizinischen Klinik und Poliklinik V, Klinikum der Ludwigs-Maximilians-Universität München

Director: Dr. Ali Önder Yildirim and Prof.Dr. Jürgen Behr

Dissertation zum Erwerb des Doctor of Philosophy
(Ph.D.) an der Medizinischen Fakultät der Ludwig-
Maximilians-Universität zu München

Oxygen Therapy in Neonatal Chronic Lung Disease – Acute and Sustained Effects and their Indicators

vorgelegt von:

Erika Gonzalez Rodriguez

aus:

San Gil, Santander, Colombia

Jahr:

2022

Mit Genehmigung der Medizinischen Fakultät der

Ludwig-Maximilians-Universität zu München

First supervisor:	PD Dr. med. Anne Hilgendorff
Second supervisor:	Prof. Dr. med. Jürgen Behr
Third supervisor:	Prof. Dr. med. Thomas Gudermann
Fourth supervisor:	Prof. Dr. Tushar Desai

Dean: **Prof. Dr. med. Thomas Gudermann**

Datum der Verteidigung:

26.09.2022

“The first problem for all of us is not to learn but to unlearn”

Gloria Steinem

Table of Content

Abstract

Premature neonates often require life-saving oxygen therapy, which increases their risk of developing bronchopulmonary dysplasia (BPD). Although survival improves with oxygen supplementation, morbidity increases with higher oxygen concentration and longer exposures. The induction of lung injury by short-term postnatal hyperoxia has been suggested by clinical observations and was in part supported by experimental studies. However, underlying mechanisms of lasting effects provoked by clinically relevant oxygen levels remain poorly understood. Despite this, most of the experimental models of BPD employ very high oxygen concentrations (FiO2 > 0.8) for several days or weeks. Thus, our knowledge of the effects of oxygen therapy in the developing lung derives from models of severity that most likely do not reflect the clinical setting. Even though the effects of treatment with severe hyperoxia concentrations have been extensively characterized, there is still a poor understanding of the maladaptive responses that lead to BPD. More importantly, a real gap of knowledge remains when it comes to clinically relevant hyperoxia concentrations i.e., $FiO_2 \leq 0.4$. Thus, it is critical to identify and understand the early mechanisms involved in the injury response to hyperoxia treatment in order to harness this knowledge towards therapeutics that restore normal lung function. Therefore, my studies addressed significant and functionally relevant changes in the three major lung cell types, i.e., ATII, EC, and MFB, and confirmed their lasting effects. This study presents previously unidentified immediate and sustained effects of the early postnatal exposure to clinically relevant hyperoxia concentrations ($FiO_2 = 0.4$). One of the main findings of this study was that treatment with O_2 ($FiO_2 = 0.4$) arrests the cell cycle potentially through the downregulation of the pre-replication complex, which is critical for cell cycle progression. The predominant downregulation of genes following hyperoxia exposure revealed a significant overlap between the MFB and ATII cell transcriptome pattern, partially shared by the lung EC. The significant overlap in the transcriptome profile between MFBs and ATII cells potentially indicates similar effects (and coping strategies) in response to oxidative stress.

In Mcm2 knockdown experiments *in vitro*, I established a causal link between cell-cycle arrest in G1 and changes in developmentally relevant gene expression

and cell function in MFB and AT2 cells. Furthermore, Mcm2 knockdown cells presented with aberrations in DNA damage response and repair genes.

In vivo, we were able to recapitulate our main in vitro findings. A model employing FiO_2 = 0.4 for 8 hours revealed indications of cell cycle arrest at the proteomic level in the absence of classical apoptosis. Longer O_2 treatment revealed a similar signature of cell cycle arrest and the regulation of other critical proteins involved in the DDR such as Parp1. Moreover, 24 hours of O_2 did not result in classical apoptosis. Interestingly, 8 hours of O_2 treatment led to the upregulation of VEGFA but no other changes in developmentally relevant proteins were observed. Remarkably, studies in 18-month-old mice that received 8 hours of O_2 as newborn pups revealed Pdgf-Rα and VE-cadherin to be significantly downregulated while eNOS, another vascular marker, was significantly increased. These results paint a picture of aberrant signaling that although not evident immediately after treatment, appears to be long-lasting.

To study deeper the potential consequences of short-term O_2 treatment, we treated mice with O_2 for 24 hours and allow them to recover after treatment. Three and seven weeks after treatment, the lungs were harvested. We observed that at the transcriptional level, the downregulation of genes like Pdgf-Rα can already be seen seven weeks after treatment. This model also revealed alterations in Wnt5a mRNA expression three and seven weeks after treatment. Remarkably, we elucidated aberrations in DDR genes i.e., Chk1 and Cdkn1a, and in BER pathway genes three weeks after treatment. Several of these changes did not return to baseline by the seven-week post-treatment.

Additionally, with a double-hit injury model, we delineated the changes in DNA damage response and the BER pathway that arise from O_2-lung priming. For several of the target genes evaluated, previous treatment with O_2 modulated the response to the second-hit injury, perhaps making the lung more vulnerable.

Finally, we translated these results to the bedside by analyzing samples collected from pre-mature babies that received oxygen therapy. Remarkably, in plasma proteome analysis from blood collected during the first week of life, protein levels of Apex1, a key BER gene, were positively correlated with O_2 days mirroring our observations *in vivo*.

In summary, the results reported in this dissertation delineate the short, long-term effects and potential epigenetic regulation in the developing lung arising from treatment with clinically relevant hyperoxia levels. Furthermore, here it is extensively established that cell cycle arrest works as an initial mechanism by which the cells respond to DNA damage arising from oxidative stress. Moreover, my findings demonstrate that priming the developing lung with clinical hyperoxia levels for short periods of time alters the response to a second-hit injury as well as leaving long-term aberrations in DNA repair. These findings have profound clinical implications beyond neonatal chronic lung disease.

1. Introduction

1.1 Anatomy and physiology of the developing lung

The lung is a vital organ that enables gas exchange between the systemic circulation and the environment. The air enters the upper airways through the nasal cavity, passing down the pharynx and larynx, and the lower airways, which consists of the trachea, primary bronchi, and the bronchial tree. From there, the air travels into the small bronchioles and alveoli within the lung tissues. In the terminal end, the airway wall is composed of alveolar ducts lined by alveolar sacs and alveoli (Fraga & Guttentag, 2012). The main function of the alveoli is gas exchange (Fraga & Guttentag, 2012; Schittny, 2017). It is estimated that in the human lung, there are about 300 million alveoli amounting to a total surface area of around 90 m^2 in women and 118 m^2 in men (Colebatch & Ng, 1992). Gas exchange is enabled via the cells lining the alveolus containing a single layer of epithelial cells *i.e.,* type 1 (AT1) and type 2 (AT2), stromal cells and capillary endothelial cells (**Fig 1.1**). AT1 cells cover most of the alveolar surface providing the necessary space for gas exchange. AT2 cells are less abundant but play critical functions like surfactant production (necessary to decrease surface tension). Moreover, some have stemness potential allowing them to differentiate into AT1 or AT2 cells following injury (Fraga & Guttentag, 2012; Nabhan et al., 2018; Schittny, 2017). Pulmonary surfactant, produced by AT2 cells, is composed of phospholipids primarily, phosphatidylcholine, and the surfactant proteins SP-A, SP-B, SP-C and SP-D. When infants are born before AT2 differentiation, the lack of pulmonary surfactant can lead to acute respiratory distress syndrome. When this is the case, oxygen supplementation and positive airway pressure can support ventilation after birth.

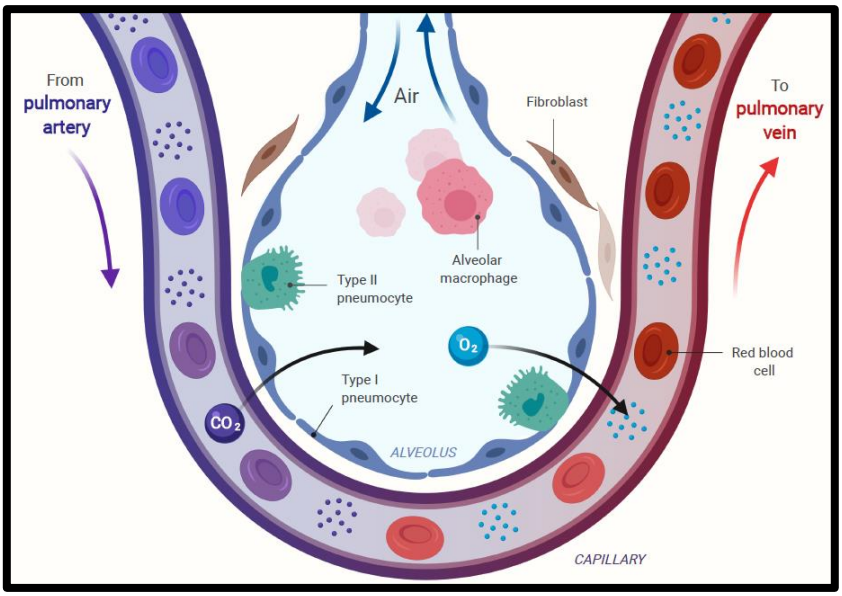

Fig 1.1: Schematics showing Alveolus structure with main cell types

This figure was created with www.Biorender.com

1.1.1 Lung development

The lung bud, the first structure that is formed, is recognizable by the 25th day of gestation. Epithelium and mesenchyme constitute the lung bud, which starts its first dichotomous divisions resulting in the primordial lung lobes. The trachea, subsegmental and subsegmental bronchi can be seen by the 7th week of gestation (pseudoglandular stage). These changes are accompanied by the separation of the thoracic from the peritoneal cavity resulting from the closure of the peritoneal folds. When this process fails, contents from the peritoneum can reach the thoracic cavity and restrict the growth of the lung as observed in diaphragmatic hernia patients (Schittny, 2017).

The process of airway branching is completed by week 16 (canalicular stage). During the canalicular phase, the primordial structures that will give rise to the alveoli start to form. Moreover, it is during this phase that the 23 airway subdivisions are completed. During the saccular phase (week 24 to 38), a barrier that can support gas exchange is formed. However, true alveoli are only evident after week 36. When mice are born, their lungs are going through the saccular phase, a fact that makes them excellent models to study prematurity (Hilgendorff et al., 2014). Postnatally, the lung continues and for the next six months, bulk alveolarization occurs. However, these alveoli are still immature and only reach full maturity when the capillary bed is remodeled from a double capillary bed to

one. This process happens from the 3rd year of life to approximately the 21st (**Table 1.1**) (Andresen & Saugstad, 2020; Behnke et al., 2021; Schittny, 2017).

Period	Stage	Duration	Characteristics
Embryonic	Embryonic	Mouse: E9.5–E12 Rat: E11–E13 Human: E26–E49 (4–7 weeks)	Anlage of the two lungs; organogenesis; formation of major airways and pleura.
Fetal	Pseudoglandular	Mouse: E12–E16.5 Rat: E13–E18.5 Human: E35–E119 (5–17 weeks)	Formation of bronchial tree and large parts of prospective respiratory parenchyma; birth of the acinus even if the acinar epithelia are not yet differentiated.
	Canalicular	Mouse: E16.5–E17.5 Rat: E18.5–E20 Human: E112–E182 (16–26 weeks)	Formation of the most distal airways leading to completion of branching morphogenesis; first air-blood barrier; appearance of surfactant, acini are detectable due to epithelial differentiation.
	Saccular or terminal sac	Mouse: E17.5–P4 Rat: E21–P4 Human: E168–E266 (24–38 weeks)	Expansion of (future) airspaces.
Postnatal	Alveolarization, classical alveolarization (first phase)	Mouse: P4 – P21 Rat: P4 – P21 Human: E252 (36 weeks* preterm) – 3 years	Formation of secondary septa (septation) resulting in the formation of the alveoli; most of the alveolar septa are still immature and contain a double layered capillary network. Depending on the species alveolarization starts before or after birth.
	Alveolarization, continued alveolarization (second phase)	Mouse: P14 – young adulthood (~P36) Rat: P14 – young adulthood (~P60) Human: 2 years – young adulthood (17–21 years)	Formation of secondary septa (septation) but now lifting off of mature alveolar septa containing a single layered capillary network.
	Microvascular maturation	Mouse: P4 – young adulthood (~P36) Rat: P14 – young adulthood (~P60) Human: ~term – ~3–21 years (timing uncertain)	Remodeling and maturation of interalveolar septa and of the capillary bed (the double layered capillary network is transformed to a single layered network). In a first approximation it takes place in parallel to alveolarization.

Table 1.1: Stages of development in the human and murine lung.

Table adapted from Schittny, J. Lung Development. Cell Tissue Res. 2017; 367(3): 427–444. (Schittny, 2017). E: embryonic day. P: postnatal

1.2 Neonatal chronic lung disease (nCLD)

Neonatal chronic lung disease *i.e.,* bronchopulmonary dysplasia (BPD) remains the most common complication of prematurity, affecting up to 30% of very low

birth weight infants (Hilgendorff et al., 2014). The persistent need for supplemental support with oxygen or mechanical ventilation is used to define the grades of BPD: A need exceeding 28 days, but less than 36 weeks postmenstrual age (PMA) defines mild BPD (Hilgendorff & O'Reilly, 2015; Niedermaier & Hilgendorff, 2015; Thébaud et al., 2019), whereas moderate and severe BPD is defined by a need greater than 36 weeks PMA. Common clinical symptoms are shortness of breath and dyspnea arising due to alveolar hypoventilation and impaired gas exchange that led to hypoxemia and hypercapnia (Niedermaier & Hilgendorff, 2015).Oxygen therapy and/or mechanical ventilation are interventions used to treat these disbalances. However, immaturity of red-ox mechanisms in the premature lung leads to deficiencies of antioxidants and inhibitors rendering the lung more vulnerable to oxidative stress (Choi et al., 2021).

Low birth weight and prematurity are two of the strongest risk factors to develop BPD. It is estimated that 95% of all infants that go on to develop BPD had very low weight at birth (Thébaud et al., 2019; Walsh et al., 2004). Other risk factors are ethnic background, male sex, prenatal smoke exposure and genetic factors (Sucasas Alonso et al., 2022; Thébaud et al., 2019).

1.2.1 Pathophysiology of Bronchopulmonary dysplasia

New clinical interventions in premature babies have succeeded to improve survival, especially in the most immature preterm infants but did not decrease the incidence of BPD significantly. Clinical interventions like exogenous surfactant administration have, however, led to increased survival of premature infants born as early as the 24th week of gestation (Hilgendorff & O'Reilly, 2015). Exogenous surfactant administration and more conservative uses of oxygen therapy have decreased the extensive interstitial atelectatic fibrosis that was commonly observed before. Although the interstitial fibrosis is milder, the histopathology of BPD is still dominated by increased smooth muscle in airways and small vessels and extensive extracellular matrix remodeling (Hilgendorff & O'Reilly, 2015; Niedermaier & Hilgendorff, 2015; Sucre et al., 2021; Thébaud et al., 2019). These changes are accompanied by increased inflammation which leads to a disbalance of matrix-metalloproteinase activity, and apoptosis. The

underlying mechanisms behind these pathological changes are believed to result from altered growth factor signaling i.e., platelet-derived growth factor (Pdgf-Rα), transforming growth factor (TGF-β), vascular endothelial growth factor A (VEGF-A), endothelial nitric oxide synthase (eNOS) and others (Hilgendorff & O'Reilly, 2015; Oak & Hilgendorff, 2017; Oak et al., 2017; Sucre et al., 2021). Studies in animal models of BPD have shown that after the initial influx of neutrophils and macrophages, the inflammatory response is perpetuated by dysregulated growth factor signaling. Decreased expression of Pdgf-Rα, VEGFA, and eNOS has been linked to the development of dysmorphic capillaries and other vascular aberrations that can promote the development of pulmonary hypertension (**Fig 1.2)** (Hilgendorff & O'Reilly, 2015; Jankov & Keith Tanswell, 2004; Oak & Hilgendorff, 2017; Oak et al., 2017).

Immaturity of red-ox mechanisms in the premature lung leads to deficiencies of antioxidants and inhibitors rendering the lung more vulnerable to oxidative stress. Animal models using excessive levels of oxygen early in life have recapitulated the pathological features of inflammation, alveolar simplification, impaired microvascular development, and mild interstitial thickening (Collaco & McGrath-Morrow, 2021; Hilgendorff & O'Reilly, 2015; Hilgendorff et al., 2014; Oak & Hilgendorff, 2017; Sucre et al., 2021). However, the evidence obtained with many of these models is limited because they usually do not reflect the clinical setting. BPD animal models use very high levels of hyperoxia (FiO_2 > 0.8) usually from postnatal day (PND) 0 to 14 which covers two distinct stages of lung development (saccular and alveolarization phases). Because lung development clearly impacts the response to oxygen exposure, addressing the effects on different lung development phases is necessary to reflect the clinical setting more accurately (Behnke et al., 2021; Bik-Multanowski et al., 2018; Choi et al., 2021; Hilgendorff et al., 2014).

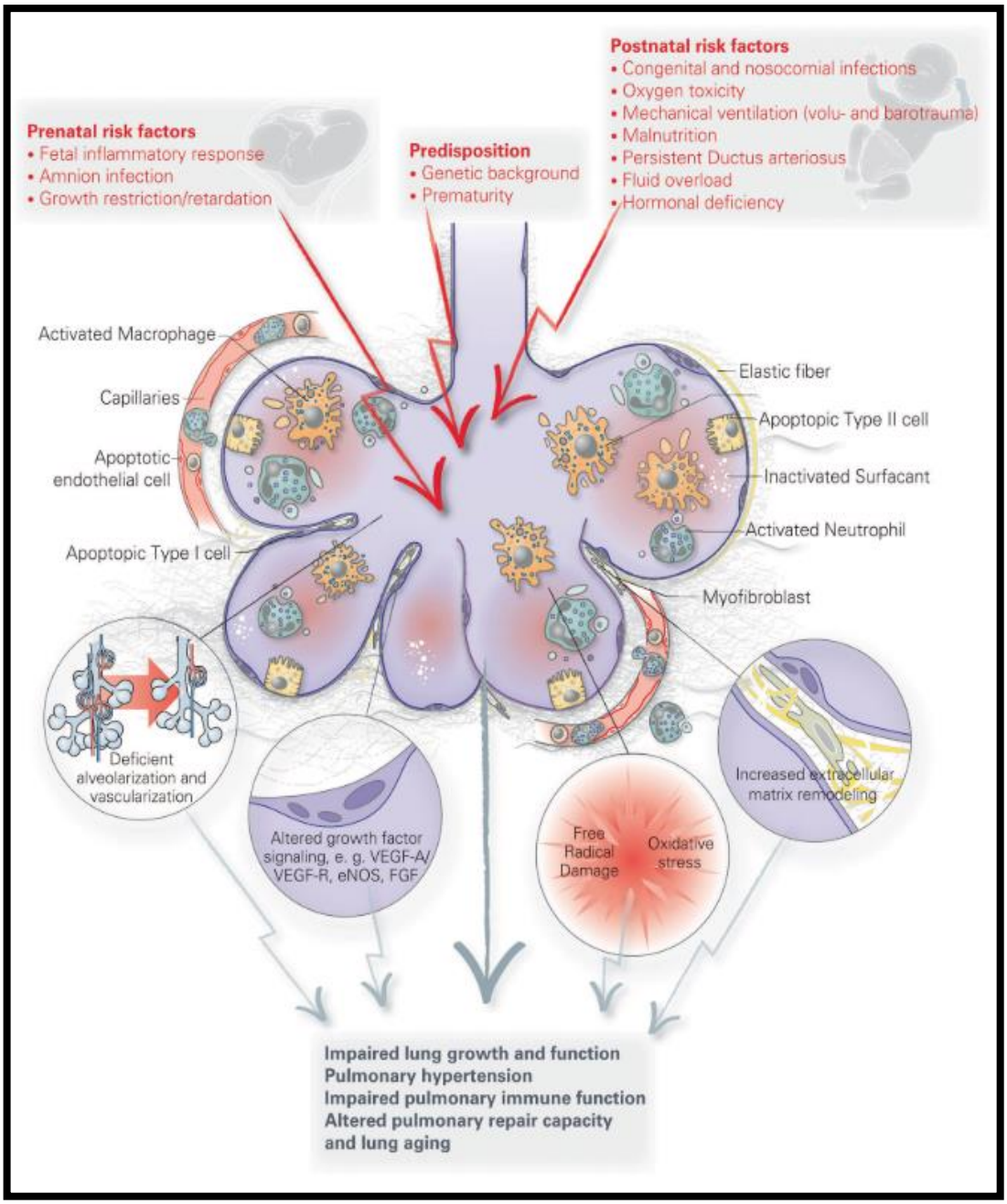

Fig 1.2: Processes involved in the pathophysiology of bronchopulmonary dysplasia (BP). This figure was published in Hilgendorff & O'Reilly, Bronchopulmonary dysplasia early changes leading to long-term consequences. Front Med (Lausanne). 2015 Feb 12; 2:2 (Hilgendorff & O'Reilly, 2015).

1.2.2 Screening and therapeutic approaches in BPD

Many studies have investigated the predictive value of computed tomography and plain chest radiography findings in the diagnosis of BPD (Gilfillan et al., 2021). Radiographic abnormalities including chronic pulmonary edema and a ‘bubbly’ cystic appearance have been associated with oxygen therapy requirements at week 36’ postmenstrual age (Hyödynmaa et al., 2012; May et

al., 2009). Other findings like elevated chest radiograph area together with reduced functional residual capacity appear to have a strong predictive value for the development of moderate and severe BPD. Ultra-short echo time MRI allows structural and functional evaluation and could play a role in defining specific BPD phenotypes (Förster et al., 2020; Gilfillan et al., 2021). Unfortunately, none of these diagnostic approaches has been fully validated in the clinical setting. Therefore, their true prognostic value for the development of BPD remains to be determined.

The identification of early predictive biomarkers of BPD remains an area of active research. Several studies using 'omic' approaches to identify markers that predict BPD, or its complications have shed light on the potential of combined diagnostic strategies that predict risk based on genetic factors, markers of disease and different disease phenotypes. **Table 1.2** shows a summary of the most important biomarker approaches that have been studied lately (Förster et al., 2020; Gilfillan et al., 2021; Lal & Ambalavanan, 2015; Piersigilli et al., 2019; Thébaud et al., 2019).

Category or causal pathway	Biomarker
Endothelial injury and dysfunction	Circulating endothelial progenitor cells
Growth and angiogenesis factors	VEGF and VEGFR, endoglin (CD105), angiopoietin 1, endostatin, PlGF and EMAP II
Epithelial injury and fibrosis	KL6, MMP9, TIMP1, TGFβ1 and NGAL
Nitric oxide deficiency and insufficiency	NOx and citrulline
Oxidative stress, redox status	Elastase, myeloperoxidase, xanthine oxidase, catalase, total sulfhydryls, carbonyls, 3-chlorotyrosine, malondialdehyde and 3-nitrotyrosine
Inflammation and host immune responses	Inflammatory biomarker panels and hyaluronan
Omics	Genomics, epigenomics, metabolomics, microbiomics, methylomics and transcriptomics
Vascular injury and pulmonary hypertension	BNP and NT-proBNP and echocardiographic measurement
Lung function	Dynamic compliance, airway resistance, functional residual capacity, etCO and exhaled NO
Lung structure	Imaging by hyperpolarized gas MRI and helium-3 MRI

Table 1.2: Biomarkers investigated in the diagnosis of BPD.
Table adapted from (Thébaud et al., 2019).

Until now treatment strategies in preterm babies have focused on minimizing the negative effects of exposure to ventilation and/or intubation. Non-invasive interventions like nasal continuous positive airway pressure, nasal intermittent positive pressure ventilation and high-flow nasal cannula have become popular strategies to prevent injury of the premature lung. Approaches to minimally invasive application of exogenous surfactant, which reduces mortality and improves outcomes, have been developed. To minimize the negative impact of oxygen administration, targets of oxygen saturation have been implemented. This has led to fraction of inspired oxygen (FiO_2) of less than 0.5 to be more commonly used to achieve the saturation goals (Askie et al., 2003; Torres-Cuevas et al., 2017). Interventions like caffeine, vitamin A, and corticosteroids have been used with varying degrees of evidence. **Table 1.3** shows some of the therapeutic interventions being used to minimize lung injury in preterm infants (Askie et al., 2018; Darlow et al., 2016; Doyle et al., 2017; "Elective high-frequency oscillatory ventilation versus conventional ventilation for acute pulmonary dysfunction in preterm infants," 2013; Keller et al., 2017; Klingenberg et al., 2017; Schmidt et al., 2007; Thébaud et al., 2019).

Intervention	Rationale	Level of evidence	Clinical implications
Caffeine	Reduced time on ventilator leading to less lung damage	High quality: large RCT with long-term follow-up	Recommended for use in extremely preterm infants at the doses used in the CAP trial
Ventilation (conventional, high-frequency oscillation or jet ventilation)	Volutrauma is an important pathophysiological mechanism	Moderate quality: despite many RCTs, evidence of a substantial benefit of one mode is lacking	BPD rates remain high in all trials, suggesting that establishing and maintaining skills with a chosen mode may be the most important factor
Less-invasive surfactant therapy	Avoids the risks of endotracheal intubation	Low quality: small RCTs, imprecise estimates of safety and efficacy	Very promising, but more research required
Vitamin A	Low levels seen in preterm infants; vitamin A required for normal lung growth	Moderate quality: meta-analysis suggests a small reduction in rates of death or BPD	Depends on local incidence of BPD; trade-off between the modest reduction in BPD and acceptability of intramuscular treatment
Targeting lower oxygen saturation levels throughout NICU stay	Avoidance of high oxygen levels may reduce BPD	High quality: individual patient data meta-analysis of five high-quality RCTs	Targeting higher oxygen saturations (91–95%) improves survival rates without increasing risk of BPD
Glucocorticoids			
Dexamethasone	Reduced inflammation allowing earlier extubation	Moderate quality: meta-analyses and meta-regression of numerous small trials	Low-dose, short courses that are useful for ventilated infants at highest risk of BPD
Hydrocortisone	Avoids adverse neurodevelopmental effects of dexamethasone	Moderate quality: small RCTs, imprecise estimates of safety and efficacy	Promising, but more research into neurodevelopmental outcomes is required
With surfactant	Better distribution of steroids and reduced systemic effects	Low quality: small RCTs, imprecise estimates of safety and efficacy	Very promising, but more research required

BPD, bronchopulmonary dysplasia; CAP, Caffeine for Apnea of Prematurity; RCT, randomized controlled trial.

Table 1.3: Therapeutic approaches to minimize lung injury in preterm infants

Table adapted from (Thébaud et al., 2019).

1.2.3 Antioxidative defense mechanisms in the developing lung and oxygen toxicity

1.2.3.1 Antioxidative defense mechanisms in the developing lung

When the fetus is developing it is exposed to oxygen tensions between 25-30 mmHg, which corresponds to a hypoxic environment. At such oxygen tensions, the physiological conditions are given for hypoxia-inducible factor (HIF) family of transcription factors to work. The HIF family, regulators of over 2000 genes, is comprised of one Hifα subunit (Hif1α, Hif2α, Hif3α) and a Hifβ subunit. The stabilization of Hifα members depends on oxygen conditions. Hypoxia stabilizes both Hif1α and Hif2α in the lungs (Andresen & Saugstad, 2020; Choi et al., 2021; Urrutia & Aragonés, 2018). Hif1α works as a key regulator of vascular development via angiopoietins, oxygen consumption and VEGF-A signaling. Under hypoxic conditions, reactive oxygen species generated by the mitochondria inhibit the prolyl hydroxylation and degradation of Hif1α. Thus, byproducts of oxidative phosphorylation work as signaling molecules for oxygen availability in the cell. The fetus has evolved to deal with hypoxic conditions through the HIF family regulation, however, the mechanisms necessary to deal with hyperoxic conditions i.e., at delivery are only developed shortly after birth (Andresen & Saugstad, 2020; Choi et al., 2021; Maltepe & Saugstad, 2009). The mechanisms to deal with hyperoxia conditions are not as well developed as those that deal with hypoxia. However, some of these mechanisms are driven by mitogen-activated kinases which result in the upregulation of antioxidant enzymes. In term babies, the transition from placental respiration to lung-based respiration does not represent a big challenge because in late gestation the lungs have evolved to allow surfactant production and antioxidant mechanisms to deal with the shift in oxygen tension (Choi et al., 2021; Haddad, 2002).

Antioxidant compounds such as lipoic acid, Vitamin A, E and C, glutathione (GSH) together with enzymes such as superoxide dismutase, catalase and glutathione peroxidase have evolved as defence mechanisms that deal with oxidative stress. Superoxide dismutase (SOD) has a dual role as antioxidant and pro-oxidant by catalyzing the dismutation of O-superoxide anion and hydrogen peroxide (H_2O_2) and Oxygen (O2) and generating H_2O_2 (Ferrante et al., 2021;

Haddad, 2002). GSH is another important system that maintains a redox conditions. This system includes Glutathione peroxidase uses glutathione as substrate to reduce H_2O_2. Glutathione S-transferase, which can reduce peroxides and glutathione reductase, in charge of reducing oxidized glutathione (Andresen & Saugstad, 2020; Choi et al., 2021; Ferrante et al., 2021; Lorente-Pozo et al., 2020; Perez et al., 2019).

To prevent injury, detoxification of ROS needs to occur in an efficient manner. In newborn infants, there is an increased in ROS generation because of their higher levels of free iron, which boosts the Fenton reaction and results in the production of free radicals. In premature neonates exposed to high concentrations of oxygen, the quick overload of the mitochondrial antioxidant systems together with mitochondrial damage render the lung more vulnerable to injury and BPD development (Choi et al., 2021).

1.2.3.2 Reactive oxygen species injury to the premature lung in BPD development

Reactive oxygen species (ROS) lead to deleterious effects in the premature lung through different mechanisms: exacerbated inflammatory response, mitochondrial dysfunction, gene regulation and epigenetic alterations, and disruption of angiogenesis (**Fig 1.3)** (Choi et al., 2021).

Exacerbated inflammatory response. Excessive activation of NF- κB, along with exacerbated production of cytokines like IL-1β, TNF-α and influx of inflammatory cells (neutrophils and macrophages) are responses triggered by ROS in the immature lung. These responses result in direct injury to alveolar structures along with impaired surfactant function and aberrations in vascular development and stem cell function (Behnke et al., 2021; Choi et al., 2021; Thébaud et al., 2019). Polymorphonuclear leukocytes have been described to perpetuate and exacerbate several of these changes because they are a major source of ROS. Moreover, these cells also activate pro-inflammatory pathways i.e., NF-κB pathway, release pro-inflammatory cytokines, and proteases that damage the tissue further and perpetuate this cycle. Other pathways like the TGF-B pathway play an important role in worsening lung injury because it upregulates pro-inflammatory mechanisms and disrupts angiogenesis (Choi et al., 2021;

Hilgendorff & O'Reilly, 2015; Oak & Hilgendorff, 2017; Oak et al., 2017; Sucre et al., 2021).

Mitochondrial dysfunction. Hyperoxia leads to the accumulation of ROS metabolites and mitochondrial stress and dysfunction. Superoxide dismutase 2 (SOD2) is an enzyme that becomes quickly overwhelmed when high amounts of ROS are released. The overload of SOD2 results in decreased availability of nitric oxide, and increased activation of NF- κB which provokes a pro-inflammatory response. Other important mitochondrial player in the response to ROS is the cytochrome P450 family. CYP1A1 and CYP1A2 activation after hyperoxia exposure are critical to reduce ROS-dependent lung injury. Interestingly, some studies have reported sex differences in the activation of CYP1A1 and CYP1A2, with males having lower activation than females, a fact that might contribute to the increased vulnerability of males to develop BPD (Andresen & Saugstad, 2020; Behnke et al., 2021; Choi et al., 2021; Haddad, 2002; Thébaud et al., 2019).

Gene regulation and epigenetic alterations. ROS and hyperoxia trigger the regulation of several genes of antioxidant genes like Nrf2 and can lead to changes in methylation patterns. Some of these changes in DNA methylation have been associated with alterations in alveolarization and growth factor gene signaling i.e., TFG-β signaling (Berkelhamer et al., 2013; Bik-Multanowski et al., 2018; Bochtler et al., 2017; Choi et al., 2021).

Disruption of angiogenesis. An important factor suppressed by ROS is Nitric oxide (NO), the downstream effector in the cascade of Hif and VEGFA. The alterations in NO signaling result in vascular pulmonary remodeling and smooth muscle cell growth. Moreover, NO has anti-inflammatory properties evidenced by the downregulation of CCXL1 and IL6 gene expression upon NO administration together with the attenuation on inflammatory cell influx (Alhayaza et al., 2020; Haddad, 2002; Hilgendorff & O'Reilly, 2015; Sucre et al., 2021; Weng et al., 2021).

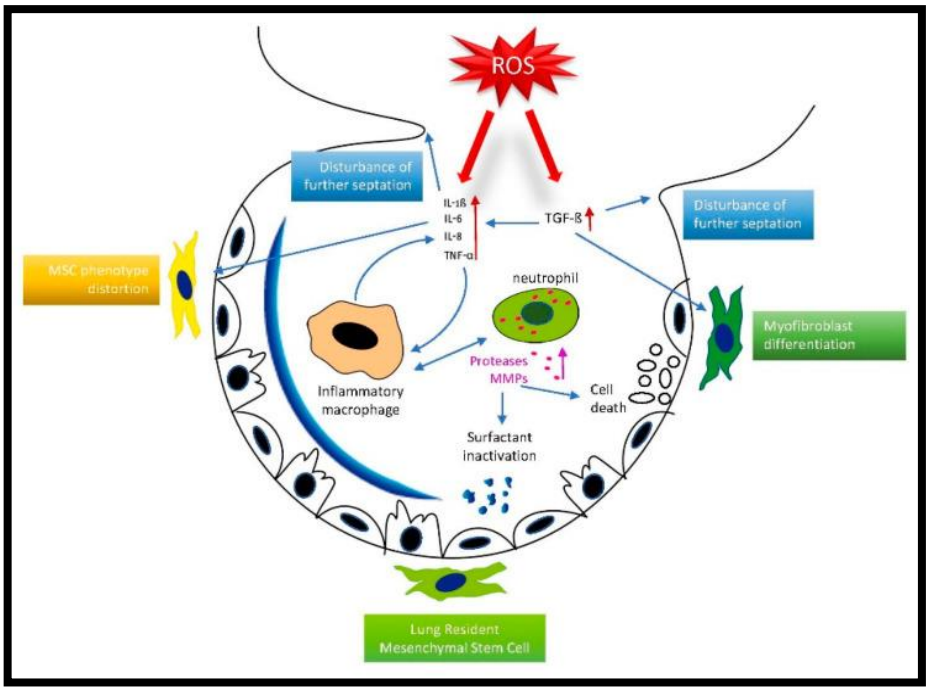

Fig 1.3: Deleterious mechanisms induced by reactive oxygen species (ROS) in the premature lung

ROS trigger the upregulation of pro-inflammatory cytokines attracting neutrophils and macrophages. This event seems to lead to cell death, surfactant inactivation, distortion of stem cell population and other pathologic BPD hallmarks. Figure adapted from Cho Y, et al. Oxygen Toxicity to the Immature Lung—Part I: Pathomechanistic Understanding and Preclinical Perspectives Int J Mol Sci. 2021 Oct; 22(20): 11006 (Choi et al., 2021).

1.2.3.3 Antioxidant therapeutic strategies

Antioxidants have been widely studied as therapeutic approaches to prevent the ROS-induced injury to the immature lung. Unfortunately, in clinical studies only Vitamin A seems to provide a small benefit in reducing BPD. Substitution of Vitamin E has been studied as well given that its deficiency has been linked to worsen lung outcomes. **Table 1.4** shows some of the antioxidant strategies that have been used to prevent ROS-mediated lung injury in premature infants.

Intervention	Study Design	Study Population	Primary Outcome	Effect on BPD/Lung Injury
Vitamin A (supplementation vs. control, placebo, or no supplementation)	Cochrane Database Syst Rev. included trials (RCTs): 11	n = 1580 BW ≤ 1500 g or GA ≤ 32	death (at 28 days and at hospital discharge) chronic lung disease (defined as oxygen use at 28 days or 36 weeks PMA) death or chronic lung disease	small benefit in reducing the risk of chronic lung disease (RR 0.87; 95% CI 0.77–0.99)
Vitamin E (supplementation vs. either placebo, no treatment, or another type, dose, or route of administration	Cochrane Database Syst Rev. included trials (RCTs): 26	n = 2028 GA < 37 or BW < 2500 g	mortality, combined outcome at 18 months including mortality	no effect on BPD (RR 0.91; 95% CI 0.73–1.14) or mortality until discharge (RR 0.97; 95% CI 0.83–1.14)
DHA	RCT	n = 1273 GA ≤ 27	BPD (physiological basis, oxygen-saturation monitoring at 36 weeks PMA or discharge)	no effect on BPD (RR 1.13; 95% CI 1.02–1.25; $p = 0.02$)
NAC (supplementation vs. placebo)	RCT	n = 391 BW 500–999 g	death or BPD (supplementary oxygen requirement at 36 weeks PMA)	no difference in the combined incidence of death or BPD (OR 1.0; 95% CI 0.7–1.6)
Caffeine (high vs. low dose)	Meta-analysis Included trials (RCTs): 6	n = 816 GA < 34	mortality during the first admission, BPD (at 36 weeks CA), cerebral palsy	fewer cases of BPD (RR 0.76; 95% CI 0.60–0.96); quality of the evidence was low due to imprecision of the estimates
iNO (supplementation vs. control with or without placebo)	Cochrane Database Syst Rev. included trials (RCTs): 17	n = 4062	death before hospital discharge BPD (oxygen dependence at 36 weeks PMA) death or BPD (at 36 weeks PMA) IVH (any grade and more severe, grades 3 and 4)	early routine use of iNO in preterm infants with respiratory disease does not improve survival without BPD (RR 0.89; 95% CI 0.76–1.04) later use of iNO to prevent BPD could be effective, but the current 95% CI included no effect; the effect size is likely small (RR 0.92; CI 0.85–1.01) and requires further study

BW—birth weight; n—number; BPD—bronchopulmonary dysplasia; PMA— postmenstrual age; RCT—randomized controlled trial; GA—gestational age; CI—confidence interval; RR—relative risk; iNO—Inhaled nitric oxide; NAC—N-acetylcysteine; DHA—docosahexaenoic acid; IVH—intraventricular hemorrhage.

Table 1.4: Antioxidant therapeutic strategies
Antioxidant therapeutic strategies studies and their effect on BPD/lung injury prevention. This table was adapted from (Behnke et al., 2021).

1.2.4 Mouse models using hyperoxia

Mouse models using high concentrations of oxygen ($FiO_2 > 0.5$) for several days or weeks have been used to recapitulate the pathological findings of BPD (Berger & Bhandari, 2014; Hilgendorff et al., 2014). Models in rodents are frequently used to model the effects of hyperoxia in the premature lung because newborn mice are born during the saccular stage of lung development which usually corresponds to the lung development stage of premature neonates. Although there are many advantages to using rodents for BPD modeling, they are limited for studying pulmonary hemodynamics, gas exchange or breathing mechanics. Regardless, thanks to rodent animal models researchers have obtained

extensive knowledge about BPD pathophysiology which has helped identified critical drivers of disease and potential therapeutic targets. To increase the clinical relevance, the concentrations of oxygen and times of exposure should be adjusted to fit the clinical setting. Thus, models using moderate concentrations of hyperoxia (FiO_2 < 0.5) for shorter exposures are needed to reflect the clinical setting (Andresen & Saugstad, 2020; Askie et al., 2003; Thébaud et al., 2019; Torres-Cuevas et al., 2017; Tracy & Berkelhamer, 2019). **Table 1.5** summarizes some of the hyperoxia models of BPD reported in the literature (Berger & Bhandari, 2014; Hilgendorff et al., 2014). For more details, see review by (Berger & Bhandari, 2014)

Strain	Experimental Model	Outcomes
FVB/N	·Hyperoxia for 28 days	·BPD pulmonary phenotype
		·Decreased cell proliferation over 14 days, which normalized by day 28
		·Increased inflammatory markers (IL-1α and MIP-1α)
C57BL/6J	·Postnatal hyperoxia at different concentrations for 3, 14, or 21 days	·BPD pulmonary phenotype
	·±Prenatal LPS	
C57BL/6	·Hyperoxia for 28 days followed by room air for 7, 14, or 28 days	·BPD pulmonary phenotype
C57BL/6N	·Hyperoxia for 28 days	·BPD pulmonary phenotype
		·Upregulation of PDE1A and 4A; downregulation of PDE5A
KunMing	·Hyperoxia for 15 days	·BPD pulmonary phenotype
		·mRNA differential expression
C3H/HeN	·Hyperoxia for 14 days followed by room air for 14 days	·Hyperoxia alone produced BPD pulmonary phenotype
	·± prenatal LPS	·Combination of hyperoxia and prenatal LPS did not result in a more severe phenotype, but the effects were more prolonged than either exposure alone
		·Combined exposure produced more inflammation, as measured by pulmonary macrophages
FVB	·Hyperoxia for 14 days	·BPD pulmonary phenotype
C57BL/6J	·Hyperoxia for 4 days	·Pulmonary fibrosis
		·Increased inflammation, measured by lymphocyte, neutrophil, and macrophage counts
		·Increased levels of MCP-1
		·Increased mortality by day of life 14
		·Increased sensitivity to influenza A as adults
C3H/HeN	·14 days hyperoxia at varying concentration	·Increased severity of BPD pulmonary phenotype with higher concentration O_2
		·Higher O_2 concentration associated with increased neutrophil counts
		·Stunted growth, worse with higher concentrations O_2

Strain	Experimental Model	Outcomes
Transgenic models		
FVB/N	·IL-1β transgenic mice	·BPD pulmonary phenotype
	·Additional gene knockouts	
C57BL/6	·Hyperoxia + macrophage MIF knockout or transgene	·BPD pulmonary phenotype
C57BL/6J	·Transgenic IFN-γ overexpressing mice	·BPD pulmonary phenotype
C57BL/6J	·TGF-β transgenic mice	·BPD pulmonary phenotype
C57BL/6	·7–14 days hyperoxia	·BPD pulmonary phenotype, which was attenuated by Vitamin A and retinoic acid exposure
	·±Exposure to Vitamin A+retinoic acid	
FVB/N	·HO-1 transgenic mice	·BPD pulmonary phenotype, right ventricular hypertrophy and arterial remodeling which was decreased by HO-1 overexpression
	·14 days hyperoxia	
FVB	·10 days hyperoxia	·BPD pulmonary phenotype Increased number of BASC in mice treated with MSC or MSC-CM; also improved pulmonary phenotype
	·Treatment with MSC or MSC-CM	
C57BL/6	·sGC-α1 knockout mice	·Knockout mouse alone produced decreased small airways and increased lung volumes but did not affect septation
	·Exposure to hyperoxia	·More complete BPD pulmonary phenotype with septation defect with hyperoxia exposure
C57BL/6	·Varying days of hyperoxia	·BPD pulmonary phenotype

Table 1.5: Mouse models of hyperoxia-induced BPD
This table describes some of the BPD mouse models reported in the literature with mouse strain, experimental design, and outcomes. *Table adapted from (Berger & Bhandari, 2014).* MCP-1, monocyte chemotactic protein-1; TLR, Toll-like receptor; PDE, phosphodiesterase; GFP, green fluorescent protein; VEGF-R2, vascular endothelial growth factor receptor 2; EYFP, enhanced yellow fluorescent protein; MIF, macrophage migration inhibitory factor; HO, heme oxygenase; BASC, bronchoalveolar stem cells; sGC, soluble guanylyl cyclase; MSC, mesenchymal stromal cells; MSC-CM, MSC conditioned media.

1.3 DNA damage response to oxidative stress

To maintain DNA integrity and prevent mutations from happening, the cell activates the DNA-damage response (DDR), which engages several pathways in order to repair DNA. The pathways that get engaged depend largely on the type of DNA lesion. DNA lesions can be single strand breaks (SSBs; breaks in phosphodiester bonds), double strand breaks (DDBs), and damage to bases including crosslinks, mismatches, and pyrimidine breaks (**Fig 1.4**) (Chatterjee & Walker, 2017; Nakad & Schumacher, 2016; Pilié et al., 2019). The first step in

this process is the recognition of DNA damage achieved by lesion-specific sensing molecules. Next, protein kinase transducers are recruited, after which cell cycle checkpoint regulators, nucleases, polymerases, helicases and ligases are engaged to remove the damage. SSBs are removed by single strand break repair, whereas DSBs are repaired by homologous end joining and homologous recombination. Base excision repair (BER) removes oxidative single base modifications while interstrand crosslinks are removed by the Fanconi anemia pathway (**Fig 1.4**) (Chatterjee & Walker, 2017; Nakad & Schumacher, 2016; Pilié et al., 2019).

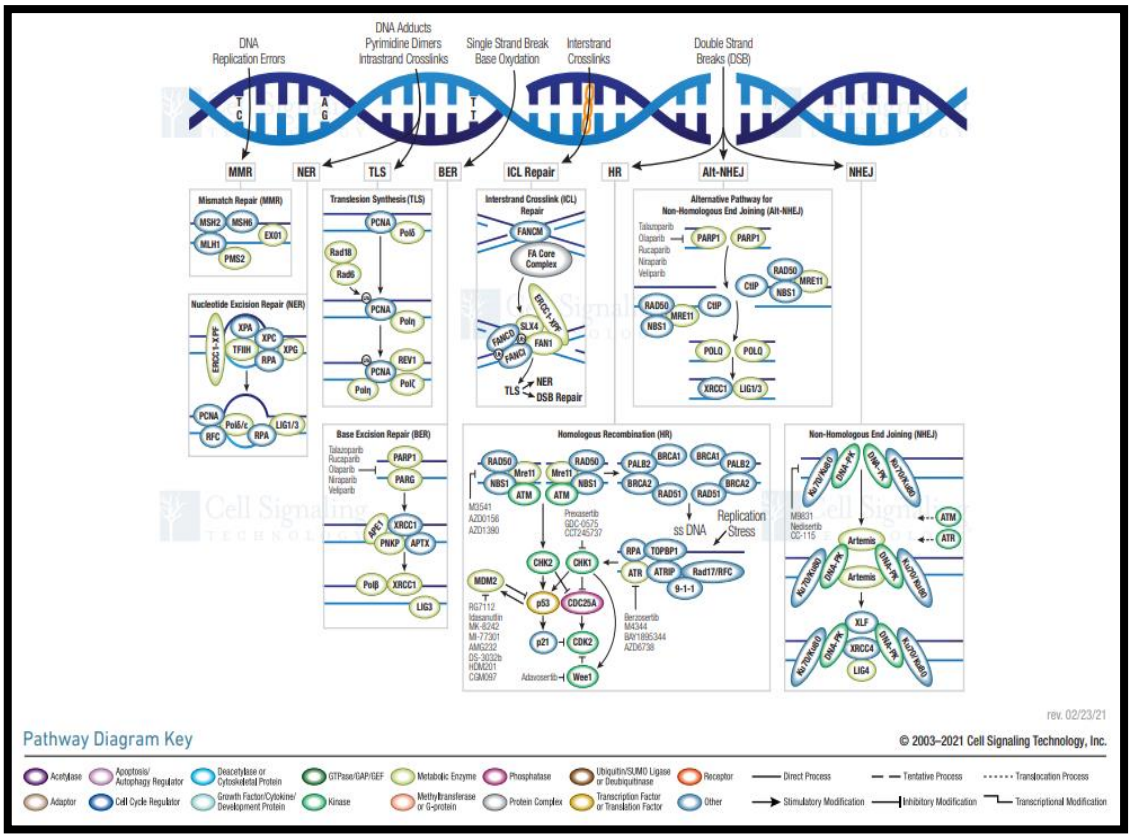

Fig 1.4: DNA damage response mechanisms

The DNA damage response is a complex network of genes that are engaged according to the type of DNA damage.

Illustration reproduced courtesy of Cell Signaling Technology, Inc. (www.cellsignal.com).

1.3.1 *DNA damage response mechanisms during oxidative stress*

Oxidative stress induces around 10000 DNA alterations in each cell per day. Representing a major source of DNA damage, oxidative stress can lead to different types of DNA damage including purine and pyrimidine damage, Apurinic/apyrimidinic (AP) sites, sugar moiety damage, single strand breaks

(SSBs), double strand breaks (DSBs), DNA interstrand crosslinks, mismatched pairs, stalled DNA replication forks, among others. When hydroxyl radicals react with pyrimidines and purines of the DNA, it can create products like 8-hydroxyguanine (8-OH-G). Singlet oxygen can generate 8-oxo-7,8-dihydroguanine (8-oxo-G) when it reacts with guanine, although it can also react with the other three deoxynucleotide bases (Agnez-Lima et al., 2012; Neeley & Essigmann, 2006). 8-oxo-G is primarily repaired by the base excision repair (BER) pathway. Th BER pathway repairs ROS-caused DNA damage that results in non-bulky lesions whereas the nucleotide excision repair (NER) pathway repairs bulky lesions like those caused by UV radiation.

To coordinate the DNA repair process and cell cycle progression, two major DNA damage response (DDR) pathways are induced upon oxidative stress DNA damage. One is the ATM- and Rad3-related (ATR)-Checkpoint kinase 1 (Chk1) and the other the Ataxia-telangiectasia mutated (ATM)-checkpoint kinase 2 (Chk2) checkpoints.

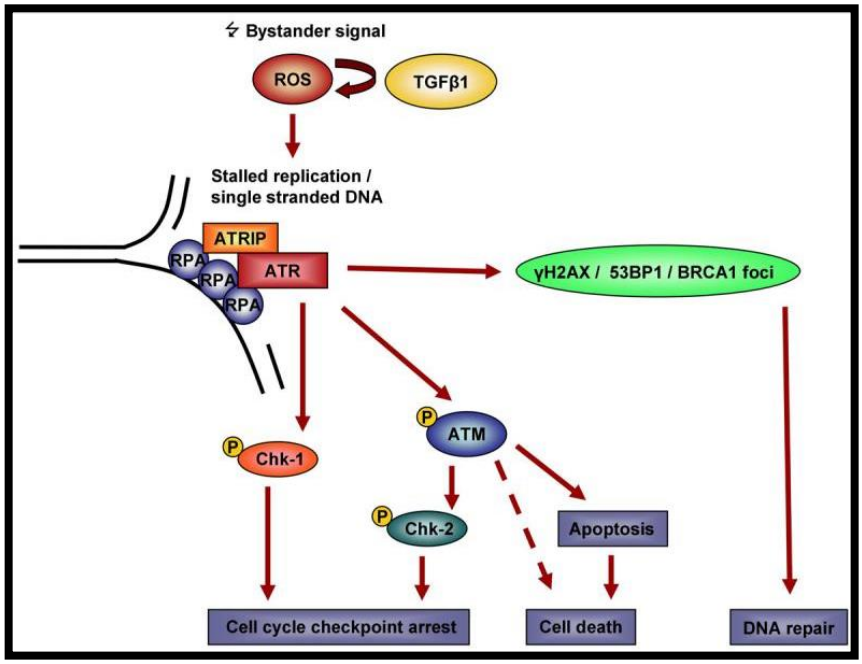

Fig 1.5: ATR and ATM are two major DNA damage response checkpoints activated upon DNA damage arising from oxidative stress. According to the downstream regulation the cell can have several fates: cell death or apoptosis, cell cycle arrest and DNA repair. This figure was adapted from (Burdak-Rothkamm et al., 2008).

ATM-Chk2 checkpoint pathway primarily responds to DSBs while the ATR-Chk1 is activated by other types of DNA damage including oxidative stress, single

strand damage and stalling of replication forks in conditions of cell cycle arrest. A study by Kulkarni et al. showed that 95% hyperoxia led to the phosphorylation of Chk1 and p53 in an ATR-dependent but ATM-independent manner in a lung epithelial cell line. This study also showed that hyperoxia activated Chk1 and p53 at different phosphorylation sites from those induced by ionizing radiation. In contrast to the 30-minute time window in ionizing radiation, in hyperoxia conditions, the phosphorylation of Ser6 and Ser15 in p53 took around 4 to 8 hours. Moreover, the authors showed that in contrast to ionizing radiation, hyperoxia triggered the phosphorylation of p53 at Ser392 in an ATR-dependent manner. Other phosphorylation of p53, Ser15 and Ser37, were also dependent on ATR. Thus, the evidence suggests that the DDR pathway activated following high levels of hyperoxia occurs in an ATR-dependent manner mostly (Agnez-Lima et al., 2012; Kulkarni & Das, 2008). For more detailed mechanisms refer to the review by (Agnez-Lima et al., 2012). **Figure 1.6** shows in more detail the ATR-Chk1/ATM-Chk2 DDR pathways and their downstream effects leading to cell cycle checkpoint regulation.

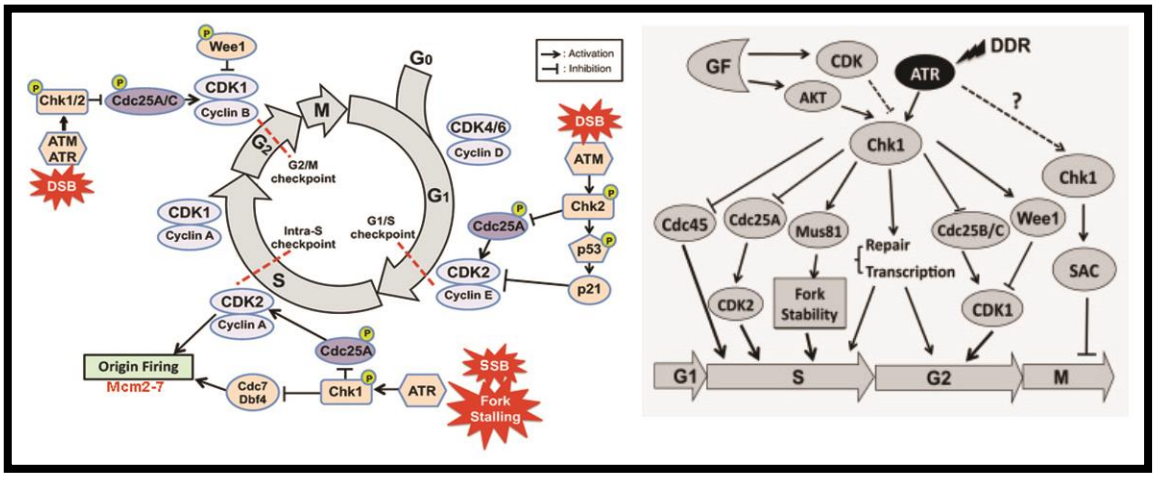

Fig 1.6: DDR response and subsequent checkpoint regulation.

Cell cycle checkpoint regulators adapted from (Kojima et al., 2017). ATR-Chk1 pathway adapted from (Zhang & Hunter, 2014)

2. Aims

Bronchopulmonary dysplasia (BPD) remains the most common consequence of prematurity (Behnke et al., 2021; Sucre et al., 2021). Premature neonates often require life-saving oxygen therapy, which increases their risk of developing BPD (Behnke et al., 2021; Hilgendorff & O'Reilly, 2015; Sucre et al., 2021). Although survival improves with oxygen supplementation, morbidity increases with higher oxygen concentration and longer exposures. The induction of lung injury by short-term postnatal hyperoxia has been suggested by clinical observations and has been in part supported by experimental studies (Dylag et al., 2021; Oak et al., 2017). In recent years, in the clinical setting, the use oxygen concentrations (FiO_2 < 0.5) have become more conservative given the evidence of severe side effects like retinopathy. However, underlying mechanisms of lasting effects provoked by clinically relevant oxygen levels remain poorly understood. This knowledge gap is perpetuated by the fact that most of the experimental models of BPD employ very high oxygen concentrations (FiO2 > 0.8) for several days or weeks (Behnke et al., 2021; Choi et al., 2021; Hilgendorff et al., 2014). Thus, our knowledge of the effects of oxygen therapy in the developing lung derives from models of severity that most likely do not reflect the clinical setting. Even though the effects of treatment with severe hyperoxia concentrations have been extensively characterized, there is still a poor understanding of the maladaptive responses that lead to BPD. More importantly, a real gap of knowledge remains when it comes to clinically relevant hyperoxia concentrations i.e., $FiO_2 \leq 0.4$. Thus, it is critical to identify and understand the early mechanisms involved in the injury response to hyperoxia treatment in order to harness this knowledge towards therapeutics that restore normal lung function. Therefore, in this study I aimed to:

1. Characterize immediate and sustained effects of treatment with clinically relevant hyperoxia concentrations in three main pulmonary cell types (fibroblasts, ATII cells, endothelial cells) obtained from healthy and diseased neonatal mouse tissue.

2. Identify the acute and persistent effects of oxygen exposure in the developing mouse lung focusing on similarities and differences in these responses.

3. Investigating whether and how oxygen ‘priming’ of the lung can alter the response to a second hit injury.

4. Translate the findings into OMIC results from biospecimen (plasma) obtained from premature neonates at risk of developing bronchopulmonary dysplasia (BPD).

3. Material and Methods

3.1 Materials

3.1.1 Antibodies

3.1.1.1 Primary Antibodies

Antigen	***Product number***	***Host Type***	***Application***	***Dilution***	***Manufacturer***
Chk1	sc-8408	Mouse	WB	1:1000	Santa Cruz
p-Chk1 (ser345)	2348	Rabbit	WB	1:1000	Santa Cruz
p21	sc-6246	Mouse	WB	1:1000	Santa Cruz
p-p21	sc-377569	Mouse	WB, IF	1:1000, 1:100	Cell signaling
p53	2524S	Rabbit	WB	1:1000	Cell signaling
p-p53 (ser15)	9284S	Rabbit	WB	1:1000	Cell signaling
p-p53(ser20)	9287S	Rabbit	WB	1:1000	Cell signaling
a-SMA	ab7817	Rabbit	WB	1:1000	Abcam
pMcm2	ab109271	Rabbit	WB, IF	1:1000, 1:100	Abcam
Mcm2	4007S	Rabbit	WB	1:1000	Cell signaling
Caspase 3	14220S	Rabbit	WB	1:1000	Cell signaling
Cleaved Caspase 3	9661S	Rabbit	WB	1:1000	Cell signaling
Caspase 7	9492s	Rabbit	WB	1:1000	Cell signaling
Caspase 9	9502S	Rabbit	WB	1:1000	Cell signaling
H2ax	ab11174	Rabbit	IF	1:1000	Santa Cruz
Ogg1	sc-376935	Mouse	WB	1:1000	Santa Cruz
8-oxoG	sc-130914	Mouse	IF	1:100	Santa Cruz
Parp	9532S	Rabbit	WB	1:1000	Cell signaling
Pro-SPC	Ab3786	Rabbit	WB	1:1000	Abcam
Rb1	sc-102	Mouse	WB	1:1000	Santa Cruz
p-Rb1	8516S	Rabbit	WB	1:1000	Cell signaling
Xrcc1	sc-56254	Mouse	IF	1:100	Santa Cruz
Cdk2	sc-6248	Mouse	WB	1:1000	Santa Cruz
Wnt5a	sc-365370	Mouse	WB, IF	1:1000, 1:100	Santa Cruz
Elastin	sc-58756	Mouse	WB	1:1000	Santa Cruz
Chop	2895S	Mouse	WB	1:1000	Cell signaling
Xbp1s	40435s	Rabbit	WB	1:1000	Cell signaling
Ki67	ab15580	Rabbit	WB	1:1000	Abcam
Gpadh-HRP	3683	Rabbit	WB	1:10000	CST
B-Actin-HRP	ab49900	Rabbit	WB	1:20000	Abcam
HIF-1a	36169S	Rabbit	WB	1:1000	Cell Signaling

Rat IgG2a, κ, FITC	553988	Rat	FACS	1:100	BD Biosciences
CD45 FITC	553080	Rat	FACS	1:100	BD Biosciences
CD11b V450	560455	Rat	FACS	1:100	BD Biosciences
CD90.2 APC	561974	Rat	FACS	1:100	BD Biosciences
CD 105 PE	130-102-548	Rat	FACS	1:100	Myltenyic Biotec
V450 IgG2b, κ	560457	Rat	FACS	1:100	BD Biosciences
APC Rat IgG2aκ	553932	Rat	FACS	1:100	BD Biosciences
PE rat IgG2aκ	557229	Rat	FACS	1:100	BD Biosciences
FITC CD326	11-5791-82	Rat	FACS	1:100	EBioscience
FITC Rat IgG2aκ	11-4321-80	Rat	FACS	1:100	EBioscience

3.1.1.2 Secondary Antibodies

Antigen	Product number	Host Type	Application	Dilution	Manufacturer
Alexa Fluor 555 Anti Mouse	A32727	Goat	IF	1:500	Invitrogen
Alexa Fluor 555 Anti Rabbit	A32732	Goat	IF	1:500	Invitrogen
Alexa Fluor 488 Anti Rabbit	A32731	Goat	IF	1:500	Invitrogen
Alexa Fluor 488 Anti Mouse		Goat	IF	1:500	Invitrogen
Anti-rabbit IgG-HRP	sc-2357	Mouse	WB	1:1000	Santa Cruz
m-IgGκ BP-HRP	sc-516102	-	WB	1:1000	Santa Cruz

3.1.2 Primers

3.1.2.1 Mouse primers

NCBI Gene Symbol	***Organism***	***Forward sequence***	***Reverse sequence***
Mcm2	Mouse	CTCAGA ATCAGGAGGTGAAGC	GCGGATACGTTGGTAG TTCTG
Hprt	Mouse	ATAGTGATAGATCCATT CCTATGACTG	TTCAACAATCAAGACAT TCTTTCCA
Wnt5a	Mouse	GACTCCGCAGCCCTGC TTTG	CCAATGGGCTTCTTCAT GGCGAG
Cdh1	Mouse	CCATCCTCGGAATCCTT GG	TTTGACCACCGTTCTCC TCC
Pdgfra	Mouse	AGGTATGTATCCACACA TGCGT	AGTTCCTGTTGGTTTCA TCTCG
Acta2	Mouse	GTCCCAGACATCAGGG AGTAA	TCGGATACTTCAGCGT CAGGA
Pcna	Mouse	TTTGAGGCACGCCTGA TCC	GGAGACGTGAGACGAG TCCAT
Gapdh	Mouse	AGGTCGGTGTGAACGG ATTTG	TGTAGACCATGTAGTTG AGGTCA
SFTPC1	Mouse	TGATGGAGAGTCCACC GGATTA	CCTACAATCACCACGA CAACGA
Spp1	Mouse	AGCAAGAAACTCTTCCA AGCAA	GTGAGATTCGTCAGATT CATCCG
Chek1	Mouse	GTTAAGCCACGAGAAT GTAGTGA	TTCAGGCATCCCTATGT CTGG
Chek2	Mouse	TGACAGTGCTTCCTGTT CACA	GAGCTGGACGAACCCT GATA
Trp53	Mouse	CTCTCCCCCGCAAAAG AAAAA	CGGAACATCTCGAAGC GTTTA
Xrcc1	Mouse	AGCCAGGACTCGACCC ATT	CCTTCTCCAACTGTAG GACCA
Apex1	Mouse	ACGGGGAAGAACCCAA GTC	GGTGAGGTTTTCTGAT CTGGAG
Neil1	Mouse	GTGGAGAGGAGGATTT TGCTG	TCCGGGATCACCCTGG AAC
Ogg1	Mouse	ACTTTCAGCTAGATGTC AGCCT	CACTCAGTGGGGTCTT GTCTC
Ungs1	Mouse	TTCGGGAAGCCGTACT TCG	CATCTGGGTCCATGTG AACAC
Cdkn2a	Mouse	CGCAGGTTCTTGGTCA CTGT	TGTTCACGAAAGCCAG AGCG

Cdkn1a	Mouse	ACATCTCAGGGCCGAAAACG	AAGACACACAGAGTGAGGGC
Mdm2	Mouse	GGATCTTGACGATGGCGTAAG	AGGCTGTAATCTTCCGAGTCC
Col41a	Mouse	TCCGGGAGAGATTGGTTTCC	CTGGCCTATAAGCCCTGGT
Gpx4	Mouse	GCCTGGATAAGTACAGGGGTT	CATGCAGATCGACTAGCTGAG
Gpst2	Mouse	TGAGCAACTATTCCAAACCAGC	GCACGTAGTCTTCGATCACTATC
Chac1	Mouse	ACTTATTGCGTTTGGCAGACT	TTCCTACGGCGTCCACAATG
Ddit3	Mouse	GGTCAGTTATCTTGAGCCTA	CTTCTGGAACACTCTCTCC
Ccne1	Mouse	GTGGCTCCGACCTTTCAGTC	CACAGTCTTGTCAATCTTGGCA
Cdk2	Mouse	ATGGAGAACTTCCAAAAGGTGG	CAGTCTCAGTGTCGAGCCG

3.1.2.2 Human primers

NCBI Gene Symbol	***Organism***	***Forward sequence***	***Reverse sequence***
Mcm2	Human	ATGATCGAGAGCATCGAGAACC	GCCAAGTCCTCATAGTTCACCA
Mcm7	Human	GCCTGTGGGAAATATCCCTCG	GTACCACCTGTCGGAACCC
Hprt	Human	AAGGACCCCACGAAGTGTTG	GGCTTTGTATTTTGCTTTTCCA
Wnt5a	Human	TCGACTATGGCTACCGCTTTG	CACTCTCGTAGGAGCCCTTG
Acta2	Human	TCAATGTCCCAGCCATGTAT	CAGCACGATGCCAGTTGT
Col41a	Human	GGGATGCTGTTGAAAGGTGAA	GGTGGTCCGGTAAATCCTGG
Gpx4	Human	GCCTGGATAAGTACAGGGGTT	CATGCAGATCGACTAGCTGAG
Gpst2	Human	TGAGCAACTATTCCAAACCAGC	GCACGTAGTCTTCGATCACTATC
Chac1	Human	ACTTATTGCGTTTGGCAGACT	TTCCTACGGCGTCCACAATG

3.1.3 Small interfering RNA (SiRNA)

SiRNA	Manufacturer	Product number
ON-TARGETplus Mouse Mcm2 siRNA	Horizon Discovery	L-062123-00-0005
ON-TARGETplus GAPD Control siRNA	Horizon Discovery	D-001830-02-05
ON-TARGETplus Non-targeting Control Pool (5 nmol)	Horizon Discovery	D-001810-10-05
DharmaFECT 1 Transfection Reagent	Horizon Discovery	T-2002-01
DharmaFECT 2 Transfection Reagent	Horizon Discovery	T-2002-01

3.1.4 Cell lines

Cell line	Species	Morphology	Catalog No	Company
IMR-90	Human	Lung embryonic fibroblast	CCL-186™	ATCC
EA.hy926	Human	Lung, Endothelial	CRL-2922™	ATCC
Hek293	Human	Kidney, Epithelial	CRL-1573™	ATCC
MLg [Mlg 2908]	Murine	Lung fibroblast	CCL-206™	ATCC
MLE-12	Murine	Epithelial	CRL-2110™	ATCC

3.1.5 Media formulations

Cell type	Culture Medium	Catalog Number	Manufacturer
CCL-206	DMEM F-12	11320033	ThermoFischer Scientific
	20% FBS	P30-3702	Pan Biotech
	100 U/mL Penicillin/Streptomycin	15140122	Gibco
IMR-90	DMEM F-12	11320033	ThermoFischer Scientific
	20% FBS	P30-3702	Pan Biotech
	100 U/mL Penicillin/Streptomycin	15140122	Gibco
EA.hy926	DMEM F-12	11320033	ThermoFischer Scientific
	10% FBS	P30-3702	Pan Biotech
	100 U/mL Penicillin/Streptomycin	15140122	Gibco
Hek293	DMEM F-12	11320033	ThermoFischer Scientific
	20% FBS	P30-3702	Pan Biotech
	100 U/mL Penicillin/Streptomycin	15140122	Gibco
MLE12	DMEM F-12	11320033	ThermoFischer Scientific
	10% FBS	P30-3702	Pan Biotech
	100 U/mL Penicillin/Streptomycin	15140122	Gibco
MFB	DMEM-1	11320033	ThermoFischer Scientific
	10% FBS	P30-3702	Pan Biotech
	100 U/mL Penicillin/Streptomycin	15140122	Gibco
EC	Endothelial cell growth medium	C-22110	PromoCell
Supplements:	0.02 ml / ml Fetal Calf Serum		
	0.004 ml / ml Endothelial Cell Growth Supplement		
	0.1 ng / ml Epidermal Growth Factor		
	1 ng / ml Basic Fibroblast Growth Factor		
	90 µg / ml Heparin		
	1 µg / ml Hydrocortisone		
AT2 cells	DMEM F-12	11320033	ThermoFischer Scientific
	5 µg/mL Insulin (I)	P07-03400	Pan Biotech

	10 µg/mL Transferrin (T)	P07-03400	Pan Biotech
	30nM Na-Selenite (S)	P07-03400	Pan Biotech
	10 mM HEPES-	H0887-100ML	Merck
	2mM L-Glutamine	25030149	Gibco
	2% FCS 10 mL (from PAA or other company)	P30-3702	Pan Biotech
	100 U/mL Penicillin/Streptomycin	15140122	Gibco
	Hydrocortisone 10nM	H0888-1G	Merck
	β-Estradiole 10nM	E2758-250MG	Merck

3.1.6 Reagents and chemicals

Reagent	Manufacturer
Dithiothreitol (DTT)	AppliChem, Darmstadt, Germany
DNase I	AppliChem AppliChem, Darmstadt, Germany
Ethanol	AppliChem AppliChem, Darmstadt, Germany
Isopropanol	AppliChem AppliChem, Darmstadt, Germany
Methanol	AppliChem AppliChem, Darmstadt, Germany
Non-fat dried milk powder	AppliChem AppliChem, Darmstadt, Germany
Random hexamers	Applied Biosystems, Life Technologies, Carlsbad, USA
Ripa Buffer	Life Technologies Darmstadt, Germany
NuPAGE® LDS Sample Buffer (4X	Life Technologies Darmstadt, Germany
NuPAGE® Reducing Agent (10X)	Life Technologies Darmstadt, Germany
NuPAGE® 4-12% Bis-Tris gels	Life Technologies Darmstadt, Germany
(Nitrocellulose/Filter Paper, catalog #LC2006, Life Technologies)	Life Technologies Darmstadt, Germany
Eosin G-solution 1% in water	Carl Roth, Karlsruhe, Germany
Hemalum solution acid acc. to Mayer	Carl Roth, Karlsruhe, Germany

3.1.7 Buffer formulations

Buffer	Formulation
Laemmli loading buffer (6x)	SDS 12% (w/v)
	Glycerol (87%) 60% (v/v)
	Bromophenol blue 0.06% (w/v)
	Tris/HCl, pH 6.8 375 mM
	DTT 600 mM
RIPA (Radio immunoprecipitation assay) buffer	Tris-Cl pH 7.4 50 mM
	NaCl 150 mM
	NP40 1% (v/v)
	Na-deoxycholate 0.25% (v/v)
TBS (Tris-buffered saline) (10x)	Tris/HCl pH 7.4 10 mM
	NaCl 150 mM
TBS-T (TBS with TWEEN®20)	TBS (10x) 10% (v/v)
	Tween®20 0.1% (v/v)
	Millipore-H2O 89.99% (v/v)
PBST washing buffer	NaCl 137 mM
	KCl 2.7 mM
	Na2HPO4 10 mM
	KH2PO4 2 mM
	Tween-20 1 % (v/v)
1X BSA (Bovine Serum Albumin)	Bovine serum albumin-5g
	20% Triton X-100-2.5ml
	10X PBS-50ml
5% Milk Blocking Solution	5 gm Skim Milk powder/100ml
	1X TBS-T
PBS (Phosphatate buffered saline) pH 7.4	NaCl 1.37 M
	KCl 27 mM
	Na2HPO4 100 mM
	KH2PO4 20 mM
	NaCl 1.37 M

3.1.8 Kits

Kit	Catalog Number	Manufacturer
H2A.X Phosphorylation Assay Kit	17-327	Merck
Cell proliferation ELISA (BrdU assay)	11647229001	Merck
CellTiter-Glo® Luminescent Cell Viability Assay	G7570	Promega
OxiSelect™ In Vitro ROS/RNS Assay Kit	STA-347	cell biolabs
TUNEL Assay Kit - BrdU-Red (ab66110)	ab66110	Abcam
QCM Chemotaxis Cell Migration Assay, 24-well (8 µm), colorimetric	ECM508	Merck
Pierce™ BCA Protein Assay Kit	23227	Thermofisher
Caspase-Glo® 3/7 Assay System	G8090	Promega

3.1.9 Consumables

Consumable	Manufacturer
96-well imaging plates, Falcon®	Corning, Thermo Fisher Scientific, Schwerte, Germany
Amicon Ultra 3K-0.5 mL centrifugal filters	Merck Millipore, Darmstadt, Germany
Cell culture dishes	Corning, Thermo Fisher Scientific, Schwerte, Germany
Cell culture multi-well plates	TPP Techno Plastic Producers, Trasadingen, Switzerland
Combitips advanced®	Eppendorf , Hamburg, Germany
Cryovials 1.5 ml	Greiner Bio- One, Frickenhausen, Germany
Falcon Tube (15 ml, 50 ml)	Corning, Thermo Fisher Scientific, Schwerte, Germany
Falcon 12 x 75 mm Tube with Cell Strainer Cap	Corning, Thermo Fisher Scientific, Schwerte, Germany
Falcon cell strainers	Corning, Thermo Fisher Scientific, Schwerte, Germany
Filter Tips	Biozym Scientific, Hessisch Oldendorf, Germany
Glas Pasteur pipettes	VWR International, Darmstadt, Germany
Westerblot Running gels	Thermo Fisher Scientific, Darmstadt, Germany
Measuring pipettes, sterile, single use (5 ml, 10 ml, 25 ml, 50 ml)	VWR International, Darmstadt, Germany
Microscope slides	Thermo Fisher Scientific, Darmstadt, Germany
Nalgene cryogenic tubes	Thermo Fischer Scientific, Waltham, MA
Nitrocellulose 40 um membranes	Thermo Fisher Scientific, Darmstadt, Germany
PCR plates, 96-well plate	Kisker Biotech, Steinfurt, Germany
Protein LoBind Tubes (1.5 ml)	Eppendorf, Hamburg, Germany
Reaction tubes (0.5 ml, 1.5 ml, 2 ml)	Eppendorf, Hamburg, Germany
Reagent reservoirs, 50 mL	Corning, New York, USA
Sealing foils for PCR plates	Kisker Biotech, Steinfurt, Germany
Sterican cannulas	BD Biosciences, Heidelberg, Germany
Syringes	Neolab, Heidelberg, Germany
ThincertTM 6-well cell culture inserts (pore Ø 8µm)	Greiner Bio- One, Frickenhausen, Germany
Tips	Eppendorf, Hamburg, Germany
white 96-well microplates	Berthold Technologies, Bad Wildbad, Germany

3.1.10 Laboratory equipment and software

-20°C freezer MediLine LGex 410	Liebherr, Biberach, Germany
2100 Antigen Retriever	Aptum Biologics, Southamptom, U.K.
-80°C freezer U570 HEF	New Brunswick, Hamburg, Germany
Aerosolizer, micro sprayer	IA-1C, Penn-Century, Wyndmoor, PA
Analytical scale XS20S Dual Range	Mettler Toledo, Gießen, Germany
Autoclave DX-45	Systec, Wettenberg, Germany
Autoclave VX-120	Systec, Wettenberg, Germany
Axiovert 40C microscope	Zeiss, Jena, Germany
Cell culture work bench Herasafe KS180	Thermo Fisher Scientific, Darmstadt, Germany
Centrifuge MiniSpin plus	Eppendorf, Hamburg, Germany
Centrifuge Rotina 420R	Hettich, Tuttlingen, Germany
Centrifuge with cooling, Micro200R	Hettich, Tuttlingen, Germany
CO2 cell Incubator BBD6620	Thermo Fisher Scientific, Darmstadt, Germany
Confocal microscope LSM 710	Zeiss, Jena, Germany
Corning® LSE™ Mini Microcentrifuge, 120V	Corning, Wiesbaden, Germany
Demineralized water	Thermo Fisher Scientific, Darmstadt, Germany
Dry ice container Forma 8600 Series, 8701	Thermo Fisher Scientific, Darmstadt, Germany
Electronic pipet filler	Eppendorf, Hamburg, Germany
Film developer Curix 60	AGFA, Morsel, Belgium
Fisher Science Education™ 4-Way Microtube Racks	Thermo Fisher Scientific, Darmstadt, Germany
Fridge MediLine LKv 3912	Liebherr, Biberach, Germany
Gel imagine system ChemiDoc XRS+	Biorad, Hercules, USA
Ice machine ZBE 110-35	Ziegra, Hannover, Germany
Light Cycler LC480II	Roche Diagnostic, Mannheim, Germany
Liquid nitrogen cell tank BioSafe 420SC	Cryotherm, Kirchen/Sieg, Germany
LSR II	BD Biosciences, NJ, USA
Magnetic stirrer KMO 2 basic	IKA, Staufen, Germany
Mastercycler Nexus	Eppendorf, Hamburg, Germany
Microdismembrator	Sartorius, Göttingen, Germany
Microm HMS740 Robot-Stainer	Thermo Fisher Scientific, Darmstadt, Germany
Multipette stream	Eppendorf, Hamburg, Germany
Nalgene® Freezing Container (Mr. Frosty)	Omnilab, Munich, Germany
NanoDrop 1000	PeqLab, Erlangen, Germany
pH meter InoLab pH 720	WTW, Weilheim, Germany
Pipettes Research Plus	Eppendorf, Hamburg, Germany
Plate centrifuge 5430	Eppendorf, Hamburg, Germany
Plate reader Sunrise	Tecan, Crailsheim, Germany
Plate reader TriStar LB941	Berthold Technologies, Bad Wildbach, Germany
Power Supply Power Pac HC	Biorad, Hercules, USA
Roll mixer	VWR International, Darmstadt, Germany
Scale XS400 2S	Mettler Toledo, Gießen, Germany
Shaker Duomax 1030	Heidolph, Schwabach, Germany
Syringe pump	AL-1000, World precision instruments, USA
Thermomixer compact	Eppendorf, Hamburg, Germany
Ultra-pure water supply MilliQ Advantage A10	Merck Millipore, Darmstadt, Germany
Vibratome	Hyrax V55, Zeiss, Jena, Germany
Vortex Mixer	IKA, Staufen, Germany
VWR® Tube Rotator and Rotisseries	VWR International, Darmstadt, Germany
Water bath Aqua Line AL 12	Lauda, Lauda-Königshofen, Germany

3.2 Methods

3.2.1 *In vitro* methods

3.2.1.1 Cell isolation from neonatal mouse lungs

3.2.1.1.1 Murine lung endothelial cell (EC) isolation

Mouse lung endothelial cells were isolated using magnetic-activated cell separation (MACS, Miltenyi Biotec, Bergisch Gladbach, Germany). In brief, following injection with a lethal dose of pentobarbital, lungs from twelve 5–7-day-old male neonatal mice were harvested. After flushing the lungs thoroughly with 1X PBS via the right ventricle, the thorax was dissected, and the lungs were removed. The lung lobes were dissected and placed in a 12-well plate in ice-cold 1X PBS. In a petri dish, the whole lung was minced 1-2 mm pieces using scissors, and then digested in 3 mg/ml Collagenase I in HBSS for 45 min at 37°C and 220 rpm in an Eppendorf thermomixer (Eppendorf, Hamburg, Germany). Thereafter, the digested tissue was filtered through a 70 µm cell strainer. Then, the cells were spun down and incubated with 40 µl of anti-mouse CD31-conjugated dynabeads (BD Biosciences, # 55370) in Buffer A (50 mL of 0.1% BSA + 100 µl of 0.5 M EDTA) for a total volume of 2 mL per tube and incubated for 10 mins at room temperature while on a shaker. Then the tubes were placed in the magnet for 1 minute. Afterwards, the buffer and contaminating cells were discarded. This procedure was repeated four times. After the 4th wash, the ECs were resuspended in EC media (PromoCell, Heidelberg, Germany) and seeded at high density on a 0.2% gelatin-coated plate. A sample was obtained to test the purity of the population by flow cytometry (3.3.4). The isolation of these cells was performed by Dr. Tina Pritzke. Former member of Dr. Anne Hilgendorff's group.

3.2.1.1.2 Murine lung fibroblast isolation

Following injection with a lethal dose of pentobarbital, lungs from twelve 5–7-day-old male neonatal mice were harvested. After flushing the lungs thoroughly with 1X PBS via the right ventricle, the sternum was excised, and the lungs were removed. The lung lobes were placed in a 12-well plate in ice-cold 1X PBS. In a

petri dish, the lung was cut into 1 mm pieces using a scalpel and distributed along the surface of the dish with 500 uL of PBS. Afterward, the dishes were left to dry out at 37°C for about 10-15 minutes. Once the tissue pieces had attached to the dish's surface, 8 mL of DMEM-1 medium (Gibco, Darmstadt, Germany) supplemented with 10% fetal bovine serum (FBS), 1% Penicillin Streptomycin, and 1% Gentamicin (Gibco, Darmstadt, Germany) was gently added. Two to three days later, the medium and floating tissue pieces were discarded, and 10 mL of fresh medium was added. On day 7, the remaining tissue pieces were discarded, and 10 mL of fresh supplemented DMEM-1 medium was added. Before the start of the experiments, the cells were characterized by flow cytometry. Experiments were started once the cells reached 70 - 80% confluency. A sample was obtained to test the purity of the population by flow cytometry.

3.2.1.1.3 Murine alveolar epithelial cell isolation

Alveolar type 2 cells (AT2 cells, $CD45^-$ / $CD31^-$/ Pro-SPC^+), and endothelial cells (ECs, $CD45^-$/ $CD31^+$) were separated by magnetic-activated cell separation (MACS, Miltenyi Biotec, Bergisch Gladbach, Germany). *The isolation of these cells was performed by Dr. Tina Pritzke, former member of Dr. Anne Hulgendorff's group.* Mouse lung endothelial cells were isolated using magnetic-activated cell separation (MACS, Miltenyi Biotec, Bergisch Gladbach, Germany). In brief, following injection with a lethal dose of pentobarbital, lungs from twelve 5–7-day-old male neonatal mice were harvested. After flushing the lungs (until almost white) with 1X PBS via the right ventricle, the thorax was cleaned, and the lungs were removed. The lung lobes were dissected and placed in a 6-well plate in ice-cold 1X PBS. In a petri dish (Corning #430167, Tewksbury MA, USA), the whole lung was minced 1-2 mm pieces using scissors, and then digested in 3 mg/ml Collagenase I in HBSS for 45 min at 37°C and 220 rpm in an Eppendorf thermomixer (Eppendorf, Hamburg, Germany). Thereafter, the digested tissue was filtered through a 70 µm cell strainer. Then, 10 µl of murine C45(Miltenyi Biotec #130-052-301) and 10 µl of murine CD31 MicroBeads (Miltenyi Biotec #130-097-418) per 10^7 total cells in Buffer A (50 mL of 0.1% BSA + 100 µl of 0.5 M EDTA) for a total volume of 2 mL per tube and incubated for 15 mins at room temperature while on a shaker. Then the tubes were placed in the magnet for 1 minute. After collecting the flowthrough, the buffer and contaminating cells were discarded. This procedure was repeated four times. After the 4th wash, the

isolated cells were resuspended in 10% FBS and seeded at high density on a plate in order to get rid of contaminating fibroblasts. After 45 minutes, the solution was collected and seeded on coated 24-well plates at a density of 5 x 10^5 / well. A sample was obtained to test the purity of the population by flow cytometry (3.2.1.2). *The isolation of these cells was performed by Dr. Tina Pritzke. Former member of Dr. Anne Hilgendorff's group.*

3.2.1.2 Flow cytometry analysis

To test the purity of the isolated cell populations (done by Dr. Tina Pritzke), flow cytometry was used using these panels:

Fibroblasts:

CD45 FITC

CD11b V450

CD90.2 APC

CD 105 PE

Epithelial cells:

CD90.2 APC

CD326 FITC

Endothelial cells:

CD45 FITC

CD31 FITC

In Annex A, **Fig A1**. shows clustering by cell type of the cells including in the RNA-sequencing analysis.

3.2.1.3 Mammalian cell cryopreservation and thawing

3.2.1.3.1 Cryopreservation

To prepare cells for cryopreservation, first, the medium was discarded, then the flasks/ dishes were washed with 1X PBS, followed by trypsinization with pre-warmed 0.25% trypsin-EDTA (Gibco) solution for 5 minutes at 37°C. Fresh complete medium was added once the cells were detached from the surface of dishes/flasks. Next, the cells were centrifuge at 450 rpm for 5 minutes. The trypsin-containing media was aspirated out and the pellet suspended in a freezing medium (90% FBS + 10% DMSO). The cell suspensions at a concentration of 1-

$2x10^6$ cells/ml were transferred to cryovials and frozen in a Mister Frosty (Omnilab) for 24 hours at -80°C. For long-term storage, the cells were kept in liquid nitrogen at -195°C.

3.2.1.3.2 Thawing of cells

After thawing the frozen cell suspension in a water bath at 37°C, the cell suspension was diluted with 1 ml prewarmed DMEM F-12 media supplemented with 100 U/ml of penicillin/streptomycin and 20% FBS and transferred to a 15 ml falcon containing 8 ml of fresh FBS-supplemented DMEM F-12 medium. After a 5-minute centrifugation, the supernatant was discarded, and the cell pellet was resuspended in 7 mL of fresh 20% FBS and antibiotic containing DMEM-F12 medium. The cell suspension was seeded in a 10 cm sterile cell culture dish and cultured under standard cell culture conditions at 37°C and 5%CO_2.

3.2.1.4 Cell culture treatments

3.2.1.4.1 Etoposide treatment

To induce DNA damage, IMR-90 fibroblasts were treated overnight with 25 nM of Etoposide (Thermofisher, #11496321).

3.2.1.4.2 Hyperoxia exposure

Platted cells were exposed to FiO_2 =0.4 for 24 hours in a C-Chamber fitted with a ProOx 110 oxygen controller (Biospherix, Parish, NY).

3.2.1.4.3 Cyclical stretch

The cultured cells were seeded in six-well plates and exposed to stretch under the following conditions: shape/sine; elongation min 0%, max 8%; frequency 2Hz; duty cycle 50%; cycles 43216 for 24 h. This experiment was performed by Dr. Tina Pritzke (a former member of the group)

3.2.1.5 Assessment of DNA damage

3.2.1.5.1 TUNEL assay

The TUNEL assay detects DNA fragmentation. Following the manufacturer's instructions, the cells were fixed with formaldehyde for 15 minutes. The cells were then incubated for 10 min in 0.3% Triton-X-100 solution at RT, followed by re-fixation with formaldehyde. After one 1XPBS wash and one wash with the wash buffer included in the kit, the slides were incubated in a humidification chamber

with DNA labeling solution for 60 min at 37ºC. For one test, the DNA labeling solution contained 10 µL of TdT Reaction Buffer, 0.75 µL of TdT Enzyme, 8 µL of Br-dUTP, and 32.35 µL of ddH_2O for a total volume of 51 µL. Thereafter, the slides were washed twice for 5 min with 1xPBS followed by 30 min incubation at RT with the antibody solution (for 1 test, 5 µL of Anti-BrdU-Red antibody, and 95 µL of Rinse buffer). After one 5-min wash with ddH_2O, counterstaining was done with DAPI (1:1000) for 5 mins, followed by one 1XPBS wash. Finally, a drop of anti-fading solution (Dako) was added to the slide and then covered with a glass coverslip. The slides were analyzed with an Axiovert 40C microscope at an Ex/Em = 488/576 nm (BrU-Red).

3.2.1.5.2 Histone Family member X Phosphorylation

The H2A.X Phosphorylation, Chemiluminescence Detection Assay Kit is a cell-based ELISA formatted for chemiluminescent detection of relative levels of phosphorylated H2A.X in microplate cell cultures. Following manufacturer's instructions, briefly, cells were cultured in 96-well plates, and following experimental treatments, fixed 100 µL/well of 95% EtOH 5% acetic acid fixing agent followed by 100 µL/well of 1% formaldehyde in TBS. After three washes, 100 µL/well of Quenching Buffer were added followed by 1 hr incubation at 37°C with 100 µL/well Blocking Buffer (3% BSA in TBS). After washing three times, 100 µL of Primary Antibody Solution (1:8000 dilution of Primary Antibody in Blocking Buffer) were added to each well. Last, 100 µL/well of the Detection Antibody solution (1:500 dilution of Detection Antibody by diluting 20 µL Goat Anti-Mouse HRP (Catalog #2003482) in 10 ml of Blocking Buffer). For Luminescence detection, 8 mL 1:1 (v/v) mixture of LumiGLO™ Chemiluminescent Substrate Reagent A (Catalog #20-212C) and LumiGLO™ Chemiluminescent Substrate Reagent B (Catalog #20-212D) were prepared. Last, 75 µL/well of prepared LumiGLO™ substrate was added to each well before

reading in a microplate Luminometer (The GloMax® Discover System from Promega).

3.2.1.6 **Functional assays**

3.2.1.6.1 Cell Titer Glo assay

The assay was performed following the protocol of the manufacturer (Promega). Briefly, cells were seeded in 96-well imaging plates at a density of 10000 – 15000 cells/100 µl. After cell treatment, 100 µl of Cell-titer Glo® Reagent mix and incubated at room temperature for 10 minutes. The signal was detected on the GloMax® Explorer Multimode Microplate Reader (Promega) following the plate reader's built-in program.

3.2.1.6.2 BrdU proliferation assay

Cells were cultured in 96-well plates and treated with hyperoxia for 24 hours before the assay was started. The BrdU proliferation assay kit from Roche was used (Cat. No. 11647229001, Roche Diagnostics GmbH, Mannheim, Germany). As per the manufacturer's instructions, 10 µl/well BrdU labeling solution was added for a final concentration of 10 µM BrdU followed by 24 hr incubation at 37°C. After discarding the medium, the cells were fixed with FixDenat (provided by the kit) and incubated at room temperature for 30 min. Thereafter, 100 µl/well Anti-BrdU-POD working solution was added followed by a 90-min incubation at room temperature. After washing three times with 1X PBS, 100 µL of Substrate solution was added per well and incubated for 30 min at room temperature. 25 µl 1 M H2SO4 Stop solution was added to each well and mixed thoroughly for 1 min. The absorbance of the plate was then measured at a test wavelength of 450 nm and a reference wavelength of 690 nm using a Sunrise TM plate (Tecan).

3.2.1.6.3 Caspase glo 3/7 Assay

The assay was performed following the protocol of the manufacturer (Promega). Briefly, cells were seeded in 96-well imaging plates at a density of 10000 – 15000 cells/100 µl. After cell treatment, 100 µl of Caspase-Glo® 3/7 Reagent and incubated at room temperature for 30 minutes. The signal was detected on the

GloMax® Explorer Multimode Microplate Reader (Promega) following the plate reader's built-in program.

3.2.1.6.4 Boyden Chamber migration assay

The Boyden Chamber migration assay (Merck Chemicals GmbH) was performed following the manufacturer's instructions. Briefly, fibroblasts were seeded in an 8 mm pore size polycarbonate membrane and allowed to migrate for 24 hr. 10% FBS was used as chemoattractant. Negative controls were done in FBS-free medium. After 24 hr of migration, cells that had migrated through the polycarbonate membrane were incubated with Cell Stain Solution, then subsequently extracted and detected on a Sunrise TM plate (Tecan) at a 560 nm wavelength.

3.2.1.7 **Preparation of cells for immunofluorescence analysis**

Cells were plated in a density of $1x10^5$ cells/well in 6-well plates in DMEM-F12 media supplemented with 20%FBS and 100 U/ml penicillin-streptomycin. The cells were kept in the incubator for 24 hrs to allow cell attachment and growth under standard cell culture conditions of 37°C and 5% CO2. Following the experimental treatments, the cells were trypsinized with 0.5 mL of 0.25% Trypsin (Gibco, Darmstad, Germany) per well and collected in fresh medium. Then, > 30000 cells/100 µl were pipeted into cytofunnels attached to a filter card, slide and slide clip, and centrifuged for 20 min at 450 rpm in a Shandon Cytospin 4 centrifuge (Thermo Fisher Scientific, Runcorn, UK). Then, the cells were fixed the next day with 4% PFA for 30 minutes at RT. The same day, the fixed cells were used for immunofluorescence staining.

3.2.2 Analytical assays

3.2.2.1 Protein isolation from cells in 2D cell culture

Cells cultured in standard 6-well dishes were washed twice with sterile 1X PBS and then trypsinized with 0.25% Trypsin or scraped with a cell scratcher in 150-400 µl of lysis buffer containing RIPA buffer enriched with Halt protease inhibitor

cocktail (Thermo Fisher Scientific). When trypsinized, complete medium was added to the mix and then the cells were centrifuged at 450 rpm for 5 minutes at 4°C. After discarding the supernatant, enriched RIPA buffer (as described above) was added. The collected cell lysates were carefully mixed by pipetting up and down and vortexing. Then, the lysates were transferred to an Eppendorf placed on ice and incubated for 45 minutes. Subsequently, the lysates were centrifuged at 15,000 RPM for 10 min at 4°C to separate the supernatant (total protein) and the pellet (cell debris). Last, cell supernatants were pipetted into LoBind Eppendorf tubes, and stored at -80°C for long-term storage.

3.2.2.2 RNA extraction from cells in 2D cell culture

RNA extraction from cells in 2D culture was done following the RNAeasy mini plus kit protocol from Qiagen. For mRNA isolation, two wells from a six-well plated were pulled and 600 µl of RLT Lysis buffer (Qiagen) supplemented with 10 µl β-ME/mL was added and incubated at room temperature for 5 minutes followed by vortexing for 30 seconds. After, the samples were first loaded into gDNA eliminator columns and spun down. The flowthrough was then mixed with 70% ethanol. After this, the samples were loaded into RNeasy spin columns. In subsequent steps, the samples were washed 1X with 700 µl RW1 buffer, 2X with 500 µl of RPE buffer, and then eluted in 35 µl of RNAse-free distilled water. The concentration of the isolated RNA was noted spectrophotometrically at a wavelength of 260 nm with the Nano-Drop 1000.

3.2.2.3 RNA-sequencing analysis

Bulk RNA-sequencing analysis was done by the Cologne Center for Genomics (CCG) using the Illumina TruSeq stranded platform. RNA extraction was done as described in *3.2.2.2*. Samples containing 2µg total RNA at a concentration range of 50–200ng/µL, solved in nuclease-free water were used for the analysis.

3.2.2.4 siRNA transfection (Mcm2 knockdown)

Mouse siRNAs used for all experiments were purchased from Horizon Discovery (Cambridge, UK) as lyophilized products, and were diluted in 1XsiRNA buffer. Following the manufacturer’s protocol for siRNA resuspension, a stock of 20µM

was made by diluting 5 nmole in 250 µl of 1XsiRNA buffer followed by 30 min room temperature incubation in an orbital shaker. Once resuspended, the stock was aliquoted and stored at -20°C or at 4°C if used within the next 6 weeks. For a 6-well plate format, the transfection mix per well was prepared by formulation of tube 1 and 2 as follows:

Solution	Reagent	Volume (µl)
Tube 1	5 µM siRNA stock	6 (CCL-206); 4 (MLE12)
	OptiMem serum-free medium	194 (CCL-206); 196 (MLE12)
Tube 2	Volume of DharmaFECT reagent 1 (µL)	10
	OptiMem serum-free medium	190
Well	Complete antibiotic-free DMEM F-12 medium	1600

Table 3.2.1: Reagents and corresponding volumes needed for each of the tube preparations in the siRNA transfection mix

At first, solutions in Tube 1 and 2 were prepared separately and incubated for 5 mins at room temperature inside the cell culture hood. Then, both solutions were pooled together in one Eppendorf and incubated for 20 mins at room temperature. Cells were seeded 48 hours before transfection at a density of $1x10^5$ in 2 ml media (DMEM, 20%FBS without penicillin/streptomycin) per well of a 6-well plate. Before transfection, the medium was aspirated, and the wells were washed with 1XPBS. Then, 400 µl of the transfection mix was added to each well along with 1600 µl of antibiotics-free cell culture medium and mixed with the 2ml of cell suspension. Three controls were included in each experiment: non-targeting control (NTC), Positive control (Gapdh siRNA), and sham (vehicle only). The NTC and positive controls were generated at a final concentration of 25 nM by adding 10 µl of the 5 µM stock to 190 µl OptiMem serum-free medium and mixing it with the solution in Tube 2 as mentioned above. The sham control was generated by adding 10 µl of 1xsiRNA Buffer with 190 µl of OptiMem serum-free medium and mixing with the solution in Tube 2 (Table 3.2.1). After 18 hr following transfection,

the medium was replaced with complete, siRNA-free, antibiotic-free medium. 24 hr (CCL-206) or 48 hr (MLE-12) after transfection the cells were collected for RNA or protein analysis. To assess the efficiency of the transfection, the mRNA expression of Gapdh in the positive control was compared to the expression of Gapdh in the NTC. Gene expression in all samples was compared to that of the NTC.

3.3 Animal experiments

3.3.1 Hyperoxia treatment

3.3.1.1 Short-term hyperoxia exposure

Five to seven-day-old, C57BL/6 wild type (WT) mice born at term gestation [3.6±0.3 g body weight (bw)] were randomized into two groups (n = 6-8 mice/group). Mice were exposed to oxygen (fiO_2 = 0.4) using the A-Chamber (Oxygen controller ProOx110, Biospherix, Parish, NY) or received room air only (RA; fiO_2 = 0.21) for either 2 hours, 8 hours, or 24 hours (short-term experiments).

3.3.1.2 Long-term experiments

A group of animals was exposed to hyperoxia ($fiO_2$0.4) for 8h on day 5-7 of life before returning to room air. Lungs were harvested at the age of 3 weeks, five weeks, or 18 months and snap-frozen or fixed in PFA for histologic analysis. All surgical and animal care procedures were reviewed and approved by the Institutional Animal Care and Use Committee (Animal Care Committee, Government of Bavaria, #17-10 and #ROB-55.2-2532.Vet_02-19-105).

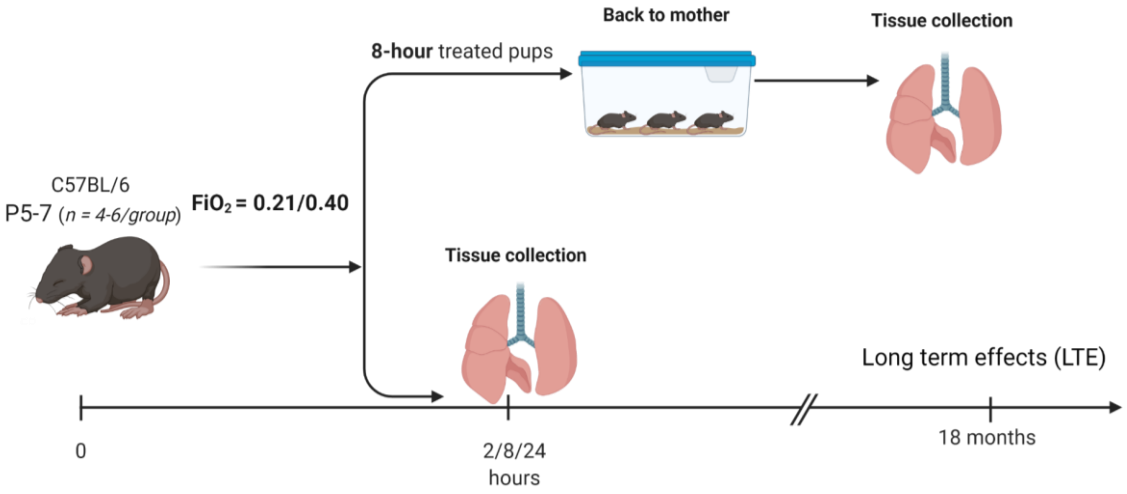

Fig 3.3.1: *In vivo* experimental design.
This figure was created in www.Biorender.com

3.3.2 Double-hit animal models

Double hit experiments were performed under the Institutional Animal Care and Use Committee (Animal Care Committee, Government of Bavaria, #ROB-55.2-2532.Vet_02-19-105) in collaboration with the laboratory of Dr. Heiko Adler and his doctoral candidate, Anna Dmitrieva at the Helmholtz Zentrum Munich. Mice were treated with hyperoxia/room air and/or infection with the murine gammaherpesvirus 68 wild-type virus.

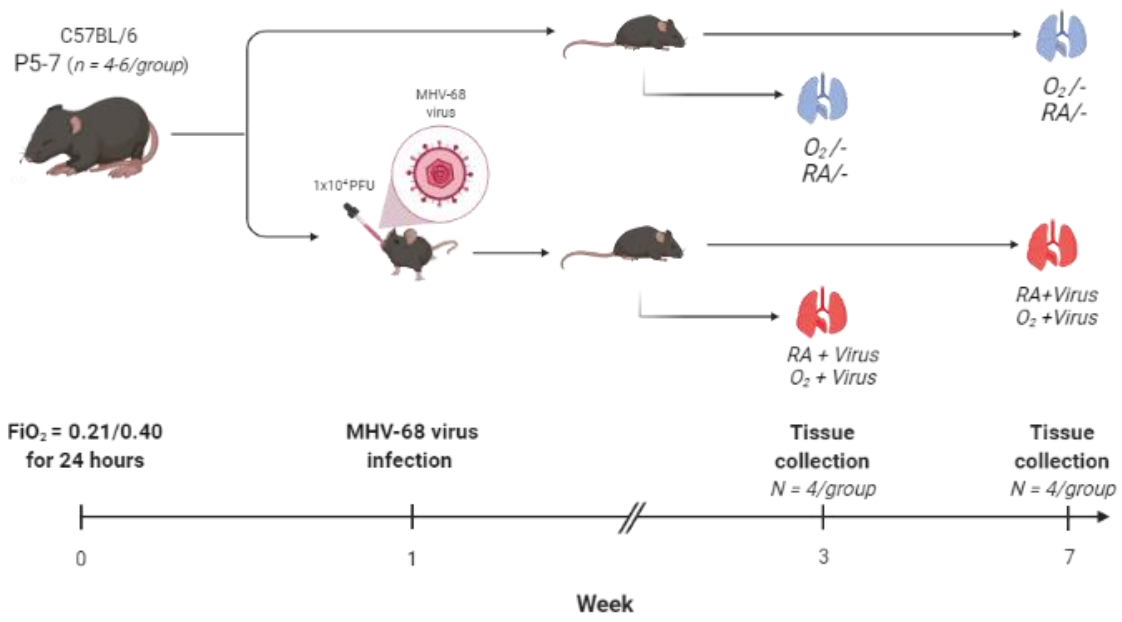

Fig 3.3.2: Double-hit model experimental design

Mice pups at PND5-7 were treated with FiO_2 = 0.4 / 0.21 for 24 hour and allowed to recover for 8 days before intranasal inoculation with the MHV-68 herpes virus. Lungs were harvested from 4-6 mice 10 days post-infection or 28 days post-infection.

P5-7: postnatal day 5 to 7. Vi: MHV-68 virus infection. MHV-68: gammaherpesvirus 68

3.3.2.1 Virus stock preparation

The original stock of MHV-68 (clone G2.4) was obtained from J. Stewart and A. Nash (University of Edinburgh, Edinburgh, United Kingdom) (1). Working stocks of virus were prepared on BHK-21 cells (ATCC CCL10; kindly provided by J. Stewart and A. Nash). The BHK-21 cells were infected by the MHV-68 virus at a 0.1 multiplicity of infection (MOI), after three days of culturing cells were frozen and thawed two times to complete the cytopathic effect (CPE). Cellular debris was removed by centrifugation, and the supernatants were stored in aliquots at −80°C. Plaque assay was performed to determine the virus titer, quality of the virus was checked by the DNA extraction, PCR amplification, and agarose gel electrophoresis.

3.3.2.2 Plaque assay (quantification of MHV-68 with the plaque-based assay)

The plaque assay was performed as described previously by (Stewart et al., 2004). In brief, for the determination of virus concentration, BHK-21 cells were

plated at a defined concentration of 5 x 10^4 cells per well in 24-well plates (Corning, Germany), 24 h before the titration. Moreover, one day before the titration, the overlay medium was made: methylcellulose (Sigma Aldrich, Germany) was dissolved in the culturing medium and stored at +4˚C. The virus aliquot was diluted in the cell culture medium (10^{-1} – 10^{-8}). The culture medium of the BHK-21 cells was removed and 900 µl of the infectious medium was added and incubated for 90 min at 37˚C. Consistently, the infectious medium was removed, a pre-warmed overlay medium was added, and the plates were incubated for 5 days at 37˚C. After the incubation period, the overlay medium was removed, and the adherent cell layer was stained with 0.1% crystal violet staining solution. For the analysis of the plaque assay, the plaques per well were determined under the microscope. The formula for the exact quantification of the virus titer was applied as follows:

PFU/ml = 1.1 x Dilution x number of the plaques

PFU/ml (plaque-forming unit) is the unit in which the virus is indicated. Factor 1.1 adjusts the volume according to the inserted 900 µl of infectious suspension. Refer to Annex A, **Fig A2**. for a detailed infection curve according to time points in female and male mice infected with the MHV-68 herpes virus.

3.3.2.3 Mice infection

Mice were anesthetized prior to infection with 2.5 µl/g of an antagonizable anesthetic containing 1 mg/ml Medetomidine, 5 mg/ml Midazolam, and 0.05 mg/ml Fentanyl. All mice were infected intranasally with (1x10^4 PFU) in 10 µl of PBS. After infection, the anesthesia was antagonized with 8.5 µl/g of the corresponding receptor antagonist (5 mg/ml Antipamezole, 0.1 mg/ml Flumazenil and 0.4 mg/ml Naloxone). Mice were killed and analyzed after 3-, 6-, 10- or 28-days post-infection.

3.3.2.4 Lung harvesting

The animals were killed at defined time points post-infection via cervical dislocation. The lungs were dissected and then transferred to sterile Eppendorf tubes and stored at -80˚C.

3.3.3 Lung fixation and paraffin embedding

Lungs were fixed intratracheally with 4% buffered PFA at 20 cmH_2O followed by measurements of lung volume.

3.3.4 Immunofluorescence staining of paraffin-embedded tissue sections

Formalin-fixed paraffin-embedded (FFPE) lung tissue sections from hyperoxia-treated mice and controls, and hyperoxia and virus-treated mice and controls were first placed in an incubator at 60°C for an hour followed by a tissue deparaffinization process. In serial steps, the slides containing the tissue sections were incubated 2x in Xylene for 5 minutes each, followed by 100%, 90%, 80%, 70% ethanol incubations 2 minutes each, followed by a 5-minute incubation in 1xPBS. The antigen retrieval was done by submerging the slides in citrate buffer p.H 6.0 at 95°C for 15 minutes. After washing steps, the tissue slides were permeabilized with 0.3% Triton-X-100 solution at room temperature for 10 minutes. Incubation with 5% BSA in PBS for 1 hour at room temperature was used to block the tissue sections. Subsequently, staining with primary antibodies was performed overnight at 4°C in a humidization chamber. The next day, two 10-minute washes with 1X PBS, were followed by 2-hour room temperature secondary incubation with fluorescence-labeled antibodies under humid conditions. After washing three times with 1X PBS, incubation with DAPI for 1 hour at room temperature was used to counterstain. Finally, the tissue slides were mounted using anti-fading mounting medium (Dako). The slides were stored at 4°C until further analysis.

3.3.5 TUNEL assay in lung tissue

Following the manufacturer's instructions, the tissues were fixed with formaldehyde, deparaffinized, and rehydrated if paraffin sections (as described in 3.3.7), followed by 5 min incubation with 0.85% NaCl, and two 5 min washes with 1XPBS. The tissues were then incubated for 10 min in 0.3% Triton-X-100 solution at RT, followed by re-fixation with formaldehyde. After one 1XPBS wash and one wash with the wash buffer included in the kit, the slides were incubated

in a humidification chamber with DNA labeling solution for 60 min at 37ºC. For one test, the DNA labeling solution contained 10 µL of TdT Reaction Buffer, 0.75 µL of TdT Enzyme, 8 µL of Br-dUTP, and 32.35 µL of ddH_2O for a total volume of 51 µL. Thereafter, the slides were washed twice for 5 min with 1xPBS followed by 30 min incubation at RT with the antibody solution (for 1 test, 5 µL of Anti-BrdU-Red antibody, and 95 µL of Rinse buffer). After one 5-min wash with ddH_2O, counterstaining was done with DAPI (1:1000) for 5 mins, followed by one 1XPBS wash. Finally, a drop of anti-fading solution (Dako) was added to the slide and then covered with a glass coverslip. The slides were analyzed with an Axiovert 40C microscope at an Ex/Em = 488/576 nm (BrU-Red).

3.3.6 Haematoxylin Eosin staining

Mouse lung slides were deparaffinized following the protocol described in 3.38. Thereafter, the slides were stained with Hematoxylin Mayer for 10 minutes. After rinsing with tap water, the slides were submerged in a 1% Eosin solution (Carl Roth) for 1 minute and then washed in VE water. Then, the slides were dehydrated under the following conditions: 80% ethanol, 90 %ethanol, 100% ethanol, Xylene (5 min), (5 min) 7. Coverslips were mounted using a Xylol-based Fast Mounting Medium (Biosystems).

After isotropic uniform random (IUR) sectioning (Scherle, 1970), alveolar area, number of incomplete and complete alveolar walls (septal density), and radial alveolar counts (≥ 30 fields of view; 400X magnification) were quantitatively assessed in 2-3 independent random 4 µm H&E tissue sections per animal (CAST-Grid 2.1.5; Olympus) (Emery & Mithal, 1960).

3.3.7 Lung tissue homogenization

For the homogenization of lung samples, the organs were transferred into specific sterile homogenization tubes containing a small ceramic bullet and 350 µl of the lysis buffer (RLT plus buffer for RNA isolation) or 500 µl of the RIPA buffer (protein isolation). The homogenization was carried out using the FastPrep-24 instrument (MP Biomedicals) with the following settings: lung samples were homogenized once at 4 m/s for 20 sec. Homogenates were directly proceeding to the RNA or protein extraction.

3.3.8 Protein analysis

3.3.8.1 Protein isolation from mouse lung tissue

Mouse lungs (n = 5-8/ group) were excised, weighed, and snap-frozen in liquid N2, and stored at -80°C for later protein extraction. Around 50-70 mg of tissue were placed in an Eppendorf along with 400-500 µl of RIPA lysis buffer and homogenized as described previously on 3.3.7. Using a tissue homogenizer, the tissue was disrupted until achieving a homogeneous mix. Subsequently, the cell lysates were pipetted into Eppendorf on ice and incubated for 45 minutes. Then, to separate the supernatant (protein) from cell debris (pellet), the cell lysates were centrifuged at 15,000 RPM for 10 minutes at 4°C. Last, cell supernatants were pipetted into LoBind Eppendorf tubes, and stored at -20°C for short-term storage.

3.3.8.2 Bicinchoninic acid (BCA) assay

The bicinchoninic acid assay (BCA assay) was used to measure protein concentrations from tissue and cell lysates according to the manufacturer's protocol (Thermo Fisher Scientific). To determine protein concentrations, a standard curve was built using known bovine serum albumin (BSA) concentrations to achieve a concentration range of 0-2 µg/µl diluted in RIPA Buffer served as a standard to determine protein concentrations. In a 96-well plate, cell lysates were mixed with RIPA buffer in a 1:4 or 1:10 ratio. RIPA buffer was used as blank. 10 µl/well of BSA standards and samples were pipetted in the same plate. All samples were pipetted in duplicates. Then, 200 µl of the BCA reagent was added per well. Following incubation at 37 °C for 30 min, the

absorbance was recorded at 562 nm using a Sunrise TM plate reader (TECAN) for estimation of protein concentrations.

3.3.8.3 SDS-PAGE and immunoblotting

Protein samples from lung tissue or cell lysates were mixed with NuPAGE® Reducing Agent (10X), NuPAGE® LDS Sample loading Buffer (4X), and deionized water. The proteins were separated using a Tris-Acetate (Life Technologies), Tris-glycine (Life Technologies) or Bis-Tris (Life Technologies) gel at a voltage of 80 - 120 V per gel. For immunoblotting, the gels containing the proteins were transferred to transfer-buffer activated Nitrocellulose membranes (Life Technologies) at 30V for 60 to 90 minutes. Then, the membranes were blocked using 5% milk in 1xTBS-T (0.1% Tween®20 in TBS) for 120 minutes followed by incubation with primary antibodies at 4°C overnight. Next day, following three 5-minute washes with 1xTBS-T, the membranes were incubated with HRP-conjugated secondary antibodies at room temperature for 2 hours. After antibody incubation, the nitrocellulose membranes were washed three times with 1X TBST for 5 minutes each. Last, the proteins were visualized using western blot chemiluminescent substrates (Femto SuperSignal®, Thermo Fisher). The Chemidoc XRS+ system from Bio-Rad was used to detect the protein signal. The primary and secondary antibodies that were used and the corresponding dilutions can be found in the materials section (**3.1.1**).

3.3.9 Quantification of DNA methylation intermediates

These experiments were done by Florian Schelter, PhD candidate in Prof.Dr. Thomas Carell research group. Institute for Chemical Epigenetics Munich (ICEM), Ludwig Maximilian University of Munich.

All experiments were performed in biological and technical triplicates to ensure reproducibility. Solvents for LC-MS/MS analysis were purchased from Honeywell, Roth and used without further purification.

To perform the analysis, we used a UHPLC-QQQ-MS/MS system fitted with a Triple Quadrupole 6490 mass spectrometer (Agilent) with an ESI source and an Agilent Infinity 1290 UHPLC. The Agilent InfinityLab Deuterium Lamp G1314 was used to monitor the elution elution at 260 nm. The MassHunter Workstation Software Version B.07.01 (Agilent)was used for data Acquisition and processing.

mdC, hmdC, fdC, cadC and 8-oxo-dG were separated on an InfinityLab Poroshell 120 SB-C8 (2.1 mm x 150 mm, 2.7 µm) column (Agilent Technologies, USA) at 35 °C. Water containing 0.0085% FA (v/v, solvent A) and MeCN containing 0.0085% FA (v/v, solvent B) was used as the mobile phase. A gradient of 0 - 3.5% B for 4 min, 3.5 - 5% B for 2.9 min, 5 - 80% B for 0.3 min, 80% B for 3.3 min was used. The flow rate of the mobile phase was set to 0.35 mL min. The source-dependent parameters were as follows, gas temperature 80 °C, gas flow 15 L/min (N_2), nebulizer 30 psi, sheath gas heater 275 °C, sheath gas flow 11 L/min (N_2), capillary voltage 2,500 V in the positive ion mode, and nozzle voltage 500 V. Delta EMV was set to 500 (positive mode). The nucleosides and labelled products were monitored using the multiple reaction monitoring mode. The MRM parameters were optimized to achieve maximal detection sensitivity.

3.3.10 RNA analysis

3.3.10.1 RNA extraction from mouse lung

The homogenization of lung samples was done as described in 3.3.7. The same kit and protocol described in 3.2.2.2 was followed.

3.3.10.2 cDNA synthesis by Reverse Transcription

To perform cDNA synthesis, 1 µg of the isolated mRNA was calculated and diluted with sterile nuclease-free water to a total volume of 20 µl. Subsequently, this mixture was denatured in a Master cycler, using the following settings:

Lid: 45°C

70°C for 10 mins

Hold: at 4°C

Next, a master-mix was prepared using the following reagents at the indicated concentrations:

Reagent	Stock concentration	Final concentration	Final volume (µl)
5X first-strand buffer	5X	1X	8
0.1 M DTT	0.1 M	0.02 M	4
dNTPs	10nM each	0.5 nM	2
Random hexamers	50µM	2.5 µM	2
Rnase inhibitor	10U/µl	20U	2
Reverse transcriptase	200U/µl	100U	0.5
dH20	-	-	1.5
Total volume master mix			20

For the reverse transcription reaction an Eppendorf Master-cycler was used following these settings:

Lid 85°CSS

37°C 60 min

75°C 10 min

Last, 160 µl of DNase-free water was added for a final concentration of 5ng/µl.

3.3.11 Quantitative Real-Time Polymerase Chain Reaction (qRT-PCR)

The SYBR Green LC480 system (Roche) was used to perform the quantitative real-time RT-PCR. The master mix was prepared as follows:

Reagent	Stock concentration	Final concentration	Final volume (µl)
SYBR green I master	2X	1X	5
Forward/Reverse Primer mix	10µM each	0.5 µM each	1
DNase-free water	-	-	1.5

In a 96-well plate, 2.5 µl of cDNA sample/well was pipetted in duplicates along with 7.5 µl of master mix Samples were always added in duplicates. The plates

were centrifuged for 1.5 minutes at 1000 rpm prior to starting measurement. The following program was used to perform the reaction:
95°C 5 minutes followed by 45 cycles of 95°C for 5 sec (denaturation)
59°C 5 seconds (annealing)
72°C 20 seconds (elongation)
60 – 95°C for 1 minute with continuous acquisition (melting curve).
After data collection, the reference gene hypoxanthine-guanine phosphoribosyltransferase (HPRT) was used to normalize the expression of target genes (Reference Gene CT value - target gene CT value). Relative gene expression was determined using the ΔCT method.

3.4 Human studies

3.4.1 Protein analysis from plasma

Whole blood samples from preterm infants hospitalized at the Perinatal Center of the Ludwig Maximilians University, Campus Grosshadern were collected in Ethylenediaminetetraacetic acid (EDTA) neonatal collection tubes after the first week and four weeks of life before discharge (Ethics approval #195-07, Munich, Ludwig Maximillian's University of Munich, Germany). The proximity extension assay (PEA) (Olink Proteomics®, Uppsala, Sweden) assay was used to measure all samples. The relative abundance of 630 proteins in plasma was determined using the cardiovascular II (v.5004), inflammation (v.3012), development (v.3511), cardiometabolic (v.3602), neurology (v.8011), metabolism (v.3402), and oncology II (v.7002) panels following the manufacturer's instructions. Real-Time PCR with the Fluidigm BioMark™ HD Real-Time PCR platform was used to measure relative protein expression. The protein expressions were reported in NPX values (normalized protein expression levels, in a log2-scale). Randomization of samples across plates was done to avoid batch effects. In this assay, each plate includes an internal control that is used to adjust for inter-plate differences. The plate median per assay was used to normalize NPX values

(Intensity Normalization v.2). Quality control was used to exclude samples or proteins of insufficient quality.

3.4.2 Genetic association analysis

DNA extraction, genotyping and association analysis were performed as previously described [50]. Briefly, DNA was extracted from EDTA cord blood samples of n=1061 preterm infants (n=278 moderate/severe BPD [19]) <=32 weeks GA (Progress Study Group: Approval was obtained by all local Ethics committees, legal representatives of study subjects provided written informed consent). Genotypes of patients were determined using Affymetrix Axiom microarrays (Axiom CEU array with custom content), imputation of the data used 1000 Genomes Phase 1, version 3 as reference panel (genome built hg19/ dbSNP 135).

3.5 Statistical analysis

3.5.1 Bioinformatics analysis

3.5.1.1 RNA-sequencing analysis

The RNA-seq Differential expression analysis was performed with DESeq2 conducted separately for each cell type (Love et al., 2014). Genes with low read counts (< 10) were removed and the samples normalized using DESeq2 calculated size factors. Statistical significance was determined using the Wald test after fitting a generalized linear model per gene taking into account the conditions under comparison (control vs treatment). A gene was deemed significantly differentially expressed if its Benjamin-Hochberg corrected q-value was less than 0.05. In-vivo-RNA-seq samples were similarly processed and analyzed. Gene set and KEGG pathway enrichment analysis was performed with gProfiler 2 using the g: SCS algorithm for multiple testing correction (Raudvere et al., 2019). Gene Ontology categories and KEGG pathways were deemed significantly enriched at an adjusted p-value of 0.05.

Common significant genes were detected between cell types following hyperoxia treatment followed by functional enrichment analysis as described above to identify commonly regulated biological processes (BP). The expression strength of each BP category detected was calculated as the mean log-fold change for up-

and down-regulated genes, respectively. This analysis was performed by Juan Henao and Benjamin Schubert, Institute of Computational Biology, Helmholz Zentrum, Munich.

3.5.1.2 Proteomics

APEX1 was analyzed in EDTA plasma (n=30) using the proximity extension assay (PEA, Olink Proteomics, Uppsala, Sweden; Olink panels C-MET, CVDII, DEV, INF, MET, NEU, ONCII). MDM2 was analyzed in EDTA plasma (n=29) using the SOMAscan® assays (SomaLogic®, Boulder, USA). Protein expression levels were $\log_2$ transformed and pareto scaled before correcting for gestational age using linear regression. The corrected protein expression levels were correlated against duration of oxygen supplementation [days] using Pearson correlation. Statistical analyses were performed in R (version 4.1.0).

3.5.1.3 Genetic association study

DNA extraction, genotyping, and genome-wide association analysis were performed as described previously (Blume et al., 2021). Briefly, DNA was extracted from EDTA cord blood of n=1061 preterm infants with less than 32 weeks gestational age. 278 infants developed moderate or severe BPD. The genotype of infants was determined using an Affymetrix Axiom Microarray (Axiom CEU array with custom content), while genotype imputation was performed using the IMPUTE v2.3.0 (Howie et al., 2009) and the 1000 Genome Phase 1 (version 3)(1000 Genomes Project Consortium et al) as reference (genome build hg19 / dbSNP135). Association of single nucleotide polymorphisms (SNPs) and BPD severity, as well as required days of oxygenation, was performed with a generalized linear mixed model (R package lme4qtl (Ziyatdinov et al., 2018)) accounting for sample relatedness (kinship), gender, gestational age, birth weight <10th percentile, and country of the mother. We filtered for SNPs with an adjusted P-value 0.05, minor allele frequency of 5%, and for close SNPs annotated for cell cycle-related genes: CCNB1, CDC25C, CCND2, CCNE1, CDKN1A, CDK2, CDK1, CCNA2, CDC25A, CDKN1B, CDT1, ORC6, CDC6, MCM2, MCM4, MCM6, XRCC1, APEX1, NEIL1, OGG1, DNMT3A, UNG, CHEK1, APE1, FEN1, MBD4.

3.5.2 Statistical analysis of small data

Statistical analysis was performed using GraphPad Prism v9.0 (GraphPad Software). Data were presented as mean ± standard deviation (SD) or median with interquartile range (IQR) according to the distribution. Statistical analysis for normally distributed data was performed using unpaired and paired t-tests (two-tailed) or One-way ANOVA with Dunnett's multiple comparison test. For non-normally distributed data, I used the non-parametric tests Mann-Whitney U tests or the Wilcoxon signed-rank for paired samples. For multiple comparisons, the Kruskal-Wallis test with Dunn's test for post hoc analysis was used.

4. Characterization of the effects of clinical hyperoxia levels in the developing lung

4.1 Background

Preterm infants often require life-saving treatment for respiratory failure with oxygen-rich gas with or without mechanical ventilation. At the same time, this postnatal intervention imposed on the developing lung provokes lung injury in the neonate, which significantly increases the risk of bronchopulmonary dysplasia i.e., neonatal chronic lung disease (Hilgendorff & O'Reilly, 2015; Hilgendorff et al., 2014; Sucre et al., 2021). Bronchopulmonary dysplasia (BPD) remains the most common complication of prematurity and leads to poor pulmonary and neurological long-term outcomes in affected infants (Stoecklein et al., 2020; Sucre et al., 2021).

When considering clinically relevant oxygen concentrations ranging between FiO_2 0.3-0.5, the specific effects of oxygen and its impact on lung developmental arrest have not been fully understood. Hyperoxic injury has been shown to promote the alteration of central developmental pathways such as the upregulation of the WNT/β-catenin or downregulation of PDGF-Rα signaling, resulting in impaired alveolar septation, septal thickening, and deformation of the gas exchange area (Hubbi et al., 2011; Jia et al., 2021; C. Li et al., 2020; Oak et al., 2017; Riccetti et al., 2022; Sucre et al., 2020). Studies in newborn mice exposed to short-term high levels of hyperoxia at birth have shown changes in expression in cell cycle checkpoint regulators genes, and the downregulation of the pre-replication complex genes hindering the initiation of replication. Some of these changes were still present weeks after the initial exposure (Kumar et al., 2020). Moreover, several studies have reported a significant increase in DNA damage and apoptosis in the lung of newborn mice exposed to severe hyperoxia levels (Hilgendorff & O'Reilly, 2015; Jiang et al., 2022). These responses to injury are likely to recruit immune cells to the area and exacerbate the inflammatory response, ultimately resulting in more cell death and damage to the alveoli (Reddy et al., 2022). Although lung effects of severe hyperoxia have been well documented, little is known about short-term exposure to clinically relevant hyperoxia concentrations i.e FiO_2 = 0.4. Thus, it is critical to investigate the

consequences of exposing the developing lung to clinically relevant hyperoxia levels for short periods of time in order to identify critical drivers of immediate and long-term changes. Here, we first focused on elucidating these effects at the cellular level using an unbiased approach at the transcriptomic level.

4.2 Results

4.2.1 Part 1: In-vitro effects of clinical hyperoxia in three major lung cell types

4.2.1.1 Transcriptomic signature of moderate hyperoxia in-vitro

The effects of severe hyperoxia (FiO_2 = 0.8 to 1.0) exposure in the lung have been described in some detail regarding immediate and longer-term effects. A study by Hurskainen *et al* that exposed neonatal mice to severe hyperoxia (FiO_2 = 0.85) for 3, 7, and 14 days showed this level of hyperoxia to dramatically alter all lung cellular compartments (Hurskainen et al., 2021). Among the most affected cells were the alveolar epithelial cells, the capillary endothelium, stromal fibroblasts, and macrophages. The authors also identified crosstalk networks in which Col13a1+ fibroblasts and myofibroblasts act as the main signal sender and receiver affecting all other cellular compartments. The TNF-signaling pathway was found to be the driver of the resulting pro-inflammatory signature that triggered the observed changes in cellular composition.

Unlike severe hyperoxia, the cellular effects of clinical hyperoxia concentrations ($FiO_2 < 0.5$) have not been studied as comprehensively. Among the few studies, You *et al* studied the effects of 7 days 40% hyperoxia exposure on lung fibroblasts. One of the main findings of the study was the potential connection between moderate hyperoxia-induced cell-cycle arrest in G2/M and senescence (You et al., 2019). A study on fetal airway smooth muscle cells found that moderate hyperoxia (FiO_2 = 0.5) led to extracellular matrix deposition in the airway wall potentially leading to airway remodeling (Vogel et al., 2017). These studies provided some insight into the effects of moderate hyperoxia on lung cells, but a comprehensive understanding of these response is still lacking. Identifying the effects of clinically relevant hyperoxia concentrations (FiO_2 = 0.4) on the three major cell types present in the alveolar unit will provide insights into

critical drivers of immediate and long-term changes. To address these knowledge gaps, we isolated alveolar epithelial cells (AT2), fibroblasts (MFB), and endothelial cells (EC) from the newborn mouse lungs at postnatal day P05-P07 as described in (**Methods 3.3.1-3**). Exposure to cyclical stretch was used in comparison to determine the specificity of the hyperoxic response (**Fig 4.1 A)**. *The bioinformatics analysis was done in collaboration with Dr. Benjamin Schubert (Institute of Computational Biology, Helmholtz Zentrum) and his doctoral candidate, Juan Henao*.

Following exposure to clinically relevant hyperoxia levels, we detected 1368, 1150, and 69 significantly regulated genes (DEG) in AT2 cells, MFBs, and EC by differential expression analysis (**Fig 4.1. B**) dominate by downregulation of gene expression including the top five significantly regulated genes (FDR < 0.05) in both AT2 and MFBs. These genes were involved in cell cycle regulation and included (Racgap1, Hells, Mcm6, Tpx2, and Anln, in AT2 cells and Atad2, Mcm6, Hjurp, and Mcm4 in MFBs. In ECs, the top 5 regulated genes (FDR < 0.05) were related to metabolic processes, as mirrored by the differential regulation of Scd2, Ldlr, and Dhcr24.

In contrast, cyclical stretch under room air conditions resulted in only 173 differentially regulated genes in the outlined cell types, dominated by their regulation in AT2 cells (n = 41 genes) (**Fig 4.1 C)**. The top two genes were Srxn1 and Gclc (in AT2 cells), both related to the oxidative stress response. Unlike hyperoxia, there was no shared signature in the three cell types (**Fig 4.1 D)**.

As depicted in the Upset graph in **Fig 4.1 D**, only a few DEGs were commonly regulated when comparing the transcriptomic response to clinical hyperoxia and

cyclical stretch. These data suggest that clinical hyperoxia triggers a distinct transcriptomic response in neonatal lung cells.

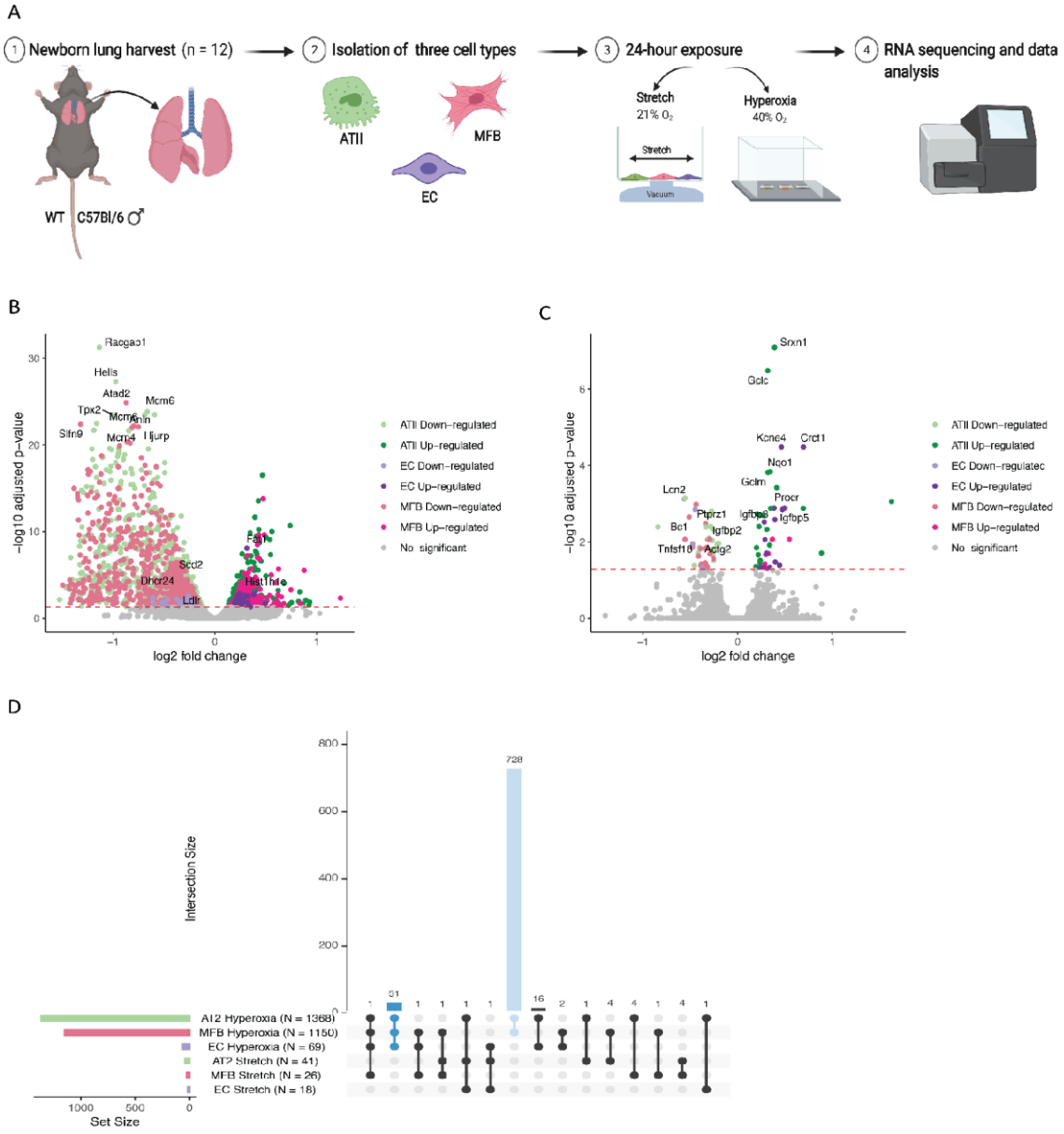

Fig 4.1: RNA-sequencing analysis of three major cell types after clinical hyperoxia exposure

Experimental design (A). Volcano plot showing differentially expressed genes (DEG) following clinical hyperoxia exposure in the three cell types (B). Volcano plot of DEGs following stretch (C). UpSET graph of commonly shared genes across cell types and treatments. In blue are represented the shared response following clinical hyperoxia (D). Each category detected was calculated as the mean log-fold change for up-and down-regulated genes. Gene ontologies were deemed significantly enriched at an adjusted p-value of 0.05 and FDR of 0.5. This analysis was performed by Juan Henao and Benjamin Schubert, Institute of Computational Biology, Helmholtz

Zentrum. AT2 = alveolar epithelial cells. MFB = mouse fibroblasts. BP = biological process. FC = fold change. FDR = false-discovery rate. DEG = differentially expressed genes.
The cell isolation experiments were performed by Dr.Tina Prtizke, postdoctoral fellow in the Hilgendorff lab. The bioinformatics analysis was performed by Juan Henao and Dr. Benjamin Schubert, Institute of Computational Biology, Helmholtz Zentrum.

4.2.1.2 Shared epithelial and fibroblast response to clinical hyperoxia

Next, the shared hyperoxia signature across the three cell types was identified. These thirty-two genes were dominated by candidates involved in cell cycle regulation (**Fig 4.2 A-B**). Remarkably, AT2 cells and MFBs shared a significant pattern of expression regulation with an overlap of 728 genes that accounted for 53,2% of DEG in AT2 cells and 63,3% of DEG in MFBs (**Fig 4.2 A**), the majority of these DEGs (90%) demonstrated a strong down-regulation. The top two DEGs included genes of the pre-replication complex, such as Mcm6 and Mcm4, and Hells, all of them significantly involved in cell-cycle progression.

Enrichment analysis of the 728 shared genes identified commonly regulated biological processes between AT2 cells and MFBs with the top eight relating to cell-cycle regulation and progression (**Fig 4.2 C**). These findings indicate a coordinated molecular response to clinically relevant levels of hyperoxia in AT2 cells and MFBs, positioning cell-cycle regulation (and arrest) as a key element in this cellular reaction. These results are in line with what has been previously observed in the single-cell analysis of models using severe hyperoxia (Hurskainen et al., 2021).

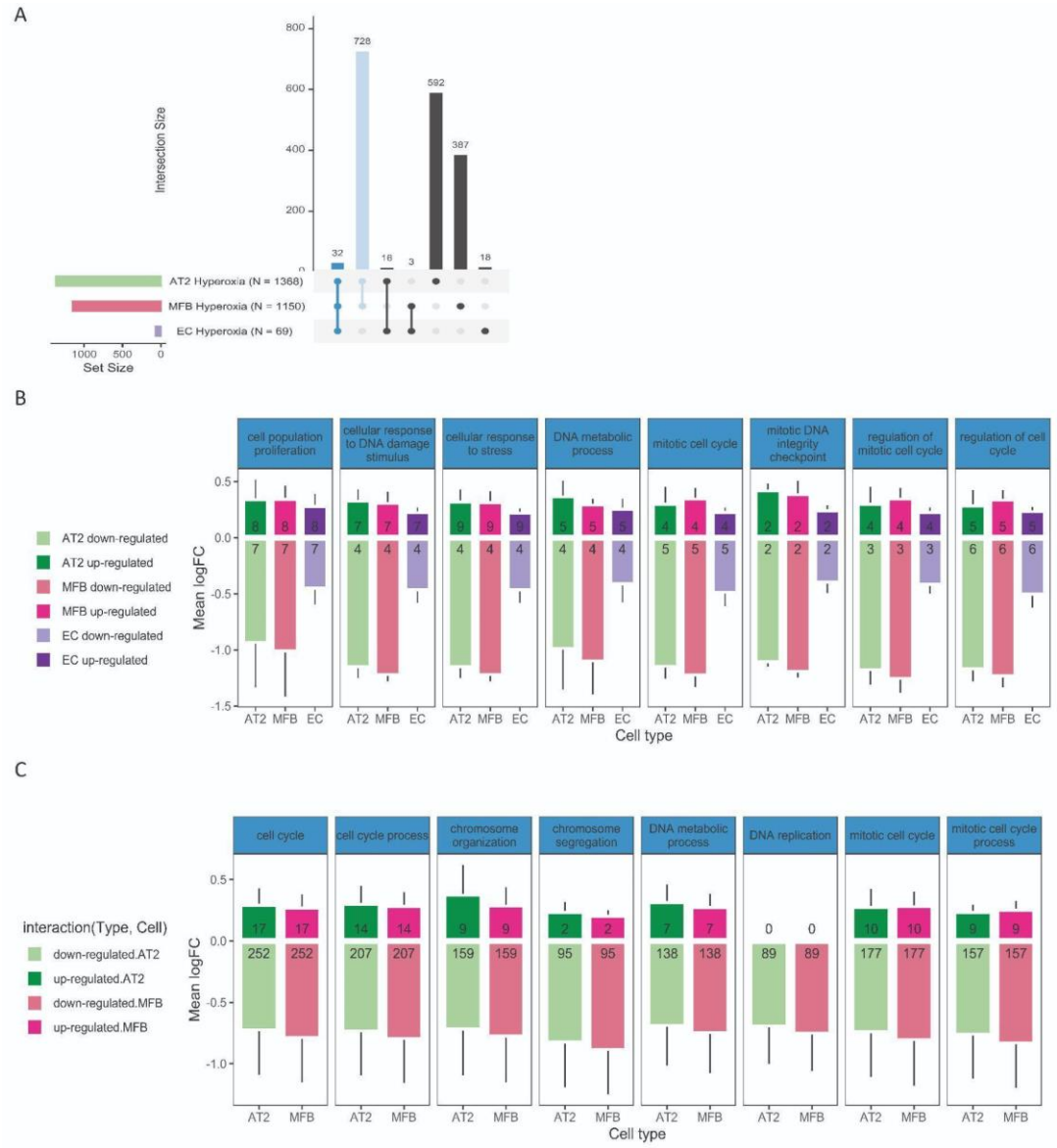

Fig 4.2: Top biological processes represented in the shared signature across cell types and between AT2 cells and MFBs

UpSet graph showing common genes shared by each cell type (A). The 32 genes in common in the three cell types were enriched in cell cycle regulation processes (B). Cell cycle regulation processes were predominantly enriched in the shared signature between AT2 cells and MFBs (C). Each category detected was calculated as the mean log-fold change for up-and down-regulated genes. Gene ontologies were deemed significantly enriched at an adjusted p-value of 0.05 and FDR of 0.5. AT2 = alveolar epithelial cells. MFB = mouse fibroblasts. BP = biological process. FC = fold change. FDR = false-discovery rate. DEG = differentially expressed genes

This analysis was performed by Juan Henao and Benjamin Schubert, Institute of Computational Biology, Helmholtz Zentrum.

4.2.1.3 Checkpoint regulation by clinical hyperoxia-induced cell cycle arrest in neonatal lung cells

There has been significant progress in recent years to understanding the abnormal molecular mechanisms causing BPD. A recent study mimicking pathophysiologic conditions relevant in BPD using precision-cut lung slices, revealed that two genes that code for critical pre-replication complex proteins, Mcm2 and Mcm3 (minichromosome maintenance complex component 2, 3) were downregulated following FiO_2 = 0.7 exposure. Interestingly, this occurred in the absence of apoptosis suggesting that cell cycle regulation could be a critical mechanism in the response to hyperoxia (Sucre et al., 2020). This study, however, did not provide any insights into what the consequences of cell cycle arrest could be in other signaling pathways. In line with these results, in our RNA-sequencing unbiased analysis, we also found cell cycle regulation processes to play a critical role in how the cells deal with FiO_2 = 0.4 exposure (**Fig 4.2**).

To comprehensively understand the role of cell cycle regulation in the response to clinical hyperoxia levels, we studied the enrichment of cell-cycle-related genes in our RNA-sequencing data and demonstrated the shared downregulation of these genes in AT2 cells and MFBs. Specifically, pre-replication complex genes, *i.e.,* Mcm2-Mcm7, critical to initiate DNA replication in S phase, as well as key regulators of cell cycle progression like Cdk2, Ccna2, the p53 downstream effector p21, and Cdk1 along with the p53 repressor Mdm2 were found to be differentially regulated (for a detailed description of cell cycle checkpoints and DNA damage response pathways see **Fig 1.6**). This response was partially shared with ECs (**Fig 4.3 A-B**). Furthermore, biological processes related to cell-cycle regulation and cell-cycle phase-dependent functions such as DNA repair were found to be enriched in all cell types (**Fig 4.3 C).** These results suggest that

short-term exposure to clinically relevant hyperoxia levels is able to induce cell cycle arrest.

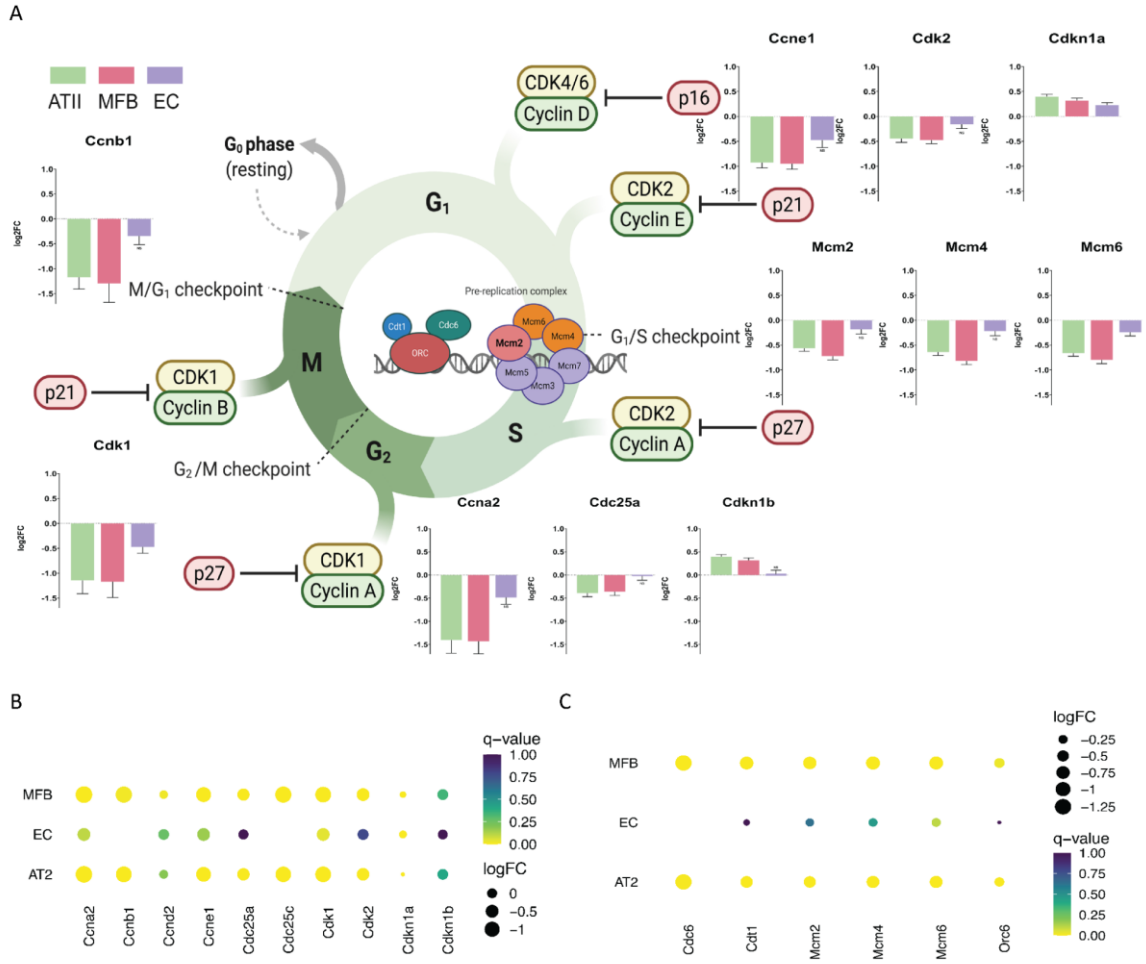

Fig 4.3: Cell cycle checkpoints were significantly regulated in all three cell types following clinical hyperoxia for 24 hours.

Enrichment of cell-cycle regulatory genes in each cell type (A). LogFC of critical checkpoint regulators per cell type (B). The enrichment per cell type of pre-RC genes showed a similar signature in AT2 cells and MFBs (C). Each category detected was calculated as the mean log-fold change for up-and down-regulated genes. Gene ontologies were deemed significantly enriched at an adjusted p-value of 0.05. AT2: alveolar epithelial cells. MFB: mouse fibroblasts. Pre-RC: pre-replication complex. FC: fold change

This analysis was performed by Juan Henao and Benjamin Schubert, Institute of Computational Biology, Helmholtz Zentrum.

Validating the detected transcriptional regulation, I employed extensively *in vitro* studies in human embryonic lung fibroblasts (IMR-90) and murine lung epithelial cells (MLE12). IMR-90 fibroblasts are embryonic Pdgf-Rα+ cells that play an important role in lung development, thus providing us with a good cellular model to study the effects of O_2 at the single cell level (Riccetti et al., 2022). IMR-90 and MLE12 epithelial cells were cultured and exposed to 24 hours of clinical hyperoxia or normoxia (FiO_2 = 0.40/0.21). After exposure, cell lysates were collected to perform RNA or protein extraction. Using RNA and protein analysis, I confirmed the significant downregulation of key checkpoint regulators in response to hyperoxia in IMR90 cells **(Fig 4.4 A-D)**. This downregulation of *Mcm2* was not counteracted by the upregulation of p53 activation (Kunnev et al., 2010) (**Fig 4.4 A-C)**. To investigate the longevity of the effects, IMR-90 cells and MLE12-cells were exposed to hyperoxia for 24 hours followed by a 'recovery' period in room air (FiO_2 = 0.21). Cell lysates were collected, and I found that both IMR-90 and MLE-12 cells showed a strong, persistent downregulation of *Mcm2* in cells that were returned to normoxia. Interestingly, in MLE12, the 'recovery' period seemed to aggravate the downregulation of *Mcm2* as determined by one-way ANOVA ($F(3,8) = 37$, $p<0.0001$) (**Fig 4.4 D-E)**.

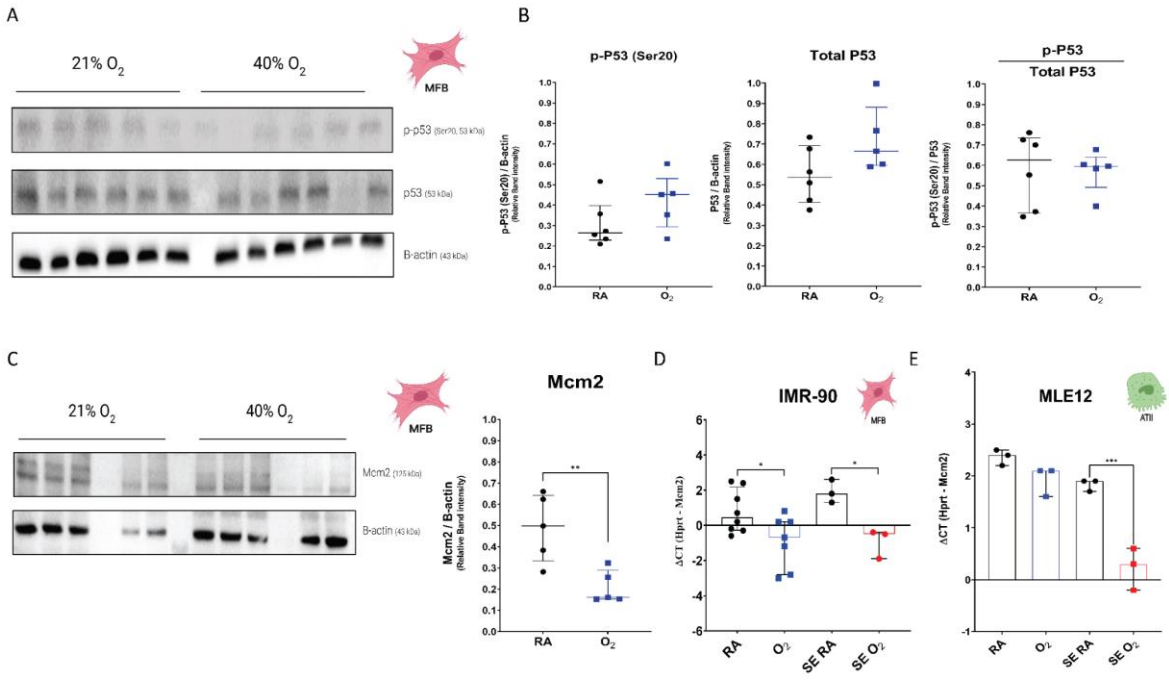

Fig 4.4: Following clinical hyperoxia, Mcm2 was downregulated at the mRNA and protein levels.

Immunoblotting was performed using protein lysates from human fibroblasts (IMR-90) treated with O_2 (FiO_2 = 0.4) or room air (RA; FiO_2 = 0.21). for 24 hours. RepresentativeS immunoblot of p-p53 (Ser 20) and p53 (A) and densitometry quantification showed no changes in protein expression between the groups (N = 5-6/group) (B). Densitometry quantification of Mcm2 (representative immunoblot) showed decreased expression in the O_2 group (N = 5/group) (C). qPCR was used to quantify the mRNA expression of Mcm2 in IMR-90 and MLE-12 cells (N = 3-7/group) exposed to O2 or RA. The Delta CT method was used to calculate relative expression with respect to the reference gene, Hprt. Mcm2 mRNA expression was downregulated under normoxia (4 days) following the previous exposure to O_2 (D-E). Densitometric protein quantification and mRNA quantification bars are represented as median with interquartile range. Statistical analysis: unpaired t-test. *p<0.05; **p<0.01; ***p<0.001. One-way ANOVA test with Tukey's test for multiple comparison correction was used when comparing more than 2 groups. MFB: Fibroblasts (IMR-90 cells). AT2: Alveolar epithelial cells (MLE12 cell line). SE: sustained effect; SE cells were exposed to O_2 for 24 hours and returned to normoxia to recover for four days.

In functional studies, I demonstrated that exposure to clinical O_2 levels resulted in decreased proliferation of IMR90 fibroblasts (BrdU assay) (**Fig 4.5 A**). These changes occurred along with the significant downregulation of Col1a1 mRNA expression (**Fig 4.5 B**). The mRNA expression of *Cdkn1a* was comparable between groups (**Fig 4.5 C**). This occurred together with the absence of classical apoptosis pathway activation as I did not detect significant differences between the experimental groups in the two cleaved subunits of Caspase-9 or Caspase 3/7 activity (**Fig 4.5 D, E**).

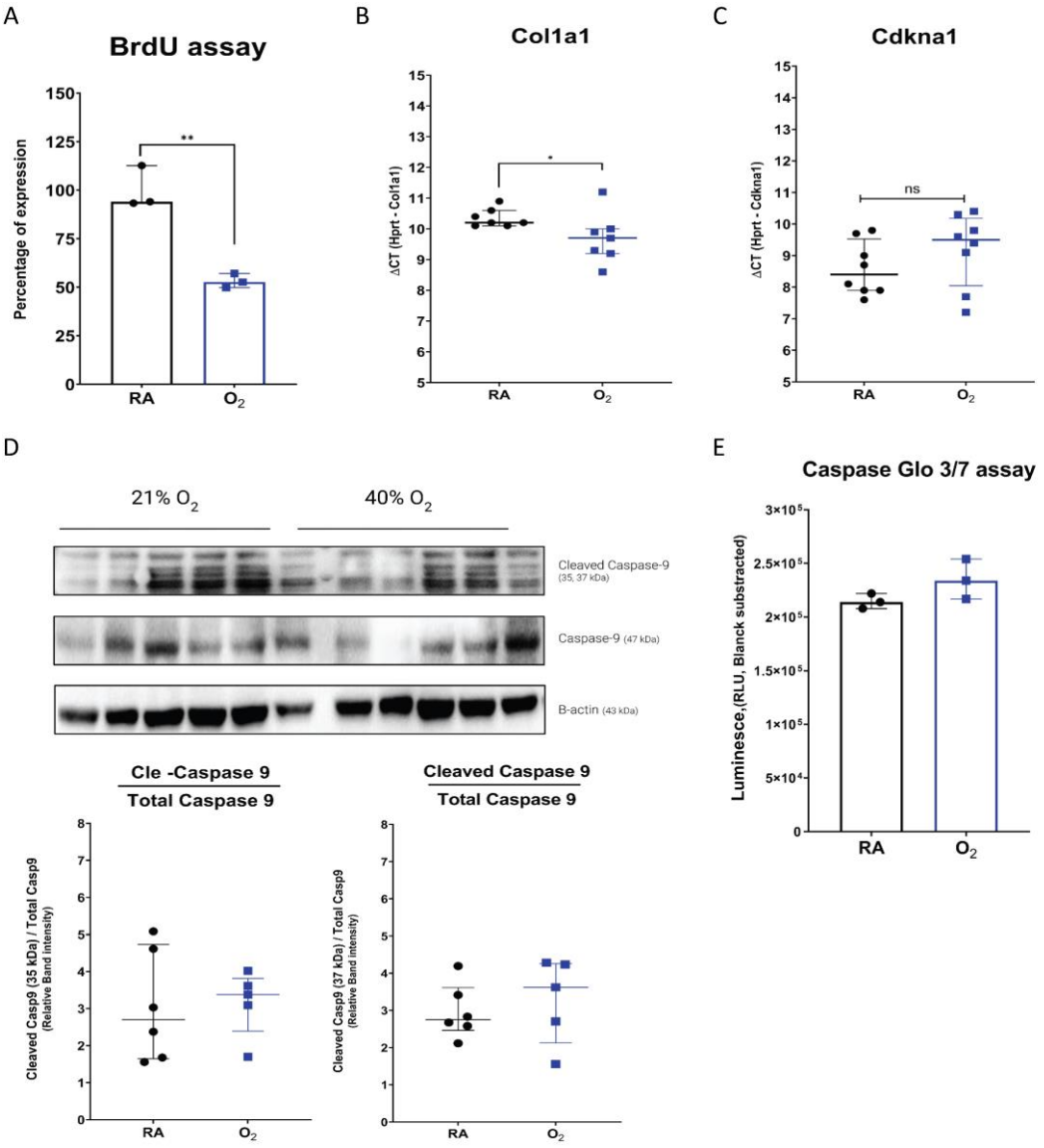

Fig 4.5: Clinical hyperoxia exposure did not trigger classical apoptosis pathways

Proliferation was evaluated with the BrdU assay in human fibroblasts (IMR-90) treated with O_2 (FiO_2 = 0.4) or room air (RA; FiO_2 = 0.21) for 24 hours (N = 3/group) (A). qPCR was used to quantify the mRNA expression of Col1a1 and Cdkn1a (N = 7-8/group) from IMR90 cells exposed to O_2 or RA. The Delta CT method (CT value reference gene - CT value target gene) was used to calculate relative expression with respect to a reference gene (Hprt). While Col1a1 was downregulated following hyperoxia treatment (B), the mRNA expression of Cdkn1a was comparable between groups (C). Immunoblotting was performed using protein lysates from IMR-90 cells treated with O_2 or RA for 24 hours (N = 5-6/group). Densitometry quantification of Cleaved Caspase 9 subunits (35 kDa, 37 kDa) and Caspase-9 (D) showed no changes in protein expression between the groups (representative immunoblot). Caspase Glo 3/7 assay was used to investigate the activity of Caspase 3/7 in IMR-90 cells treated with O_2 or RA for 24 hours (N = 3/group). Densitometric protein quantification and mRNA quantification bars are represented as median with interquartile range. Statistical analysis: unpaired t-test. *p<0.05; **p<0.01. qPCR: quantitative polymerase chain reaction. MFB: Fibroblasts (IMR-90 cells). AT2: Alveolar epithelial cells (MLE12 cell line).

To rule out the activation of non-classical apoptosis pathways like ferroptosis, we assessed the mRNA expression of *Chac1*, *Gpx4,* and *Spgt2,* again not identifying significant differences between the normoxia and hyperoxia groups (**Fig 4.6 A-C**). In line with the transcriptomic signature described above, my data suggest cell-cycle arrest in G1 induced by exposure to clinical hyperoxia for 24 hours. Moreover, the changes in cell cycle regulatory genes in the absence of classical apoptosis hint at potential alterations in a cell cycle phase-dependent gene expression.

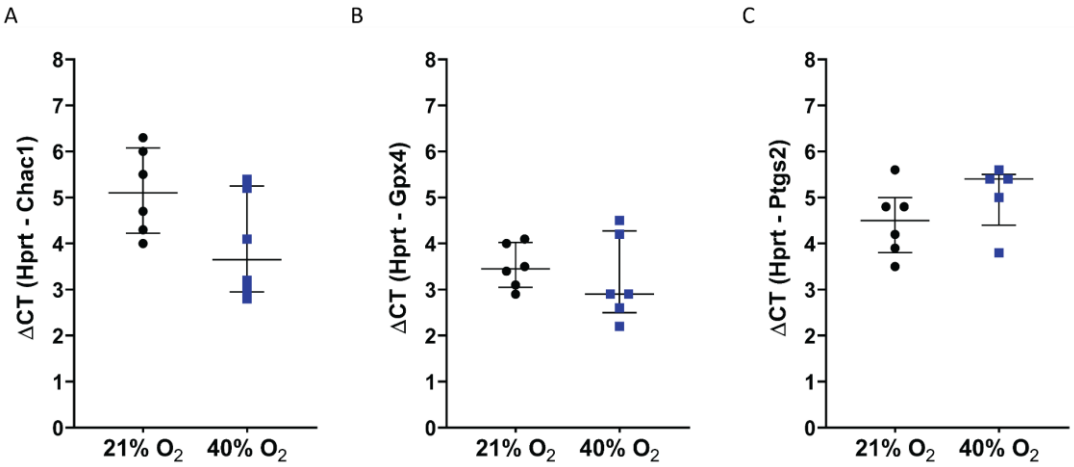

Fig 4.6: mRNA expression of Ferroptosis genes were comparable between groups

qPCR was used to quantify the mRNA expression of ferroptosis genes, Chac1, Gpx4, Ptgs2 (N = 5-6/group) from human fibroblasts (IMR-90) exposed to O_2 (FiO_2 = 0.4) or room air (FiO_2 = 0.21). The Delta CT method (CT value reference gene - CT value target gene) was used to calculate relative expression with respect to a reference gene (Hprt). Chac1 was downregulated in the O_2 group, but this difference was not significant (A). Gpx4 median mRNA expression was lower in the O_2 group (B) while the median Ptgs2 expression was up (C). However, none of these differences reached statistical significance. mRNA quantification bars are represented as median with interquartile range. Statistical analysis: unpaired t-test.

As the next logical step to study the response to clinically relevant hyperoxia levels (O_2: FiO_2 = 0.4) at the cellular level, I investigated the longevity of these effects. I expected that stemming from cell-cycle arrest, some of these responses would still be present days after O_2 cessation. In MLE12, I studied sustained effects induced by hyperoxia (FiO_2 = 0.4) in 'recovery' experiments. To do so, we treated cells with hyperoxia for 24 hours and then allowed them to recover for four days in normoxia (sustained effects, SE). We found that in addition to *Mcm2* (**Fig 4.4 E**), *Cdkn1a* and functional genes *Cdh1* and *Hif1a* were significantly downregulated four days after recovery from hyperoxia (**Fig 4.7 A, B, D**). *Sftpc* was downregulated immediately after hyperoxia but following the recovery period, it was significantly upregulated compared to normoxia control cells (**Fig 4.7 C**). To investigate the organ-specificity of the hyperoxia response *in vitro*, I treated Hek293 epithelial cells with FiO_2 = 0.4/0.21 for 24 hours and allowed them to recover for 4 days. The median *Mcm2* mRNA expression was lower in the O_2 group, but it returned to baseline levels after 4 days of 'recovery' (E). The median *Cdkn1a* in the O_2 group was more than one-fold lower than in controls but it recovered after 4 days in normoxia (F). After 24 hours of treatment, proliferation (BrdU assay) was comparable between groups

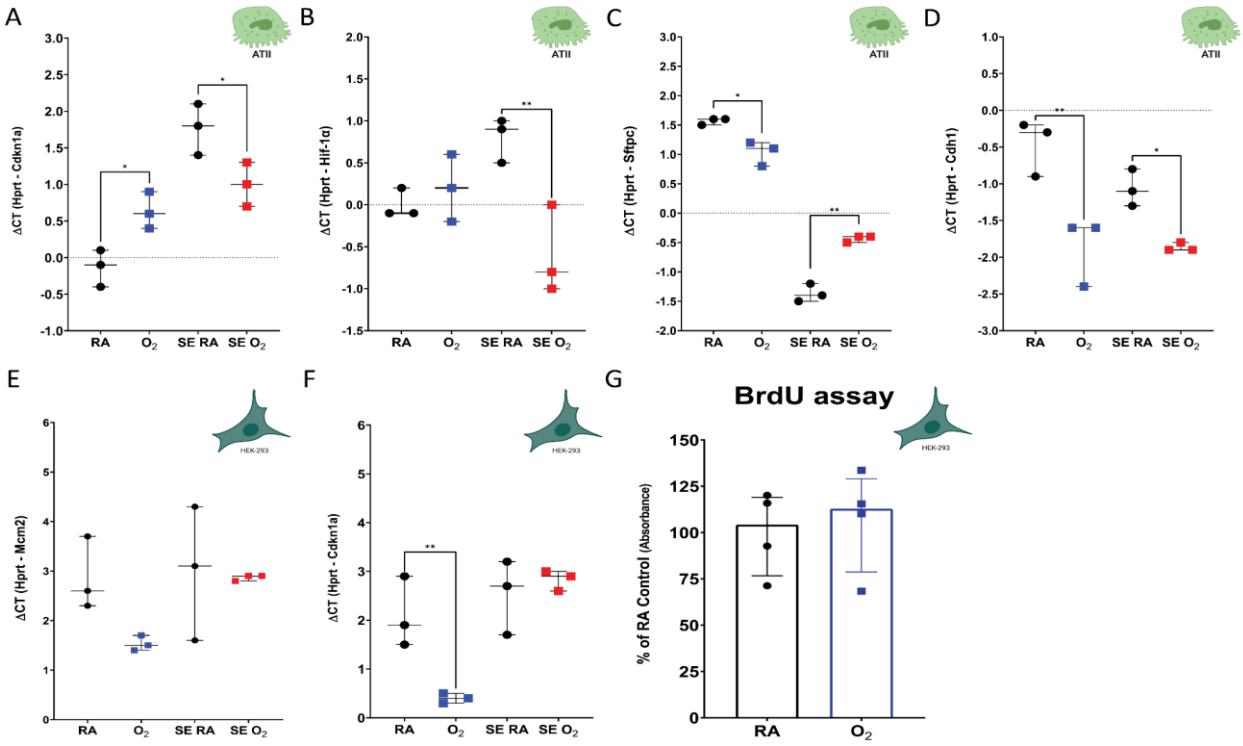

Fig 4.7: Sustained effects and organ specificity of the response to hyperoxia

qPCR was used to quantify the mRNA expression of target genes (N =3/group) from mouse lung alveolar epithelial cells (MLE-12) and human kidney cells (Hek-293) exposed to O_2 (FiO_2 = 0.4) or room air (FiO_2 = 0.21). Cdkn1a (A) and functional genes Cdh1(B) and Hif1a (D) were significantly downregulated four days after 'recovery' from hyperoxia. The mRNA expression of Sftpc was downregulated after 24 hours of hyperoxia but recovered after 4 days in normoxia (C). In human kidney cells, the Mcm2 mRNA expression was lower in the O_2 group, this difference was not statistically significant. Moreover, after 4 days of recovery, it returned to baseline levels (E). The median Cdkn1a in the O_2 group was more than one-fold lower than in controls but it recovered after 4 days in normoxia (F). After 24 hours of treatment, proliferation (BrdU assay) was comparable between groups(G). The Delta CT method (CT value reference gene - CT value target gene) was used to calculate relative expression with respect to a reference gene (Hprt). mRNA quantification bars are represented as median with interquartile range. Statistical analysis: unpaired t-test. *p<0.05; **p<0.01. One-way ANOVA test with Tukey's test for multiple comparison correction was used when comparing more than 2 groups. MFB: Fibroblasts (IMR-90 cells). AT2: Alveolar epithelial cells (MLE12 cell line). SE: sustained effect; SE cells were exposed to O_2 for 24 hours and returned to normoxia to recover for four days.

4.2.1.4 Mcm-2 silencing mimics the effects of clinical hyperoxia in neonatal lung cells

To start DNA replication in the S-phase, the licensing of replication origins in the G1 phase needs to occur. The pre-replication complex (pre-RC) composed by

several proteins including two hexamers of the Mcm2–7 helicase. The assembly of the pre-RC at thousands of origin sites is a critical step to start replication (Chang et al., 2019). Previous studies have revealed Mcm2 and Mcm3 to be downregulated following 7 days of 70% hyperoxia in an ex-vivo model (Sucre et al., 2020). This together with our data showing a strong downregulation of pre-RC genes i.e., *Mcm2*, *Mcm4, Mcm6, Orc1, Cdc6* following O_2 exposure is notable and suggests that the pre-RC plays an important role in the response to O_2. To gain mechanistic insight into the role of checkpoint regulation in cell cycle-dependent signaling and subsequent cellular functions and in order to thereby understand the hyperoxia-induced effects, I silenced Mcm2 as a key player in the pre-RC and one of the top DEGs identified by RNA-sequencing (log2FC = -0.56; adjusted *p-value* = $5.62E^{-17}$). Using a pool of 4 siRNAs targeting *Mcm2* gene expression, the temporal knockdown of Mcm2 was achieved in CCL-206 fibroblasts. *Gapdh* was used as positive control addressing transfection efficiency, whereas anon-targeting control (NTC) and sham (transfection reagent only) were used as negative controls. The cells were incubated with the transfection media for 18 hours. After this time, the medium was replaced, and a comparable number of cells were placed in either normoxia (FiO_2 = 0.21) or hyperoxia (FiO_2 = 0.4). Cell lysates for mRNA analysis were collected 24 hours after hyperoxia exposure.

After confirming optimal transfection conditions (**Fig 4.8 A-B),** I investigated the effects of the *Mcm2* knockdown on cell cycle progression. I found that, like hyperoxia, *Mcm2* knockdown in CCL-206 fibroblasts led to the changes in cell-cycle regulation-related gene expression (**Fig 4.8 C-E**) without affecting cell viability. Moreover, in *Mcm2*-silenced cells, critical cell-cycle regulators, *Trp53* and *Cdkn1a*, were downregulated when compared to the NTC (**Fig 4.8 F-G**). Hyperoxia did not exacerbate the downregulation of *Trp53* in silenced cells resulting in no significant differences between NTC-O_2 and siRNA-O_2 treated cells (**Fig 4.8 F**). In contrast, both under normoxia and O_2 conditions, there was a significant downregulation of *Cdkn1a* in silenced cells as compared to controls (**Fig 4.8 G**). The observed regulation in silenced cells mimicked the results

obtained by hyperoxia supporting the role of the Pre-RC in hyperoxia-induced cell cycle arrest.

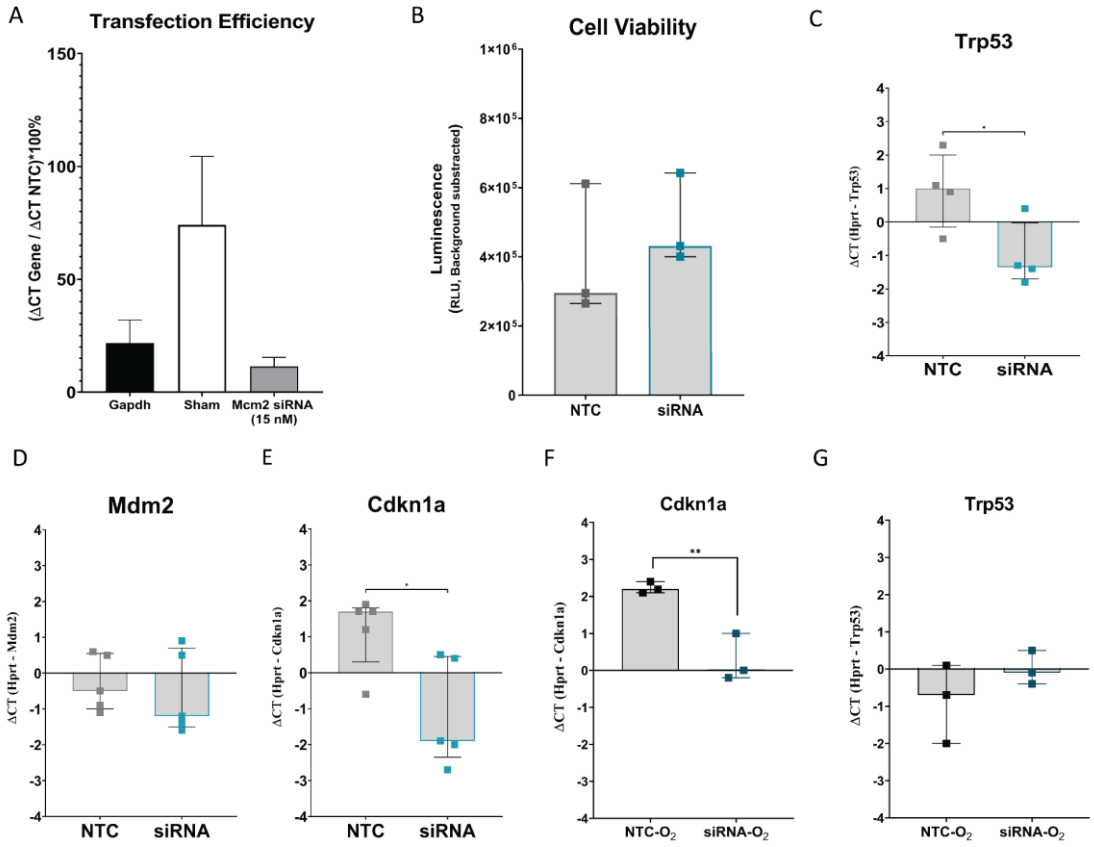

Fig 4.8: Cell-cycle master regulators were downregulated in *Mcm2*-silenced cells

qPCR was used to quantify the mRNA expression of Mcm2 in CCL206 mouse fibroblasts. Transfection efficiency in CCL206 fibroblasts is represented as the percentage of expression with respect to the NTC control. knockdown of Gapdh expression was used as the positive control (A). There was no difference in cell viability between the NTC group and the *Mcm2*-knockdown group (B). The mRNA expression of Trp53 (C), Mdm2 (D), and Cdkn1a (E) were downregulated in *Mcm2*-knockdown cells under normoxia conditions. This effect was also observed under O_2 (FiO_2 = 0.4) conditions for Cdkn1a but not for Trp53 (G). The Delta CT method (CT value reference gene - CT value target gene) was used to calculate relative expression with respect to the reference gene, Hprt. Bars are represented as median with interquartile range from at least three independent biological experiments (N = 3-5/group). Statistical analysis: unpaired t-test. *p<0.05; **p<0.01. siRNA: *Mcm2*-knockdown. NTC: Non-targeting control. O_2: FiO_2 = 0.4 for 24 hours.

One-way ANOVA test with Tukey's test for multiple comparisons correction was used when comparing more than 2 groups.

4.2.1.5 Cell cycle arrest resulted in impaired developmental cell signaling and function

Previous studies have shown that severe hyperoxia treatment ($FiO_2 > 0.7$) leads to the upregulation of the canonical WNT/β-catenin signaling as well as the decrease of Pdgf-Rα-expressing fibroblasts (Riccetti et al., 2022; Sucre et al., 2020). Pdgf-Rα and PDGFA are necessary for alveologenesis to happen (Lau et al., 2011; Oak & Hilgendorff, 2017; Oak et al., 2017). Moreover, Pdgf-Rα expressing fibroblasts drive the process of secondary septation during the saccular and alveolar phase of lung development (Oak et al., 2017; Riccetti et al., 2022). Thus, decreases in Pdgf-Rα signaling lead to aberrant septation and changes in myofibroblast function (Riccetti et al., 2022).

The dysregulation of Wnt5a, a non-canonical WNT ligand, in the saccular phase decreased the differentiation of alveolar epithelial type I cells, myofibroblasts and endothelial cells, thereby blocking distal airway development (C. Li et al., 2020). Hif1a is another gene critical to normal lung development given its main role as oxygen sensor (Kirschner et al., 2022).

To assess the effects of cell cycle regulation on central developmental pathways and cell function in ATII cells and MFBs, the mRNA expression of genes such as *Wnt5a*, *Sftpc*, *Pdfra*, and Hif-1α was evaluated in *Mcm2*-knockdown cells in normoxia and hyperoxia ($FiO_2 = 0.4$). I demonstrated that these genes were significantly downregulated upon *Mcm2* knockdown in normoxia but the effect was not exacerbated by O_2 exposure (**Fig 4.9 A-D**). Addressing cell-function related genes, we observed that *Acta2* and *Spp1* were significantly downregulated in silenced cells as compared to the NTC under normoxia conditions (**Fig 4.9 E-F**). Given the downregulation of *Acta2* and *Spp1* in *Mcm2*-knockdown cells and previous observations by others of the effects of hyperoxia on fibroblast function (Riccetti et al., 2022), I assessed whether *Mcm2*-knockdown led to changes in fibroblast migration using the Boyden chamber assay. when culturing *Mcm2*-silenced cells and NTC controls on transwells, their capacity to migrate was assessed following 24 hours under normoxia. I observed decreased migration in *Mcm2*-silenced cells as compared to the normoxia NTC.

Interestingly, O_2 exposure did not aggravate the effect of *Mcm2*-silencing on cell migration. In consequence, we observed the impairment of developmentally relevant cell functions, *i.e.,* migration in addition to the decreased proliferation outlined above (**Fig 4.9 G**).

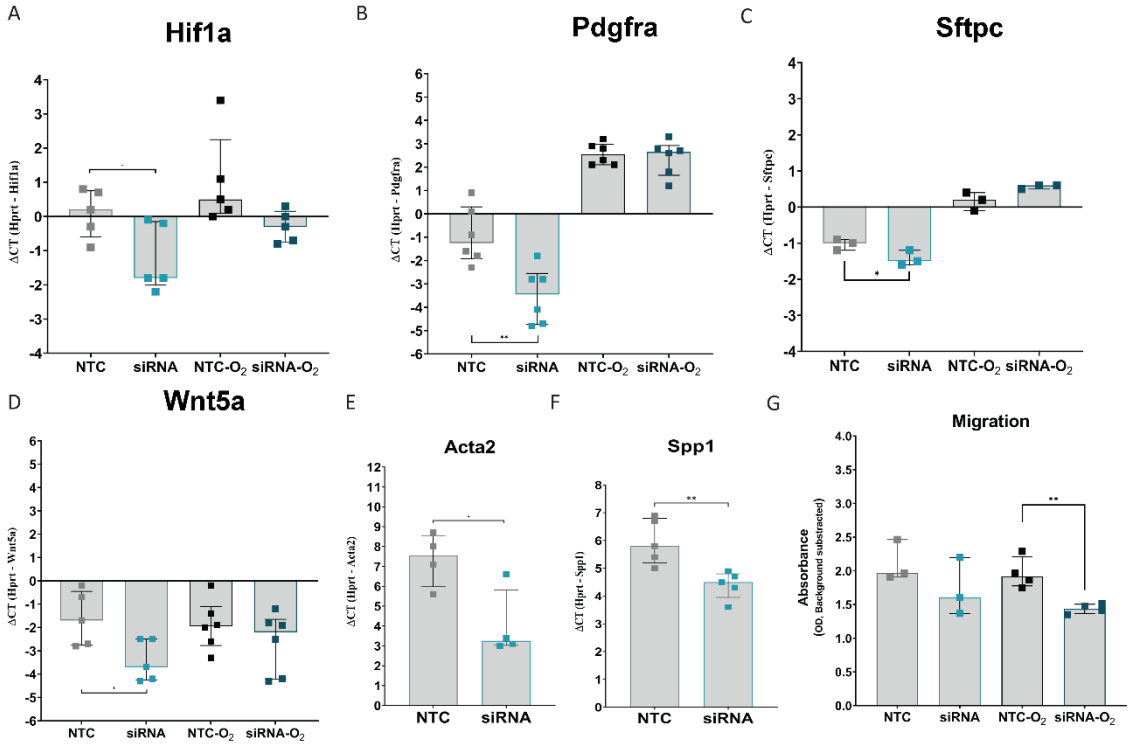

Fig 4.9: *Mcm2*-knockdown leads to gene expression changes in developmental genes, and alters cell migration

Under normoxia and hyperoxia, Hif1a was downregulated in *Mcm2*-knockdown cells (A). The mRNA expression of Pdgfra (B), Sftpc (in MLE12 cells) (SC), and Wnt5a (D) were downregulated in silenced cells under normoxia but not under hyperoxia. Functionally relevant genes Acta2 (E) and Spp1 (F) were downregulated in *Mcm2*-knockdown cells. The Boyden chamber assay showed that *Mcm2*-silenced cells had decreased migration, an effect aggravated by hyperoxia (G). Hprt was used as a reference gene. Bars are represented as median with interquartile range (N = 3-5/group). Statistical analysis: unpaired t-test. *p<0.05; **p<0.01. One-way ANOVA test with Tukey's test for multiple comparisons correction was used when comparing more than 2 groups. siRNA: *Mcm2*-knock out cells. NTC: Non-targeting control. O_2: FiO_2 = 0.4 for 24 hours. BER: Base-excision repair

4.2.1.6 Hyperoxia-induced cell cycle arrest is linked to DNA damage

Cell cycle progression into the S phase is critical for DNA repair. I hypothesized that the cell cycle arrest induced by hyperoxia could alter DNA damage response pathways (DDR) and DNA repair pathways. From our RNA-sequencing data, we learnt that DDR genes like Chk1 were significantly regulated. ATR-Chk1

regulation is expected given its role in responding to DNA damage resulting from hyperoxia exposure (Kulkarni & Das, 2008). Kulkarni et al. showed that 95% O_2 activated the ATR-Chk1 pathway *in vitro* (Kulkarni & Das, 2008). Here, our RNA-sequencing data and *in vitro* experiments suggest that even short-term, moderate O_2 leves (FiO_2 = 0.4) induce the ATR-Chk1 DDR pathway (**Fig 1.6**). The recruitment of the ATR-Chk1 complex to DNA damage sites is mediated by Apex2, a base excision repair (BER) protein (Willis et al., 2013). Thus, altered expression of any of these key genes would likely result in impaired DDR or DNA repair. The BER pathway has evolved to deal with oxidative stress damage. Among the main genes in this pathway are *Apex1, Apex2, Xrcc1, Neil1, Ung* and *Ogg1* (Willis et al., 2013). Furthermore, previous studies have shown an increase in 8-OxoG, an oxidative-stress DNA lesion that is primarily repaired by the BER pathway. Because of this close link between Chk1 and the BER pathway, and the potential role the BER pathway can play in the response to clinically relevant hyperoxia levels, I decided to study the changes in mRNA expression in genes associated with the DNA damage response and BER pathway. To address the consequences of clinical hyperoxia exposure in DDR and repair pathways, we first quantified the phosphorylation of H2A.X, a marker of DNA damage (**Fig 4.10 A**). H2A.X phosphorylation was increased in IMR-90 cells exposed to 24 hours of O_2 (FiO_2 = 0.4), although this increase did not reach statistical significance. Second, I studied the mRNA expression of critical DNA response and repair genes in *Mcm2*- knockdown CCL206 fibroblasts. We found that next to impaired developmental signaling, cell cycle arrest resulted in the downregulation of DNA damage and repair-related genes demonstrating the importance of cell-cycle-phase dependent gene expression and the potential role of Mcm2 in DDR (Ge & Blow, 2010; Kong et al., 2016; Kunnev et al., 2010)(**Fig 4.10 B-D**). *In vitro, Mcm-2* knockdown in CCL-206 cells revealed the upregulation of *Apex1* and *Xrcc1*, which happens in the presence of single strand breaks. Paradoxically, knockdown cells were exposed to O_2, this led to the downregulation of *Apex1* mRNA expression. In contrast, in the NTC-O_2 group, *Apex1* was upregulated compared to the expression in NTC cells that did not receive hyperoxia. These two findings suggest that cell cycle arrest makes the cells more vulnerable by causing aberrant DNA damage repair. In line with these data, *Xrcc1*, another important BER gene, was downregulated in *Mcm2*-knockdown cells exposed to

O_2. Although *Neil1* regulation followed a similar pattern to *Apex1*, the differences between groups did not reach statistical significance (**Fig 4.10 A**). Taken together, these results provide evidence that short exposure to clinically relevant levels of O_2 leads to DNA damage as well as aberrant DNA repair.

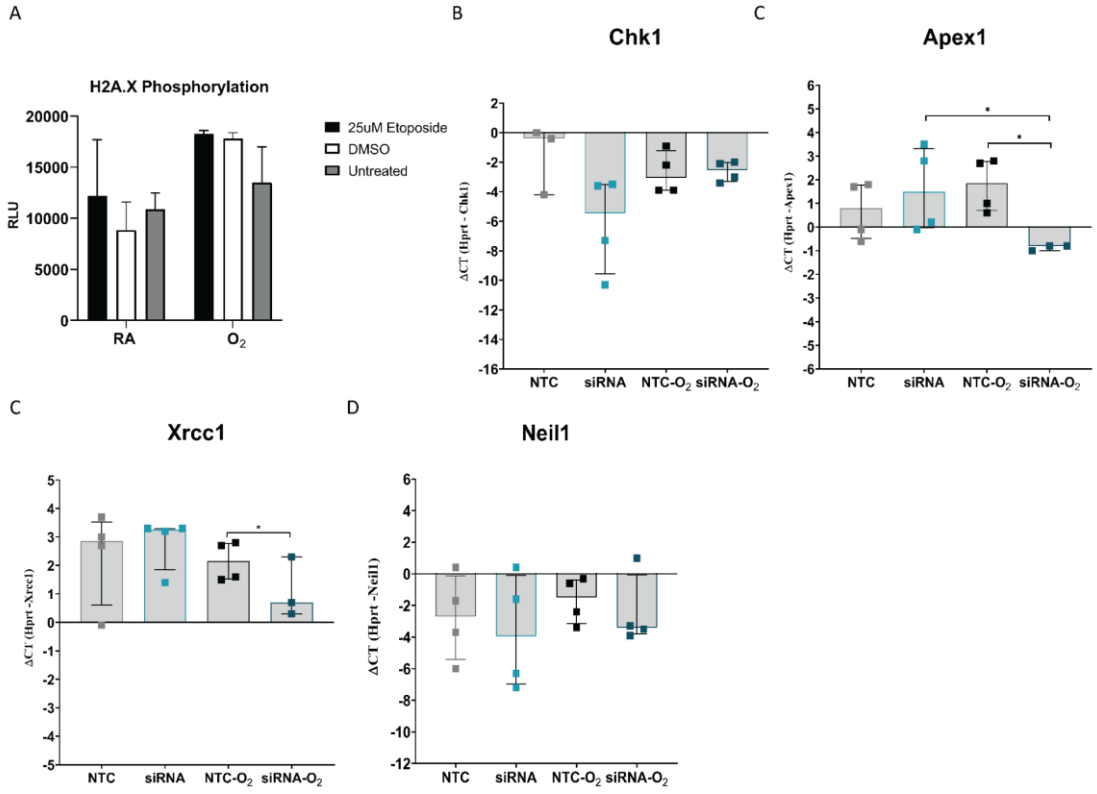

Fig 4.10: DNA damage and repair genes are downregulated in *Mcm2*-silenced cells. mRNA expression of Chk1 in *Mcm2*-silenced fibroblasts was downregulated when compared to the NTC under normoxia (A). Apex1 (B) and Xrcc1(C) BER pathway genes, were significantly downregulated in silenced cells in O_2 conditions. The mRNA expression of Neil1, showed a trend towards downregulation in *Mcm2*-knockdown cells both under normoxia and hyperoxia conditions (D). Hprt was used as reference gene. Bars are represented as median with IQR from at least three independent biological experiments. Statistical analysis: unpaired t-test. *p<0.05; **p<0.01. siRNA: *Mcm2*-knockdown. NTC: non-targeting control. O_2: FiO_2 = 0.4 for 24 hours. BER: Base-excision repair

4.2.1.7 Cell-specific effects of clinical hyperoxia

Next, we investigated the cell-specific biological responses in the three cell types (**Fig 4.10**). Here, enrichment analysis demonstrated small compound metabolic processes, and response to endoplasmic reticulum stress amongst the top 10 biological processes in AT2 cells (**Fig 4.10 A)**, whereas MFBs showed regulation of cellular component processes and energy-related metabolomic processes (**Fig**

4.10 B). Enrichment analysis of EC-specific regulated genes did not discover any biological processes.

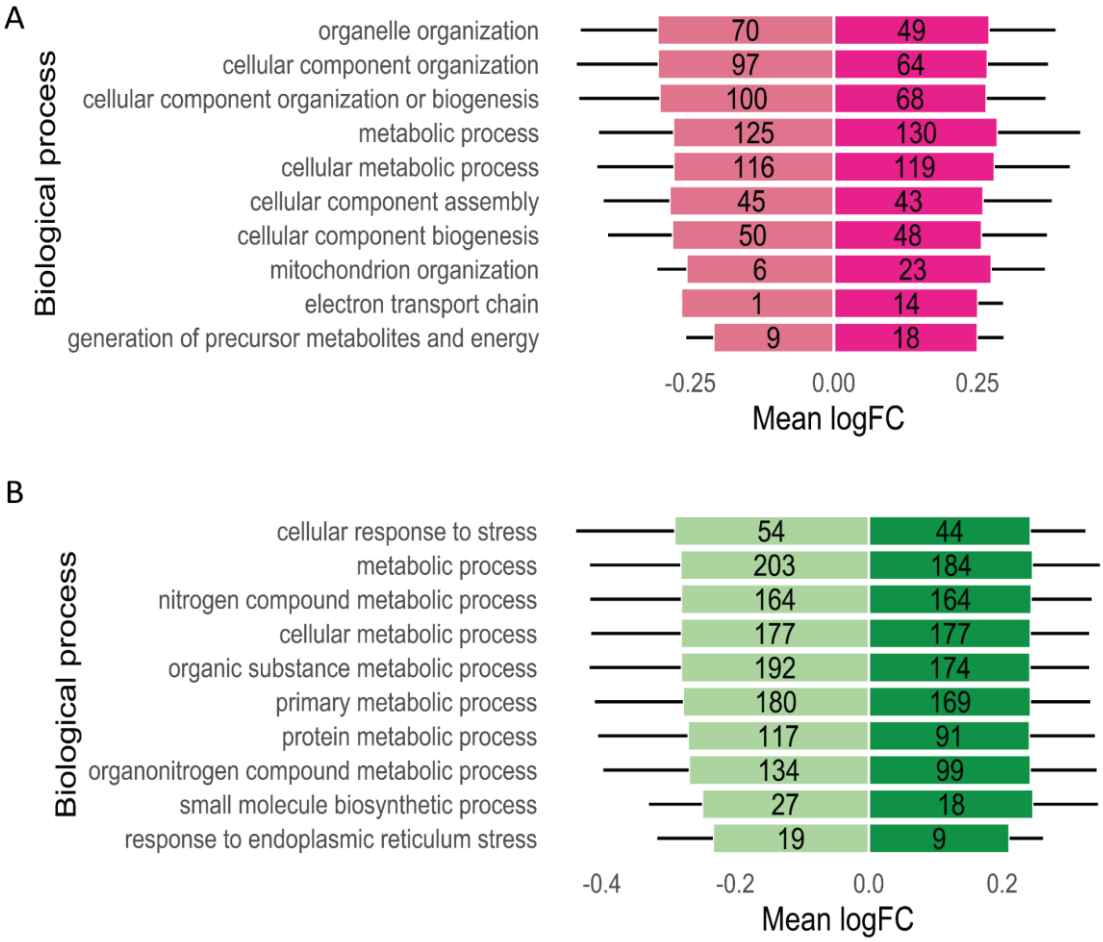

Fig 4.9: Cell-specific biological processes in MFB and AT2 cells

Top ten biological processes enriched in AT2 (A) cells and MFBs (B) with the number of genes representing upregulation or downregulation. The expression strength of each BP category detected was calculated as the mean log-fold change for up-and down-regulated genes. Gene

ontologies were deemed significantly enriched at an adjusted p-value of 0.05. AT2: alveolar epithelial cells. MFB: mouse fibroblasts. BP: biological process. FC: fold change.
This analysis was performed by Juan Henao and Benjamin Schubert, Institute of Computational Biology, Helmholtz Zentrum.

Collectively, the data showcase cell cycle regulation as a central part of the response to clinical hyperoxia in vitro.

4.2.2 Part2: *In vivo* short and long-term effects of clinical hyperoxia in the developing lung

4.2.2.1 Cell cycle arrest following clinical hyperoxia exposure in vivo

Most animal models used to study the consequences of hyperoxia (O_2) exposure on the developing lung have employed severe O_2 (Fi O_2 > 0.5) for several days and/or weeks (Hilgendorff et al., 2014; Thébaud et al., 2019). As our in vitro results demonstrated that 24 hours of clinically relevant hyperoxia (Fi O_2 = 0.4) led to a vast transcriptomic signature that leading to cell-cycle arrest. Thus, we hypothesized that short treatment (8 hours or 24 hours) of newborn mice with clinical O_2 concentrations results in cell cycle arrest and long-term changes in the lung. To test this hypothesis, I (1) determined whether O_2 (Fi O_2 = 0.4 I) in vivo leads to cell cycle arrest and alters cell cycle-phase dependent gene expression, i.e., DDR genes, DNA repair, and developmentally relevant pathways. After establishing the in vivo signature arising from short treatment with Fi O_2 = 0.4, I (2) I moved on to investigate sustained and long-term effects as well as their potential implications in development, DDR, and DNA repair. I last (3) investigated whether preceding injury with FiO_2 = 0.4 primes the lung to an altered response subsequent (second hit) injury.

To achieve the first aim, I treated C57BL/6 pups at postnatal day (PND) PND5-PND7 with clinically relevant hyperoxia levels (Fi O_2 = 0.4) for 8 or 24 hours and measured protein expression by immunoblotting and immunofluorescence (**Fig 4.11 A**). Protein lysates from lungs collected at the end of the experiment revealed that, in line with the in vitro results, p-Mcm2 protein levels were downregulated after 8 hours of O_2 treatment (Fig 4.11 B). I then validated this finding by immunofluorescence staining in Formalin-fixed paraffin-embedded (FFPE) lung sections from hyperoxia-exposed mice and normoxia littermate controls (**Fig 4.11 C**). In addition, critical cell cycle regulators Rb (retinoblastoma protein) and p21 were evaluated as well by measuring their phosphorylated protein concentrations. The dephosphorylation of p-Rb occurs in response to growth-inhibitory signals (**Fig 1.5**) (Riccetti et al., 2022).In whole lung lysates of mice exposed to 8 hours of clinical hyperoxia concentrations, I found the ratio of p-Rb to total Rb protein levels to be lower when compared to normoxia controls, indicating dephosphorylation of the Rb protein as a hallmark of cell cycle arrest (**Fig 4.11 D**). Interestingly, there was no difference between groups in levels of p-p21 protein at 8 hours. This likely due to p21 phosphorylation needing longer than 8 hours to be activated (some studies have reported a peak of p-p21 18 hours after genotoxic agent treatment (Dash & El-Deiry, 2005)) (**Fig 4.11 E**). Mirroring our in vitro findings, the changes occurred in the absence of classical apoptosis pathway activation after 8 hours of O2 treatment (**Fig 4.11 F**).

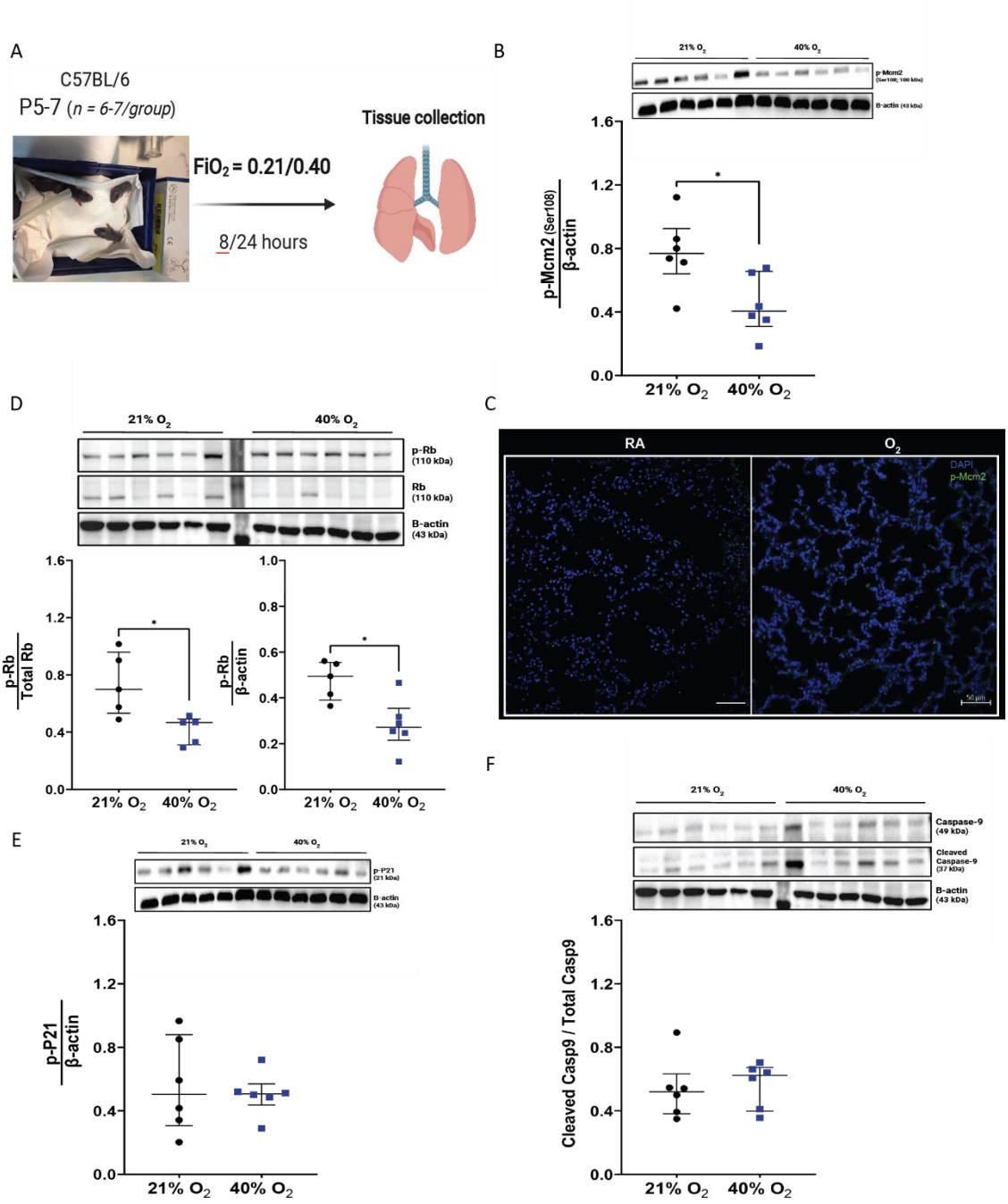

Fig 4.11: FiO_2 = 0.4 treatment for 8 hours triggered the activation of G1-cell cycle checkpoint regulators

Experimental design (A). By immunoblotting I demonstrated the protein downregulation of the p-Mcm2 (B), p-Rb and total Rb (D). No changes in p-p21 (E), and cleaved Caspase-9 and pro-Caspase-9 (F) were observed (representative images of immunoblots). Furthermore, the downregulation of p-Mcm2 was further validated by immunofluorescence staining in Formalin-fixed paraffin-embedded lung slides from mice pups treated with 8 hours of O_2 (FiO_2 = 0.4) showing downregulation in the O_2 group. Scale bars: 50 µm. Expression of p-Mcm2 was normalized with DAPI to obtain relative expression of p-Mcm2. p-Mcm2 and DAPI staining were quantified in the Image J software. Data are expressed as RFU per 100 nuclei. B-actin was used

as the loading control. Densitometric protein quantification bars are represented as median with interquartile range. Statistical analysis: unpaired t-test. *p<0.05.
Immunofluorescence staining was performed by Dr. Motaharehsadat Heydarian, postdoctoral fellow at the Comprehensive Pneumology Center, Hilgendorff lab.

4.2.2.2 Prolonged hyperoxia exposure aggravates lung signature of cell cycle arrest

To address whether prolonged O_2 exposure aggravated the effects observed after 8 hours, we then treated mice pups with FiO_2 = 0.4 for 24 hours. Spatial resolution of protein expression assessed by immunoblotting and immunofluorescence showed that 24-hour O_2 exposure significantly decreased the ratio of p-Mcm2 to total Mcm2. However, prolonged O_2 exposure did not aggravate the decrease in p-Mcm2 expression already observed at 8 hours (**Fig 4.12 A, B**). I next studied the expression of Chk1 and Cdk2. Chk1 is a key DNA damage response effector that is rapidly activated by ATR as a response to single-strand DNA damage. Moreover, Chk1 responds to genotoxic stresses in the S phase and by inducing Cdc25A degradation, leads to the decreased activity of the Cdk2/cyclin E or Cdk2/Cyclin A complex. Without the activity of Cdk2, the pre-replication complex (pre-RC) cannot be loaded onto chromatin to initiate replication (see **Fig 1.6** for more details) (Chou-Wei Chang, 2019; You et al., 2019). In O_2-exposed pups, it was revealed that while p-Chk1 lung protein expression was significantly increased (**Fig 4.12 C, D**), protein levels of Cdk2 were significantly lower compared to the control group (**Fig 4.12 E**). To maintain cells arrested in G1/S, the p53-mediated activation of p21/Cip1/WAF1 is required (Chou-Wei Chang, 2019). Like Chk1, p21/Cip1/WAF1 is also an inhibitor of Cdk2/cyclin complexes (see Fig 1.6 for more details). In contrast to the 8-hour time point, 24 hours O_2 resulted in an increase in p-P21 (**Fig 4.12 F**), providing further evidence of sustained cell cycle arrest in G1/S. Cleaved Parp is involved in apoptosis when cleaved by caspase-3 but also plays a role in the BER pathway.

Again, and although cleaved Parp was increased in the O2-exposed group (**Fig 4.12 G**), the protein expression of Caspase-3 was comparable between groups (**Fig 4.12 H**).

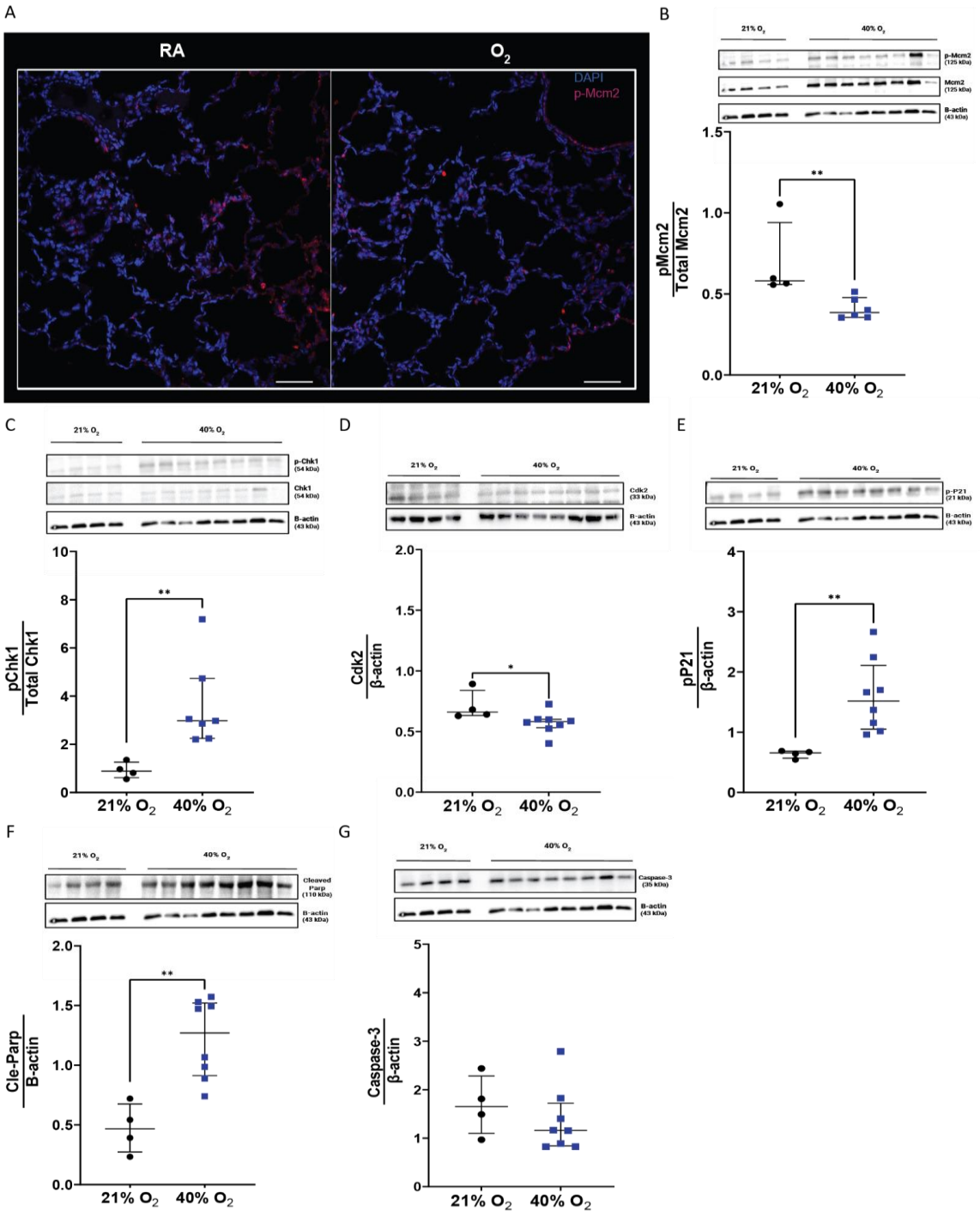

Fig 4.12: FiO_2 = 0.4 treatment for 24 hours triggered the activation of G1-cell cycle checkpoint regulators

Immunofluorescence staining of Formalin-fixed paraffin-embedded lung slices from PND5-7 mice pups treated with O_2 or room air for 24 hours showing decreased protein expression of p-MCm2 (representative image) (A). With immunoblotting (representative images of immunoblots), I measured the relative protein concentrations of p-Mcm2 (B), p-Chk1 (C), Cdk2 (D), p-p21 (E), cleaved Parp (F) and pro-Caspase-3 (G). B-actin was used as the loading control. Densitometric protein quantification bars are represented as median with interquartile range. Statistical analysis:

unpaired t-test. *p<0.05. Scale bars: 50 µm. Expression of p-Mcm2 was normalized with DAPI to obtain relative expression of p-Mcm2. p-Mcm2 and DAPI staining were quantified in the Image J software. Data are expressed as RFU per 100 nuclei.
Immunofluorescence staining was performed by Dr. Motaharehsadat Heydarian, postdoctoral fellow at the Comprehensive Pneumology Center.

These results not only validated the observed *in vitro* hyperoxia signature but suggest that even short exposures to moderate hyperoxia levels trigger cell cycle arrest and DNA damage response mechanisms.

4.2.2.3 Short-term treatment with clinically relevant hyperoxia provokes aberrant signaling in developmental pathways

In vitro, we found that the exposure to clinical hyperoxia levels (FiO_2 = 0.4) led to *Mcm2* downregulation and cell cycle arrest. From *Mcm2*- knockdown experiments, we concluded that cell cycle arrest led to decreased migration and aberration in developmental pathway gene expression *i.e.,* Pdgf-Rα, Hif-1α, and Wnt5a. In line with our findings, previous studies have shown that treatment with severe hyperoxia leads to the downregulation of Pdgf-Rα+ expressing fibroblasts and aberrations in Wnt-signaling. These pathways are then critical for alveolarization and lung development and repair (Riccetti et al., 2022). To investigate whether short-term exposure in vivo provoked changes in developmentally relevant pathways, I looked at the protein expression of Pdgf-Rα, eNOS, VE-cadherin, Hif-1α, and VEGFA in PND5-7 mice pups treated with FiO_2 = 0.4 / 0.21 for 8 hours that were sacrificed at the end of treatment (baseline) (**Fig 4.13 A**). 8 hours after exposure, we found no significant differences in protein expression between the O_2 and control groups in all (**Fig 4.13 B-F**) but one protein, VEGF-A (**Fig 4.13 G**). This result is notable given that the over-expression of VEGF-A during the period of postnatal adaptation can cause lung injury. Moreover, increased VEGF-A expression has been observed in the antiproliferative plexiform lesions in the lungs from newborns with persistent pulmonary hypertension (Tuder et al., 2001).

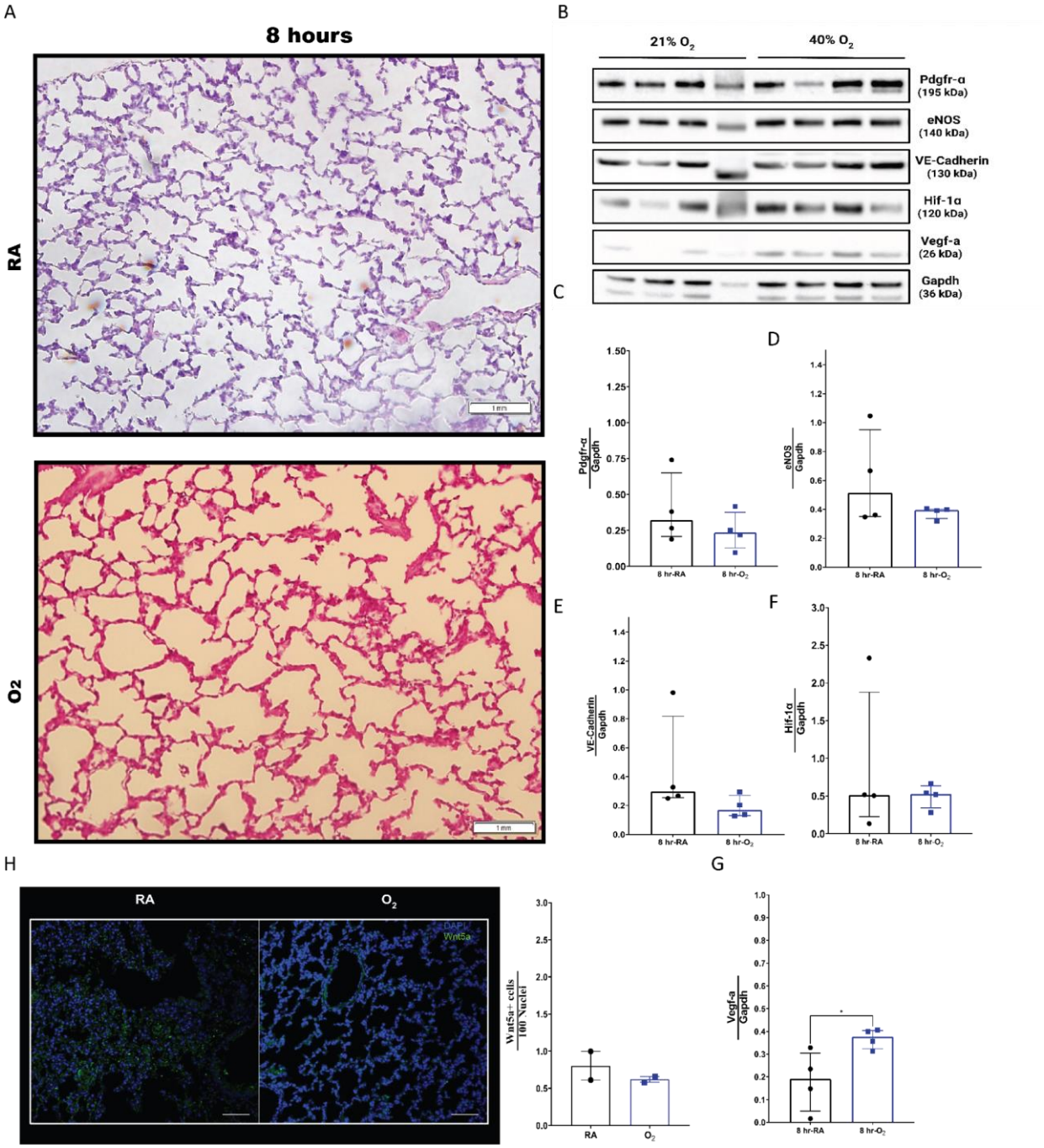

Fig 4.13: PND5-7-day mice treated with FiO_2 = 0.4 for 8 hours showed increased protein expression of VEGF-A.

H&E staining was performed on PND5-7 mouse lung sections after 8 hours of FiO_2 = 0.4/0.21 treatment (A). Scale bars = 1 mm. Representative immunoblot (B) of protein expression of Pdgf-Rα, eNOS, VE-Cadherin, Hif-1α, and VEGF-A. Densitometry protein quantification of Pdgf-Rα (C), eNOS (D), VE-Cadherin (E), Hif-1α (F), and VEGF-A (G). While VEGF-A protein expression was significantly upregulated in the hyperoxia group, the other target protein concentrations were similar between groups. Immunofluorescence staining of FFPE fixed newborn lungs (N = 2) after 8 hours of treatment showed a modest decrease in Wnt5a protein expression (representative image) (H). Scale bars: 50 uM. Expression of Wnt5a was normalized with DAPI to obtain relative

expression of Wnt5a. Gapdh was used as the loading control. Densitometric protein quantification bars are represented as median with interquartile range. Wnt5a and DAPI staining were quantified in the Image J software. Data are expressed as RFU per 100 nuclei. Statistical analysis: unpaired t-test. *p<0.05. H&E: hematoxylin and eosin. RFU: relative fluorescence units. *H&E staining was performed by former lab member, Dr. Nona Kampari. Immunofluorescence staining was performed by Dr. Motaharehsadat Heydarian, postdoctoral fellow at the Comprehensive Pneumology Center.*

In vitro, I demonstrated that 24-hour exposure to FiO_2 = 0.4 resulted in sustained changes in mRNA expression of developmentally relevant genes that were present four days after recovery in normoxia (**Fig 4.4 D, E; Fig 4.7**). To investigate long-term effects (LTE) after short-term exposure to clinically relevant levels (FiO_2 = 0.4), we exposed mice pups at PND5-7 to O_2 for 8 hours. After exposure, mice pups were returned to their mothers, weaned at the age of 3 weeks and maintained to grow for 18 months in room air **(Fig 4.14 A)**. We demonstrated that Pdgf-Rα protein expression was significantly downregulated in the O_2 group, an effect that was not evident immediately after exposure cessation (8-hour time point) **(Fig 4.14 B)**. This finding is in line with previous studies indicating that hyperoxia treatment decreases the populations of Pdgf-Rα expressing myofibroblasts (Riccetti et al., 2022). Regarding vessel marker expression, eNOS was significantly upregulated while VE-cadherin was significantly downregulated in the hyperoxia group despite no apparent differences between groups at baseline **(Fig 4.14 C, D)**. The upregulation of eNOS and the downregulation of VE-cadherin have been observed following acute lung injury (Yu et al., 2021). These results suggest that these mechanisms do not fully resolve and instead lead to long-term changes in the lung vasculature.

In contrast, Hif-1α protein expression was comparable between groups both at baseline and 18 months after treatment. However, this could be due to the observed variability in protein expression within groups **(Fig 4.14 E)**. VEGF-A was significantly upregulated in the hyperoxia group after exposure, but at 18 months, this difference was no longer statistically significant **(Fig 4.14 F)**. These results together demonstrate that exposure to O_2 provoke changes in developmentally relevant pathways that can be traced into adulthood and potentially lead to changes in lung development and repair mechanisms.

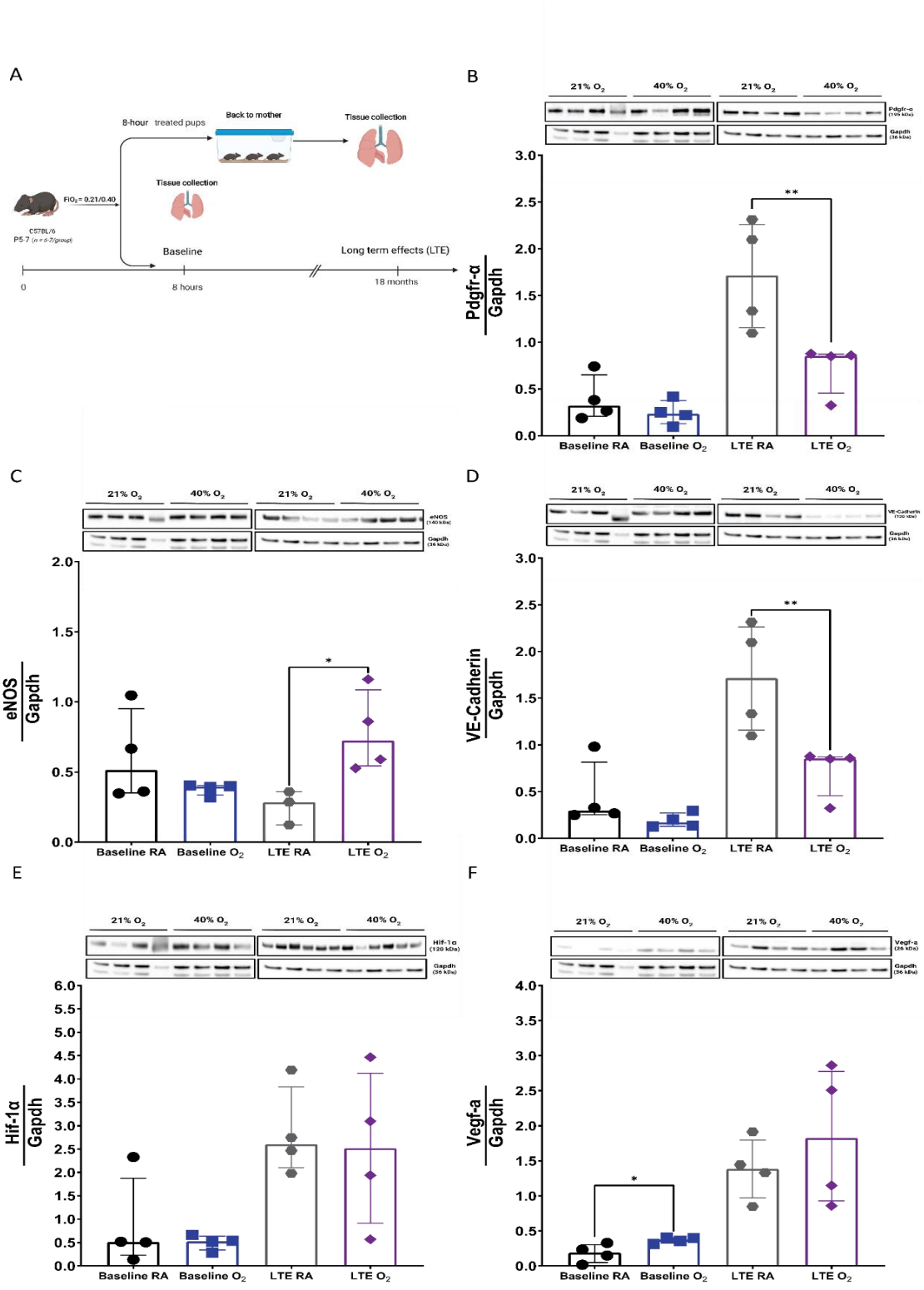

Fig 4.14: Eight hours of clinical hyperoxia treatment results in long-term changes in developmental pathways

Experimental animal model design of mice treated with FiO_2 = 0.4/0.21 for 8 hours (baseline) and long-term effect mice (LTE; mice treated as neonates and sacrificed 18 months after) (A). Densitometry quantification of Pdgf-Rα (B) and VE-Cadherin (D) showed significant downregulation of protein expression in the lungs of adult mice treated with O_2; (FiO_2; = 0.4) as neonates (representative immunoblot). Despite comparable protein expression at baseline between groups, eNOS protein expression was upregulated 18 months after treatment (C). Hif-1α was comparable between groups at both time points (E). VEGF-A protein levels were upregulated in the LTE O_2 group, but this increase was not statistically significant (F). Gapdh was used as the loading control. Densitometric protein quantification bars are represented as median with interquartile range. Statistical analysis: unpaired t-test. *p<0.05. **p<0.01 Baseline data can also be seen in **Fig 4.13 B-G.** FiO_2 = fraction of inspired oxygen. LTE: long-term effects (mice treated as pups but allowed to grow for 18 months after treatment). RA: room air. O_2: FiO_2 = 0.4. Some of these experiments were performed by Markus Koschlig, a former lab member.

4.2.2.4 Dynamics in transcriptional regulation in developmentally relevant genes

Studies in adult mice exposed as newborns to O_2 (FiO_2 = 0.4) for 8 hours (LTE group) revealed the abnormal regulation of several developmentally relevant proteins (**Fig 4.14**). However, immediately after 8-hour exposure, most of the investigated proteins were similarly expressed in O_2-treated and untreated mice. To explore this observation further, we also investigated the time-dependent changes in mRNA expression of genes that were shown to be altered *in vitro* after 24 hours of O_2 and in *Mcm2* knockdown cells (G1-cell cycle arrest). For this purpose, we treated PND5-7 mice pups with O_2 (FiO_2 = 0.4) or room air (FiO_2 = 0.21) for 24 hours. After treatment, a group of untreated and treated mice were immediately sacrificed while the rest returned to normoxia and were allowed to grow for three or seven weeks (**Fig 4.15 A**). At these timepoints, lungs were harvested and changes in target genes were evaluated by qPCR at the transcriptional level or with immunofluorescence at the protein level.

Reflecting what I observed in the mice exposed to O_2 for hours (**Fig 4.14**), three weeks after O_2 treatment, the mRNA expression of Pdgfra was comparable between groups. Furthermore, immunofluorescence staining of Pdgf-Ra in FFPE-fixed lungs showed only a small decrease in the O_2 group (D). Surprisingly, by the seven-week time point, there was a marked downregulation in both groups but more pronounced in the O_2 group leading to a statistically significant

difference between groups (A). Wnt5a gene expression was significantly upregulated at the three-week time point (B). However, Wnt5A protein expression showed a modest downregulation (E). Similar to Pdgfra, the mRNA expression of Wnt5a decreased in the control and O_2 exposed groups at the seven-week time point. However, only when comparing Wnt5a expression in the O_2 group at 7 weeks to that at 3 weeks (O_2 group), this difference was statistically significant. Although a reduction was observed in the RA group at seven weeks compared to at 3 weeks, this change was only modest. In line with my previous finding (**Fig 4.14**), Hif1a mRNA expression was comparable between groups at both time points. In summary, short-term exposure to O_2 on PND5-7 leads to sustained changes in Pdgfra and Wnt5a expression.

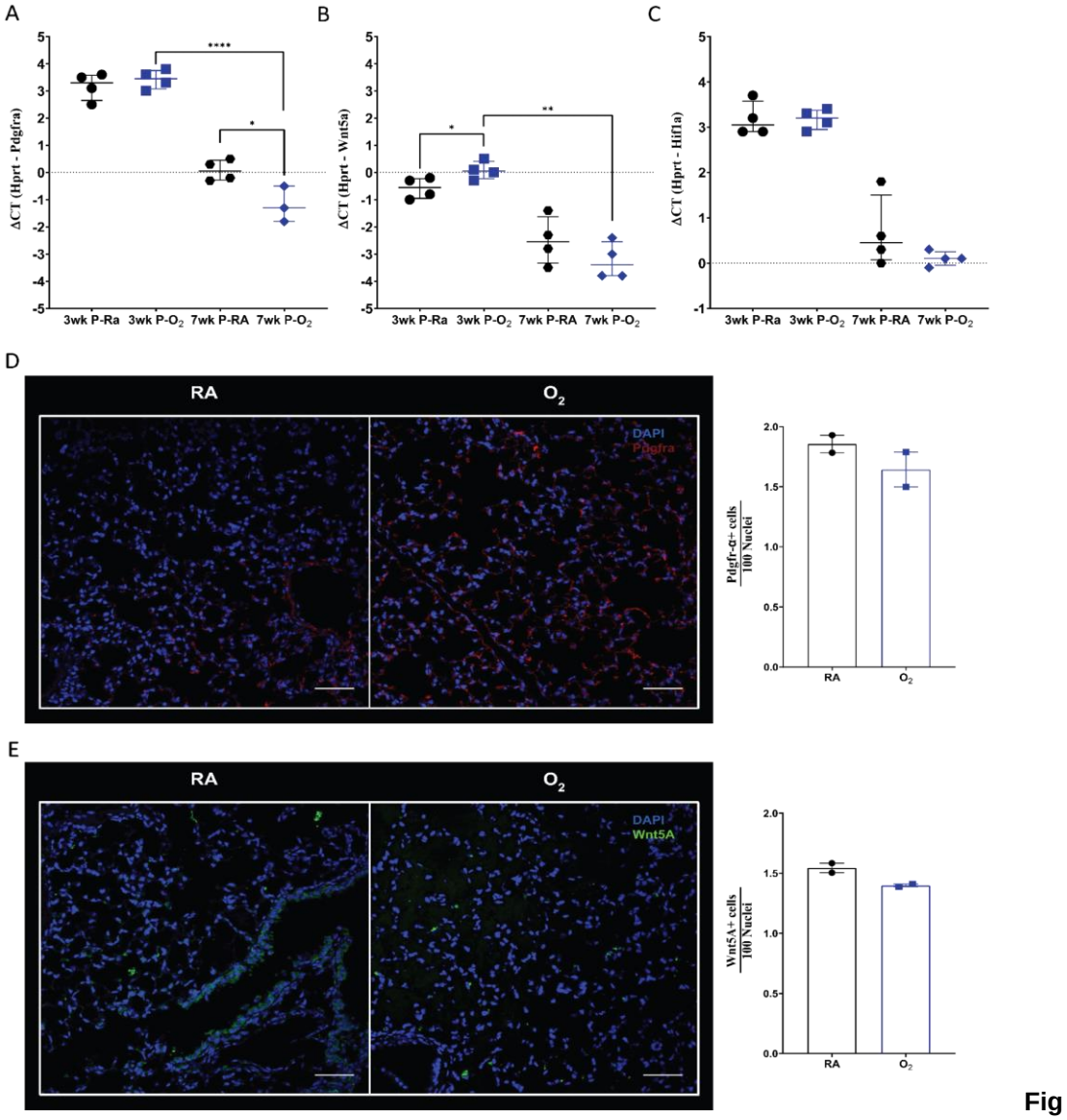

Fig 4.17: Sustained changes in developmental pathway genes is a hallmark of clinically relevant hyperoxia exposure in vivo

qPCR was used to quantitate the mRNA expression of Pdgfra (A), Wnt5a (B), and Hi1a (C) in whole-lung lysates from O_2-treated mice and controls harvested three and seven weeks after O_2 treatment. Hprt was used as a reference gene. Relative expression was calculated with the delta CT method (Hprt CT value - target gene CT value). Immunofluorescence staining (representative images) was performed to assess the protein expression of Pdgf-Rα (D) and Wnt5A (E) (N = 2). Scale bars: 50 µm. Expression of Pdgf-Rα and Wnt5A were normalized with DAPI to obtain the relative expression of each protein. Data are expressed as RFU per 100 nuclei. Quantification bars are represented as median with interquartile range. Statistical analysis: one-way ANOVA test with correction for multiple comparisons. *p<0.05. **p<0.01.***p<0.001. ****p<0.0001. qPCR: quantitative polymerase chain reaction. RFU: relative fluorescence units. 3/7wk P-RA: three- or seven-weeks post room air (controls). 3/wk P-O_2: three or seven weeks post-O_2 treatment. RFU: relative fluorescence units. *Immunofluorescence staining was performed by Dr. Motaharehsadat Heydarian, postdoctoral fellow at the Comprehensive Pneumology Center.*
In vivo experiments were performed in collaboration with Dr. Heiko Adler and Anna Dmitrieva, Ph.D. candidate

4.2.2.5 Sustained changes in DNA damage and repair mechanisms

In vitro, I showed that cell cycle arrest in Mcm2- knockdown cells was causally linked to the downregulation of DNA-damage response (DDR) genes, Trp53 and Cdkn1a (**Fig 4.8**), and base-excision repair (BER) pathway genes, Apex1 and Xrcc1 (**Fig 4.10**). Moreover, *in vivo*, I demonstrated that treatment with $FiO_2 = 0.4$ for 8 hours and 24 hours leads to the activation of cell-cycle checkpoint regulators and triggers the DNA damage response in the absence of classical apoptosis (**Fig 4.11; Fig 4.12**). In contrast to these results, I hypothesized that short-term treatment (24 hours) with clinically relevant hyperoxia concentrations ($FiO_2 = 0.4$) results in sustained alterations in DNA-damage-related pathways. To test this hypothesis, we treated PND5-7 mice pups with hyperoxia (O_2: $FiO_2 = 0.4$) or room air for 24 hours. After treatment, a group of untreated and treated mice were immediately sacrificed while the rest returned to normoxia and were allowed to grow for three or seven weeks (**Fig 4.15 A**). At these timepoints, lungs were harvested and changes in target genes were evaluated by qPCR at the transcriptional level or with immunofluorescence at the protein level.

First, we studied DDR effector genes. As shown before (**Fig 4.12**), following 24 hours of O_2 treatment, we observed that the protein expression of p-p21 and p-Chk1 were significantly upregulated in the O_2 group (**Fig 4.12 B-D**). Here, we

observed that 24 hours of O_2 treatment led to a notable increase in H2.ax protein expression in the lungs of pups sacrificed immediately after treatment (**Fig 4.15 B)**. Against our expectations, in the O_2 group, we did not observe any differences between groups in 8-oxoG, a common DNA lesion that results from reactive oxygen species (Lio & Rao, 2019; Lorente-Pozo et al., 2020; Sejersted et al., 2009; Weber et al., 2016) (**Fig 4.15 C)**. Then, we studied the mRNA expression changes in key DDR genes, Cdkn1a and Chk1. We observed that the mRNA expression of Cdkn1a was comparable between groups three weeks after O_2 treatment cessation. However, seven weeks after treatment, it was significantly downregulated in the O_2 group (**Fig 4.15 D**). In contrast, Chk1 was still upregulated at the transcriptional level three weeks following O_2 treatment, but seven weeks after treatment, no differences between groups were detectable (**Fig 4.15 E**).

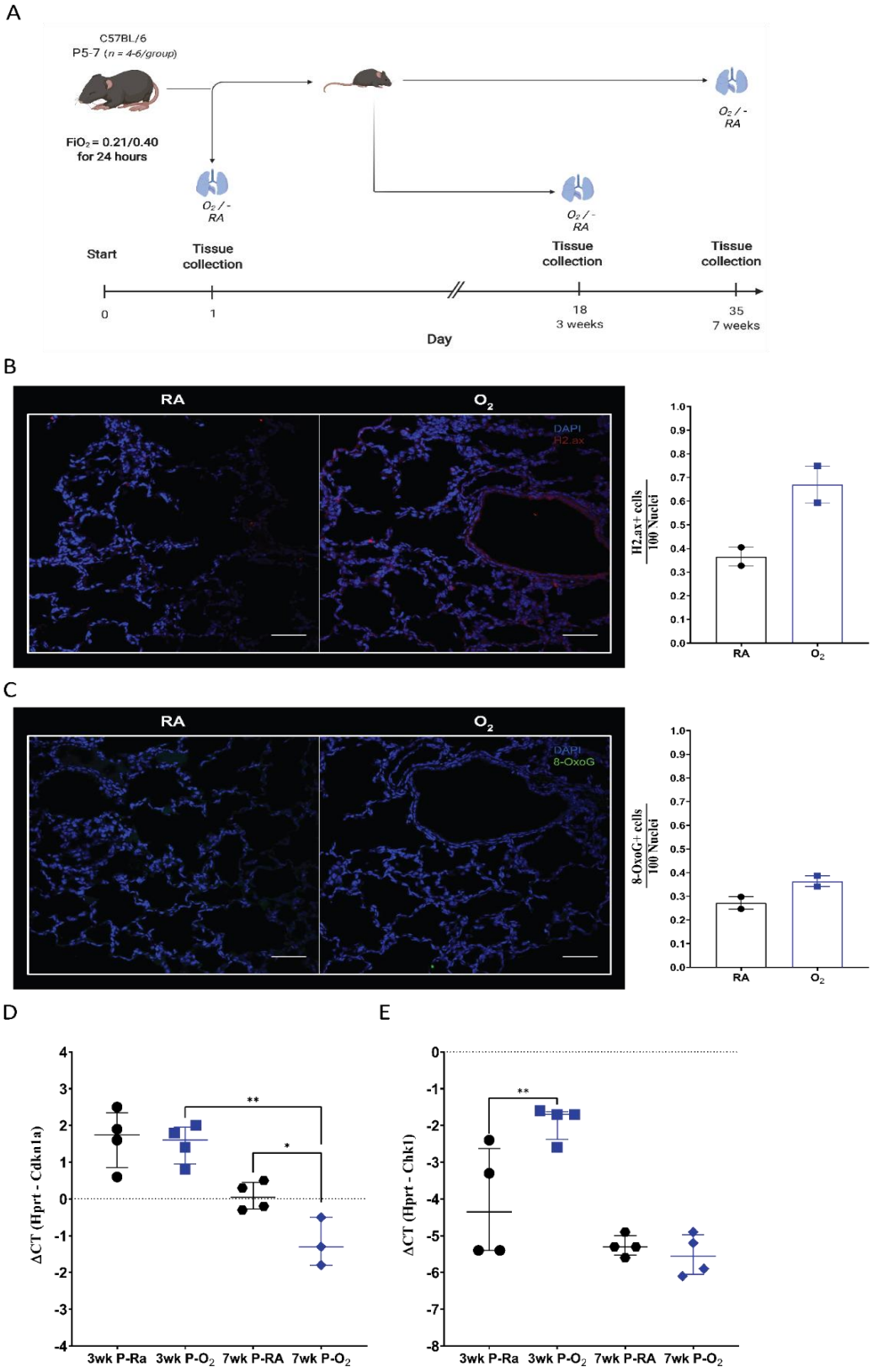

Fig 4.15: Hyperoxia treatment led to sustained dysregulation of DNA-damage response genes

Experimental design (A). Immunofluorescence staining (representative images) of p-H2A.X (B) and 8-OxoG (C) revealed higher DNA damage in mice treated with FiO_2 = 0.4 for 24 hours (N = 2). Scale bars: 50 µm. Expression of H2A.X and 8-OxoG were normalized with DAPI to obtain

relative expression of each protein. Data are expressed as RFU per 100 nuclei. qPCR was used to quantitate the mRNA expression of Cdkn1a (D), and Chk1 (E) in whole lung lysates from O_2-treated mice and controls harvested three and seven weeks after O_2 treatment. Hprt was used as a reference gene. Relative expression was calculated with the delta CT method (Hprt CT value - target gene CT value). Quantification bars are represented as median with interquartile range. Statistical analysis: one-way ANOVA test with correction for multiple comparisons. *p<0.05. **p<0.01. qPCR: quantitative polymerase chain reaction. RFU: relative fluorescence units. 3/7wk P-RA: three- or seven-weeks post room air (controls). 3/wk P-O_2: three or seven weeks post-O_2 treatment. RFU: relative fluorescence units. *Immunofluorescence staining was performed by Dr. Motaharehsadat Heydarian, postdoctoral fellow at the Comprehensive Pneumology Center.*
In vivo experiments were performed in collaboration with Dr. Heiko Adler and Anna Dmitrieva, Ph.D. candidate

To investigate the changes in DNA repair, we studied alterations in BER pathway genes (**Fig 4.16**). Based on our previous in vitro findings, we expected to find sustained changes in the expression of BER pathway genes. Three weeks after O_2 treatment, Apex1 mRNA expression was significantly upregulated but by week seven downregulation of Apex1 mRNA expression occur returning the expression of this gene to baseline levels (**Fig 4.16 A**). Xrcc1 was significantly upregulated in the O_2 group three weeks after treatment (**Fig 4.16 B**). However, immunofluorescence staining did not reveal any differences between groups suggesting that this regulation is happening primarily at the transcriptional level (**Fig 4.16 C**). Notably, seven weeks after treatment, Xrcc1 mRNA expression was significantly lower compared to that of the control group, and to the three-week Xrcc1 mRNA expression in the O_2 group (**Fig 4.16 B**). I also investigated the mRNA expression dynamics of two other BER genes, Ung1 and Ogg1 (**Fig 4.16 D, E**). Both Ung1 and Ogg1 were upregulated in the O_2 group three weeks after treatment however not in a statistically significant manner. Seven weeks after treatment, the mRNA expression of both genes was comparable between groups. However, from week three to seven there was a statistically significant decrease in the mRNA expression of Ung1 and Ogg1 in the O_2 group suggesting the expression of these genes returned to baseline levels. Given the modest increase in 8-oxoG 24 hours after O_2 treatment, the increase in Ogg1 mRNA expression by the three-week time point and its return to baseline go in line with that result.

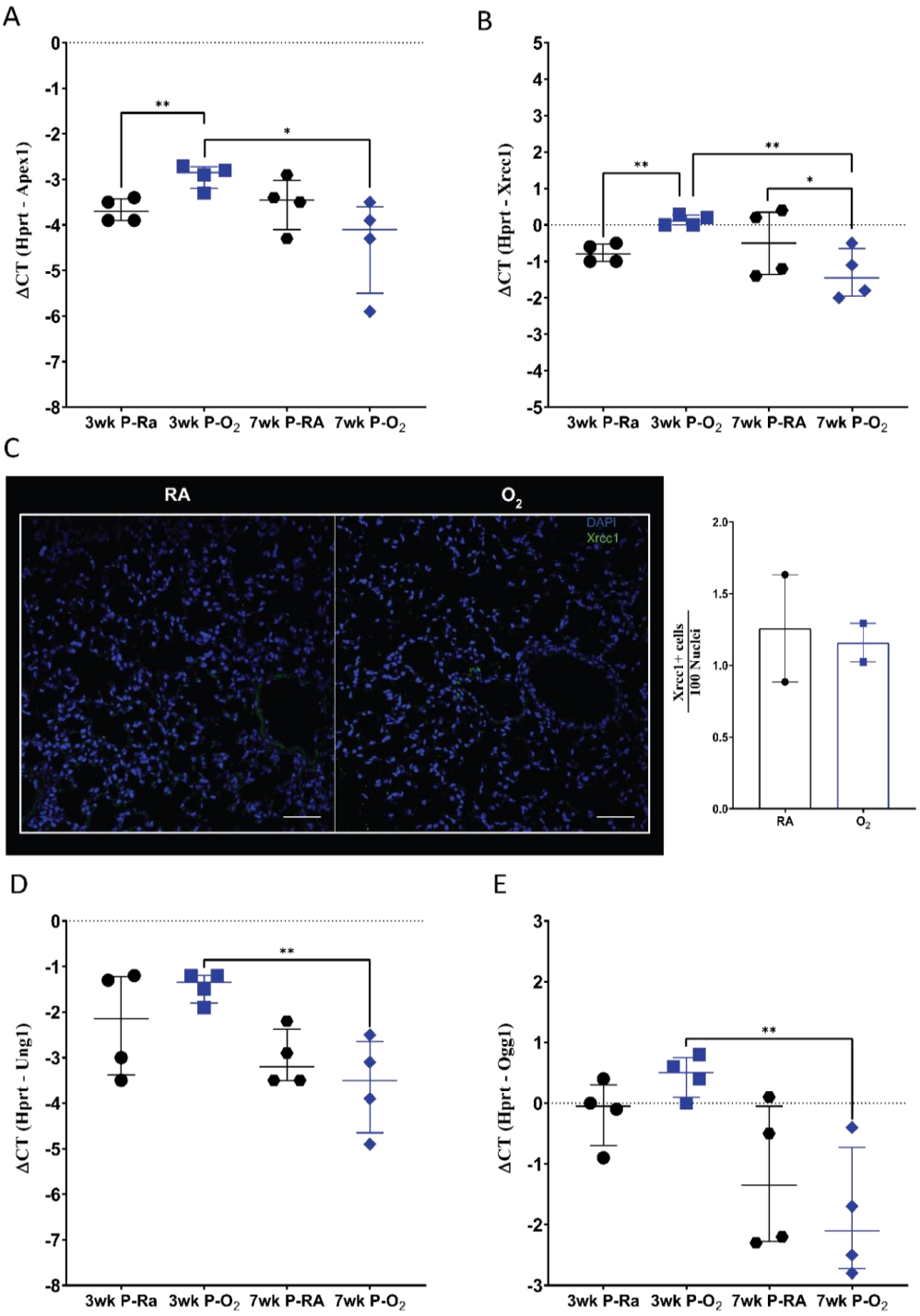

Fig 4.16: Hyperoxia treatment triggered long-term dysregulation in BER pathway genes
qPCR was used to quantitate the mRNA expression of Apex (A), Xrcc1 (B), Ung1 (D) and Ogg1 (E) in whole lung lysates from FiO_2 = 0.4-treated mice and controls harvested three and seven weeks after treatment. Hprt was used as a reference gene. Relative expression was calculated with the delta CT method (Hprt CT value - target gene CT value). Immunofluorescence staining of O_2-treated FFPE fixed newborn lungs (N = 2) harvested three weeks after treatment revealed a modest decrease in Xrcc1 protein expression (representative image) (H). Scale bars: 50 µm. Expression of Xrcc1 was normalized with DAPI to obtain relative expression of Xrcc1. Data are expressed as RFU per 100 nuclei. Quantification bars are represented as median with

interquartile range. Xrcc1 and DAPI staining were quantified in the Zen software. Statistical analysis: one-way ANOVA test with correction for multiple comparisons. *p<0.05. **p<0.01. qPCR: quantitative polymerase chain reaction. RFU: relative fluorescence units. 3/7wk P-RA: three- or seven-weeks post room air (controls). 3/wk P-O_2: three or seven weeks post-O_2 treatment. *Immunofluorescence staining was performed by Dr. Motaharehsadat Heydarian, postdoctoral fellow at the Comprehensive Pneumology Center.*
In vivo experiments were performed in collaboration with Dr. Heiko Adler and Anna Dmitrieva, Ph.D. candidate

To investigate whether the dysregulation of the DDR response and BER genes resulted in increased DNA damage long-term, we studied the presence of DNA damage in mice that were exposed to O_2 for 8 hours on PND5-7 and sacrificed as 18-month-old adults (LTE). By immunofluorescence staining, we measured the lung protein expression of p-H2A.X. The phosphorylation of H2A.X occurs in the presence of single strand and double strand DNA damage (Kulkarni & Das, 2008) (**Fig 4.17 A, B**). Here I found that p-H2A.X was more expressed in the lungs of mice that were treated with O_2 although it was not statistically significant. In line with this finding, the TUNEL assay, which also detects DNA damage, further corroborated that mouse lungs from the O_2 group presented with significantly more DNA damage than mouse lungs from the control group ($p<0.001$).

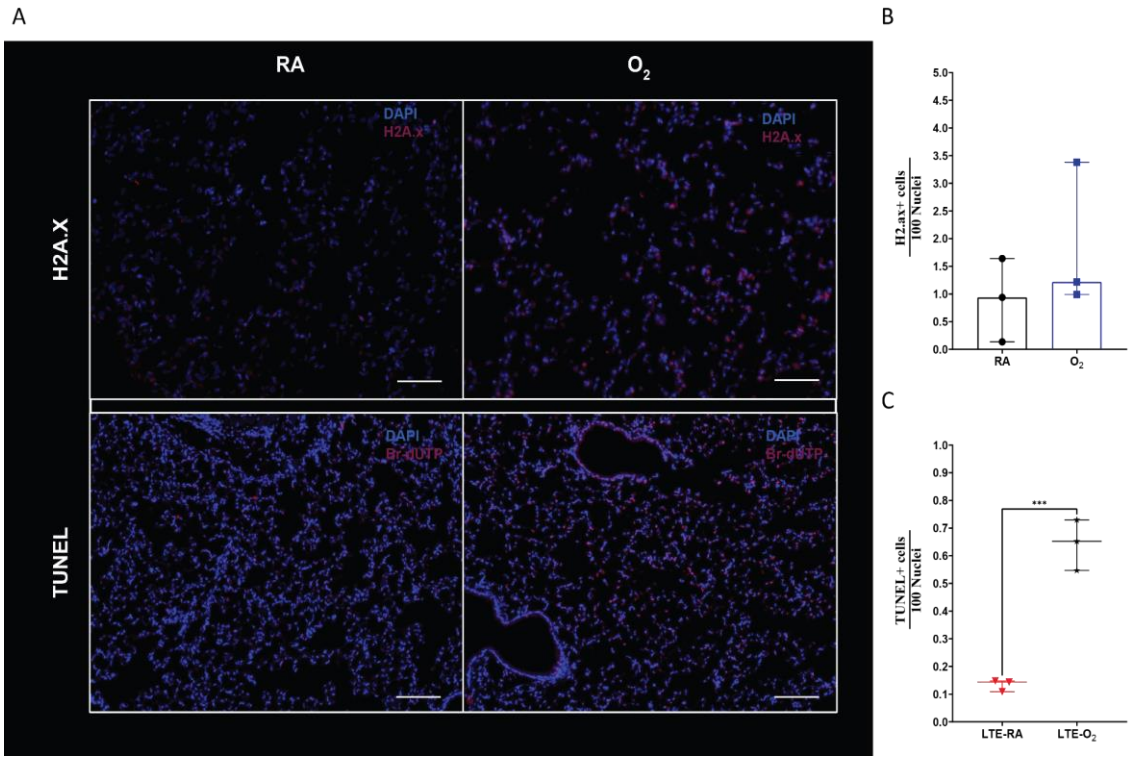

Fig 4.17: DNA damage was increased in 18-month-old adult mice that were treated as neonates with FiO_2 = 0.4 for 8 hours

Immunofluorescence staining of O_2-treated FFPE fixed newborn lungs (N = 3) harvested 18 months after O_2 treatment revealed an increase in p-H2A.X protein expression (representative image). Likewise, the TUNEL assay, also indicative of DNA damage, revealed a much higher number of TUNEL+cells in the O_2 group ($p<0.001$) (A). Scale bars: 50 µm. Expression of p-H2A.X or Br-dUTP was normalized with DAPI to obtain the relative expression of each target. Data are expressed as RFU per 100 nuclei. Quantification bars are represented as median with interquartile range. p-H2A.X and Br-dUTP and DAPI staining were quantified in the Image J Fiji software. Statistical analysis: Student t-test. ***$p<0.001$.

Because of the previously presented data indicating a sustained dysregulation of the BER repair pathway, we explored the ten-eleven translocation (TET) enzyme-mediated DNA demethylation reactions given the intricate mechanism that exists between the TET enzyme pathway and the BER pathway (Bochtler et al., 2017; Mahfoudhi et al., 2016; Rasmussen & Helin; Weber et al., 2016). TET enzymes catalyze the hydroxylation of DNA intermediates 5-methylcytosine (5mC) to 5-hydroxymethylcytosine (5hmC), and the oxidation of 5hmC to 5-formylcytosine (5fC) and then to 5-carboxycytosine (5caC) (Bochtler et al., 2017; Rasmussen & Helin; Weber et al., 2016). 5fC and 5caC can be removed from the DNA base sequence by base excision repair (BER) and replaced by cytosine in the base sequence. Ogg1 recruits TET1 when reactive oxygen species have acted on

guanine leading to 8-hydroxy-2'-deoxyguanosine (8-OHdG or its tautomer 8-oxo-dG). The recruitment of TET1 facilitates the start of the demethylation pathway (Rasmussen & Helin).

We measured the intermediates of DNA demethylation in newborn (PND5-PN7) mice pups treated with O_2 (FiO_2 = 0.4) for 8 hours and sacrificed immediately, 18-month-old adult mice treated with O_2 as neonates and adult mice treated with O_2 for 8 hours and sacrificed immediately after treatment. At the end of the experiment, lungs were harvested and processed for protein analysis by mass spectrometry (**Fig 4.18**). This analysis revealed that the levels of all intermediates of DNA methylation were downregulated in newborn pups treated with O_2 and sacrificed immediately after treatment. Levels of cadC were dramatically downregulated in adult mice treated with O_2 as newborns. This could have resulted from decreased enzymatic activity in the TET system that catalyzes the conversion from fdC to cadC (Mahfoudhi et al., 2016; Rasmussen & Helin). In adult mice treated as adults, there was an increase in 8-oxo-dG of about 40% whereas the levels in newborn mice showed almost no change. Unexpectedly, in adult mice treated as newborns, the levels of 8-oxo-dG were 60% lower. This downregulation could have resulted from the activation of other DNA repair mechanisms other than the BER pathway (Higgs et al., 2021) (**Fig 4.18 A**). Moreover, both in old mice and adult mice treated as neonates, there was an increase in mdC and nmdC levels accompanied by decreasing dfC and cadC levels. This pattern suggests a potential epigenetic link between short-term O_2 treatment and the resulting effects.

These data not only provide further evidence that O_2 treatment as newborns leads to long-term consequences in DNA repair pathways but also point to epigenetic regulation as an underlying mechanism.

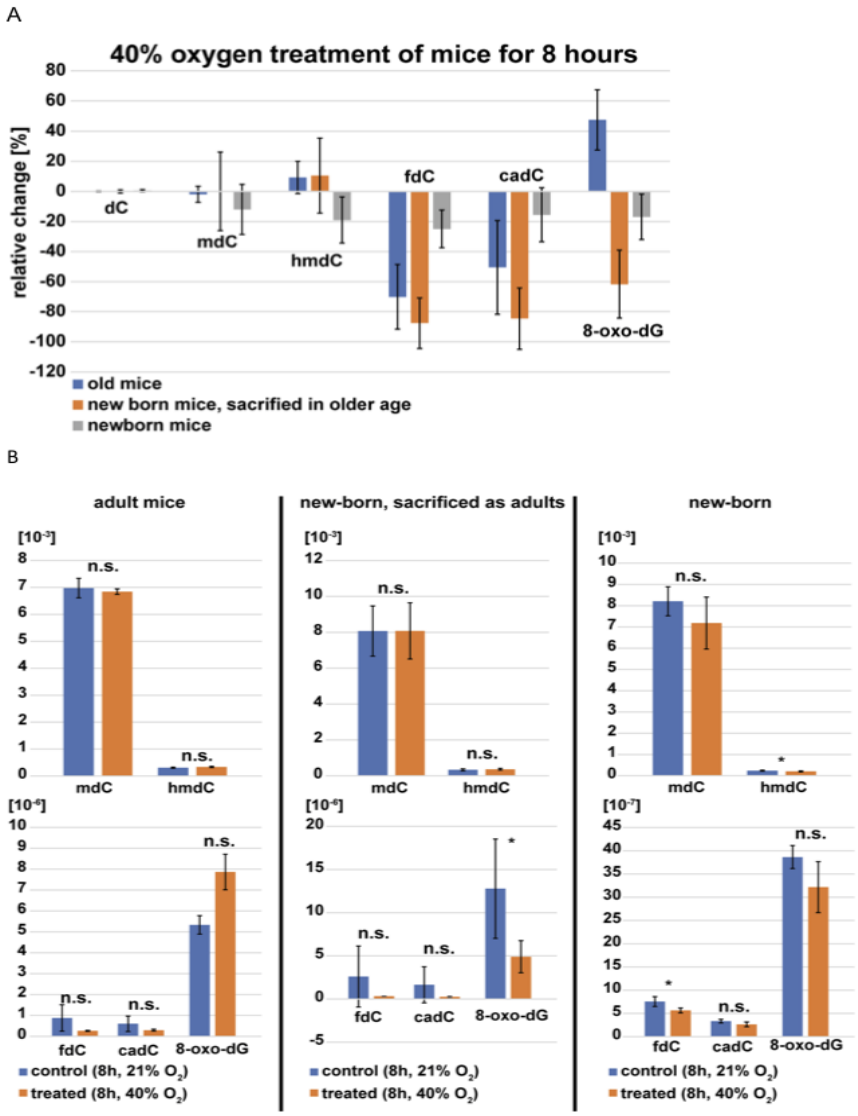

Fig 4.18: Mass-spectrometry analysis of DNA methylation intermediates

DNA methylation intermediates normalized to controls were measured by LC-MS/MS (A). Comparison of treated and control levels for each methylation intermediate measured (B). Graphs show data of three different conditions from different biological replicates (N = 3-6/ group) measured as technical duplicates. Comparison Bars show mean, error bars show standard deviation (s.d.). (Students t-test, Two-sample t-test assuming equal variances. *p < 0.05.

This analysis was performed in collaboration with Florian Schelter, PhD candidate and Dr. Markus Müller, member of Prof. Thomas Carell lab.

4.2.2.6 Double hit injury in newborn mice undergoing clinical hyperoxia exposure and virus infection

I have demonstrated that short-term O_2 ($FiO_2 = 0.4$) treatment *in vitro* and *in vivo* leads to aberrations in the DDR response, DNA repair, and developmental

pathway signaling. Remarkably, many of these changes persist several weeks after exposure cessation. In the clinical setting, premature babies spend several days in intensive care and are at high risk of complications like bacterial or viral infections (Buczynski et al., 2013; Sucre et al., 2020). Understanding whether and how previous short-term hyperoxia treatment increases the risk of future complications paves the way for the identification of targets with therapeutic potential. Parting from these observations, we hypothesized that hyperoxia treatment primes the neonatal lung and increases its vulnerability to a second-hit injury. To test this hypothesis, we exposed newborn mice at PND5-7 to O_2 for 24 hours and returned to room air after treatment cessation. One week later, in a randomized manner, mice were subjected to intranasal inoculation with the MHV-68 herpes virus or 0.89% saline solution (controls). The mice were then sacrificed on week three or seven after the initial O_2 treatment (**Fig 4.18 A**). *In vivo experiments were performed in collaboration with Dr. Heiko Adler and Anna Dmitrieva, Ph.D. candidate, Comprehensive Pneumology Center, Helmholtz Zentrum, Munich.*

We started our investigations by studying histology changes in the lung (**Fig 4.18 B**). At three weeks, mice treated with FiO_2 = 0.4 showed signs of airway simplification and remodeling and enlargement of air spaces. However, by seven weeks, only mild differences between O_2 and RA groups were evident. Infected lungs with or without hyperoxia showed signs of ongoing inflammation at both time points. In contrast to the groups that received O_2 or virus infection only, in the O_2+virus group the airspace area was still enlarged seven weeks after the first hit.

A

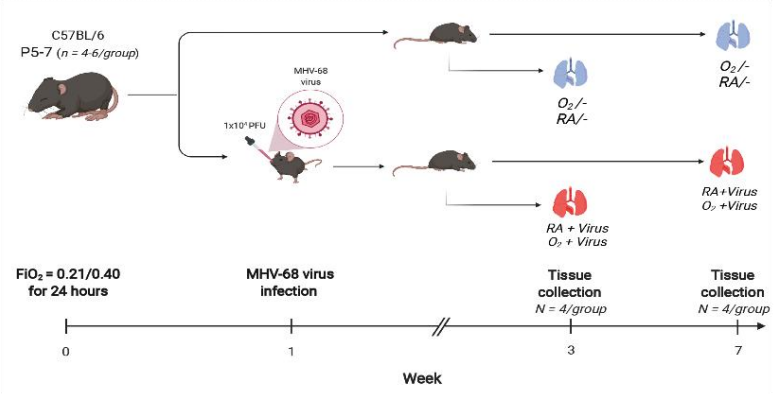
C57BL/6
P5-7 (n = 4-6/group)
MHV-68 virus
1x10⁵ PFU
O2/-
RA/-
O2/-
RA/-
RA+Virus
O2 +Virus
RA + Virus
O2 + Virus
FiO2 = 0.21/0.40
for 24 hours
MHV-68 virus
infection
Tissue
collection
N = 4/group
Tissue
collection
N = 4/group
0
1
3
7
Week

B

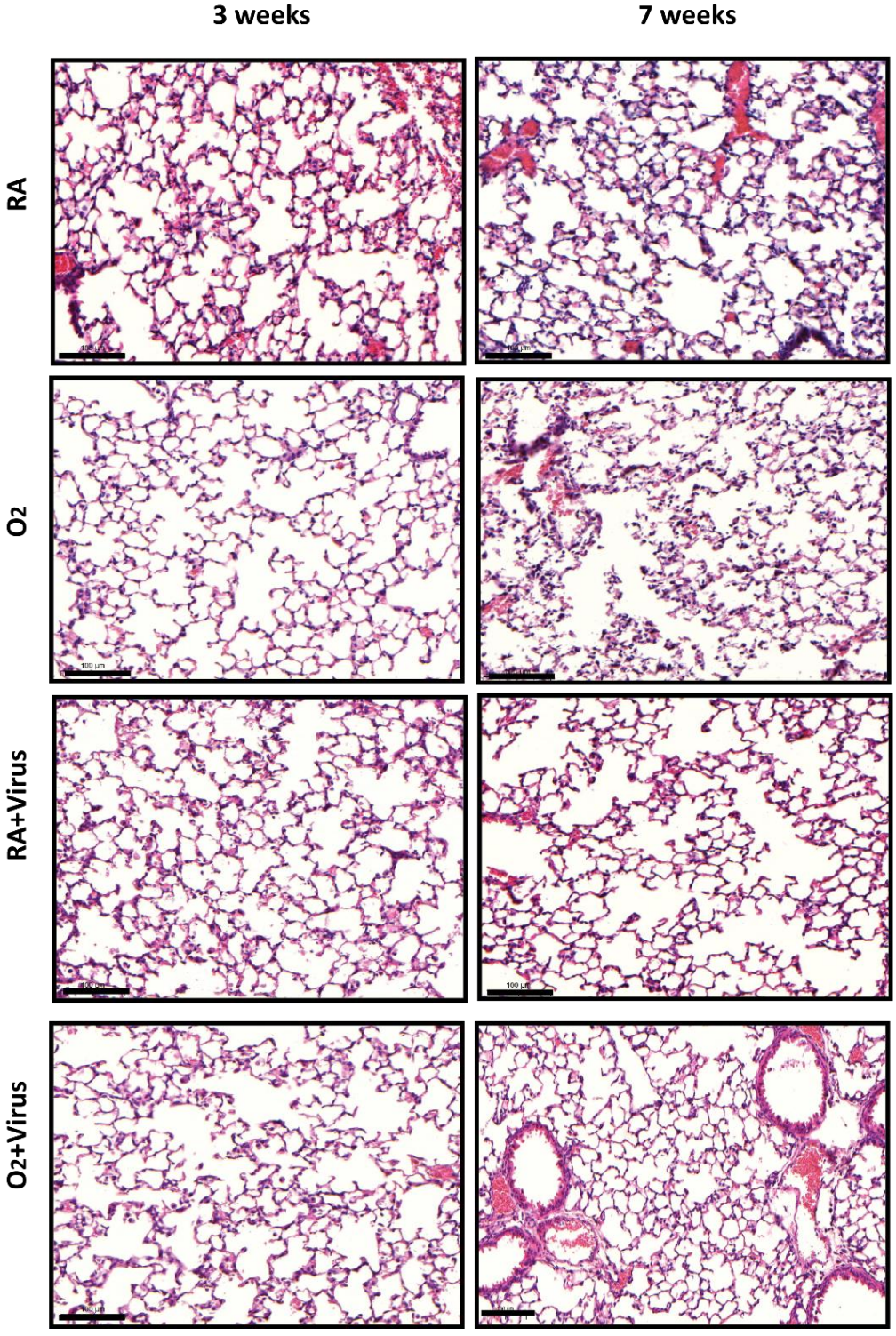
3 weeks
7 weeks
RA
O2
RA+Virus
O2+Virus

Fig 4.18: A mouse model of hyperoxia and subsequent herpes virus infection
Experimental design. PND5-7 mice pups were given an initial hit with O_2 (FiO_2 = 0.4) or room air (RA). One week after the initial hit, the second hit was induced by inoculating mice intranasally with the MHV-68 herpes virus. Three or seven weeks after the first hit, lungs were harvested for analysis (A). H&E staining of lung sections of RA controls, O_2 treated mice, RA+ MHV-68 virus infection, and O_2+ MHV-68 virus infection on weeks 3 and 7 after O_2 treatment (B). Scale bars: 100 µm.

4.2.2.6.1 O_2 priming alters the regulation of developmentally relevant genes following a second hit with viral infection

In section **4.2.2.3,** I showed that Pdgf-Rα protein expression was markedly downregulated in 18-month-old mice that were treated as neonates with FiO_2 = 0.4 for 8 hours. In addition, vascular factors like VE-cadherin and eNOS were abnormally regulated as well. Moreover, in **4.2.2.4** I demonstrated that 8 or 24 hours of FiO_2 = 0.4 treatment led to downregulation of *Pdgfra* mRNA expression seven weeks after hyperoxia treatment. The mRNA expression of Wnt5a, another developmentally relevant gene, was also distinctly regulated in the O_2 group. We followed the experimental design described in **4.2.2.** to investigate whether O_2 priming makes the lung more vulnerable to a second hit (MHV-68 virus infection) aggravating the dysregulation of developmental pathways following O_2 treatment, **6**. We investigated the transcriptional regulation of *Pdgfra, Wnt5a,* and *Hif1a* three weeks after the first hit. We did not observe any differences in the mRNA expression of *Pdgfra* or *Hif1a* between the groups that received virus infection (**Fig 4.19 A**, **B**). However, comparing the RA group to the RA group that received virus infection, we observed downregulation of *Pdgfra* expression in what seemed to be a virus-driven effect (**Fig 4.19 A**). In contrast, Wnt5a mRNA expression was significantly upregulated in the group that received both O_2 treatment and virus inoculation (O_2+virus). Interestingly, the expression levels in the O_2+virus group were similar to the expression levels observed in the O_2 group without virus inoculation suggesting that the effect on Wnt5a is mostly driven by O_2 treatment without aggravating effects of virus exposure (**Fig 4.19 C**).

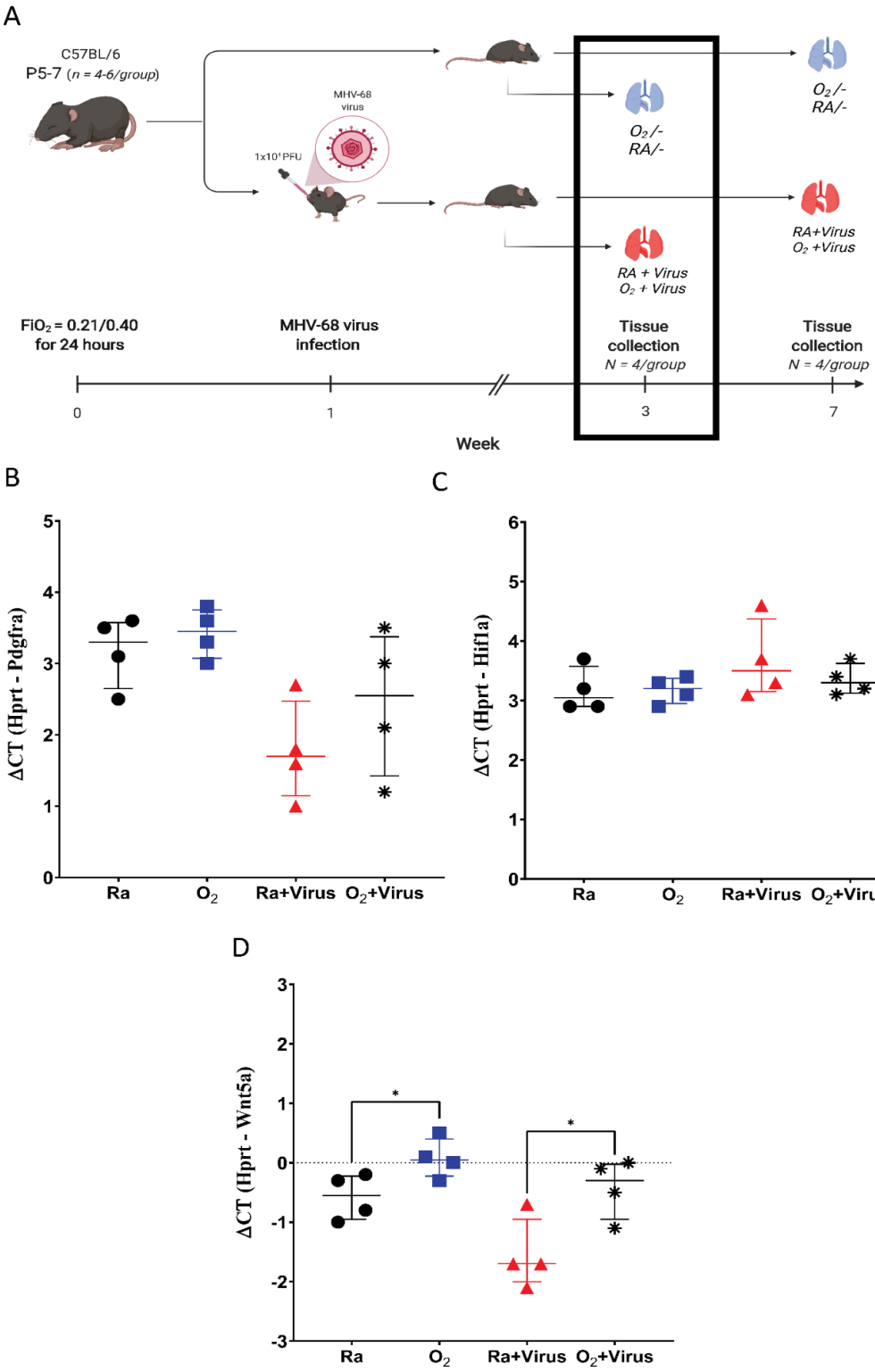

Fig 4.19: development is affected in double hit injury model after 3 weeks

Experimental design showing the double hit injury model in which PND5-7 pups were exposed to 24 hours of O2 and inoculated with the MHV-68 herpes virus one week later (A). qPCR was used to quantitate the mRNA expression of Pdgfra (B), Hif1a (C), and Wnt5a (D) in whole lung lysates from FiO2 = 0.4-treated mice and controls harvested three weeks after treatment (N = 4 mice/group). Hprt was used as a reference gene. Relative expression was calculated with the delta CT method (Hprt CT value - target gene CT value). Quantification bars are represented as

median with interquartile range. Statistical analysis: one-way ANOVA test with correction for multiple comparisons. *p<0.05. qPCR: quantitative polymerase chain reaction.
In vivo experiments were performed in collaboration with Dr. Heiko Adler and Anna Dmitrieva, Ph.D. candidate

At the seven-week time point (A), we did not find detectable changes in mRNA expression in *Hif1a* (B) and *Wnt5a* (C) in any of the groups. Virus infection did not have any effect on the mRNA expression of *Pdgfra* in the absence of O_2 treatment (D). Compared to the group that received virus inoculation only, the O_2+virus group presented with lower *Pdgfra* mRNA expression. Immunofluorescence staining showing decreased Pdgf-Rα expression in the O_2+virus group suggested that this regulation also happened at the protein level (E). Although not statistically significant, virus infection after O_2 treatment seemed to induce a small but opposite effect to the downregulation observed under O_2 only. When comparing the expression in those mice that received both hits (O_2 followed by virus inoculation) to those that received only O_2, a small upregulation of *Pdgfra* expression was observed.

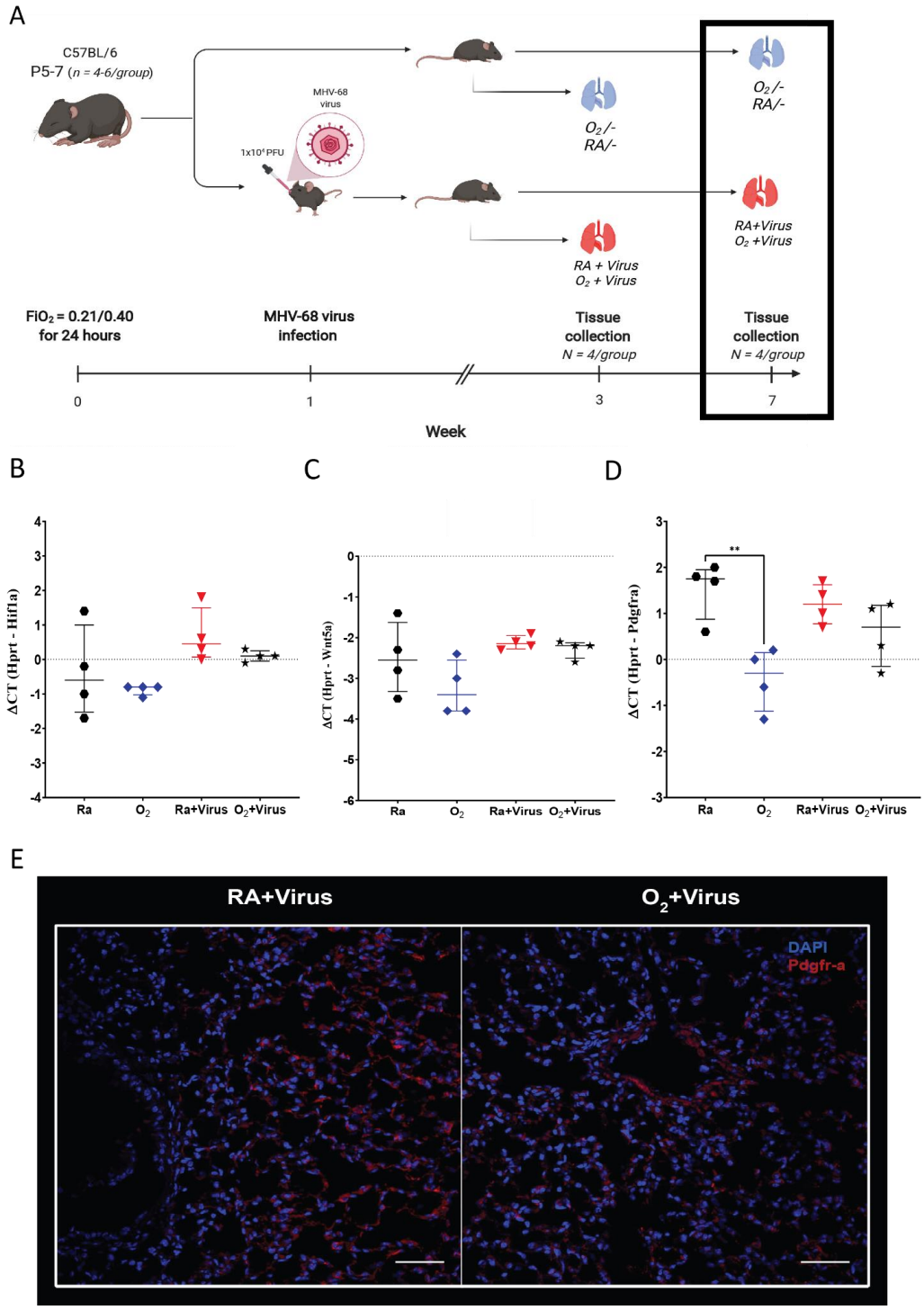

Fig 4.20: development is affected in a double hit injury model after 7 weeks

Experimental design indicating the seven-week time point (A). qPCR was used to quantitate the mRNA expression of Pdgfra (B), Hif1a (C), and Wnt5a (D) in whole lung lysates from FiO_2 = 0.4-treated mice and controls harvested three weeks after treatment (N = 4 mice/group). Hprt was used as a reference gene. Relative expression was calculated with the delta CT method (Hprt CT value - target gene CT value). Quantification bars are represented as median with interquartile

range. Immunofluorescence staining on FFPE fixed lung tissue from mice that received virus inoculation only (Ra+virus) and mice that received both hits (O_2+virus) FFPE fixed newborn lungs (N = 2/group) harvested seven weeks after treatment revealed a modest decrease in Pdgfr-α protein expression (representative image) (H). Scale bars: 50 µm. Expression of Pdgfr-α was normalized with DAPI to obtain relative expression of Pdgfr-α. Data are expressed as RFU per 100 nuclei. Quantification bars are represented as median with interquartile range. Pdgfr-α and DAPI staining were quantified in the Zen software. Statistical analysis: one-way ANOVA test with correction for multiple comparisons. **p<0.01. qPCR: quantitative polymerase chain reaction. RFU: relative fluorescence units.

Immunofluorescence staining was performed by Dr. Motaharehsadat Heydarian, postdoctoral fellow at the Comprehensive Pneumology Center.

In vivo experiments were performed in collaboration with Dr. Heiko Adler and Anna Dmitrieva, Ph.D. candidate

4.2.2.6.2 Lung priming with O_2 treatment alters the DNA damage response and repair at the transcriptional level

Next, we investigated changes in DNA damage response (DDR) genes and BER pathway genes in our double-hit injury model three weeks after O_2/RA exposure (**Fig 4.21 A**). *The in vivo experiments were performed in collaboration with Dr. Heiko Adler and Anna Dmitrieva, Ph.D. candidate*

First, we found that, DDR gene, *Chk1* was significantly upregulated in the mice that received O_2 treatment followed by virus challenge compared to the group that received virus inoculation only (Ra+Virus) (**Fig 4.21 B**). Interestingly, this effect was likely driven by O_2 treatment only given the comparable mRNA expression between the O_2+virus group and the O_2 only group. Comparison of the mRNA expression between the O_2 group and the O_2+virus group revealed that virus infection drove the upregulation of *Cdkn1a* (**Fig 4.21 C**). In contrast to what we have found shortly after O_2 treatment both *in vivo* and *in vitro*, *Mcm2* mRNA expression was significantly upregulated in the O_2 only group compared to the RA control group. In this case, virus infection without O_2 challenge seemed to trigger the upregulation of *Mcm2*, an effect that was markedly aggravated when mice received both hits (O_2+virus) (**Fig 4.21 D**). This increase could be the pro-apoptotic role that Mcm2 may play when it is in the cytoplasm and not in the nucleus (Abe et al., 2012). In line with this finding, we found the expression of *Pcna* to be significantly higher in the O_2+virus compared to the Ra+virus group. This effect seemed to arise from the presence of both hits given the comparable

mRNA regulation between controls and the other two groups (O_2 and Ra+virus) (**Fig 4.21 E**). *Apex1* and *Xrcc1* mRNA expression was upregulated in the O_2+virus group compared to that of the Ra+virus group (**Fig 4.21 F, G**). However, like for *Chk1* and *Mcm2*, this upregulation seemed to be driven by O_2 treatment. Similar to *Pcna*, the upregulation of *Ung1* in the O_2+virus group resulted from a distinct effect of receiving both hits (**Fig 4.21 H**).

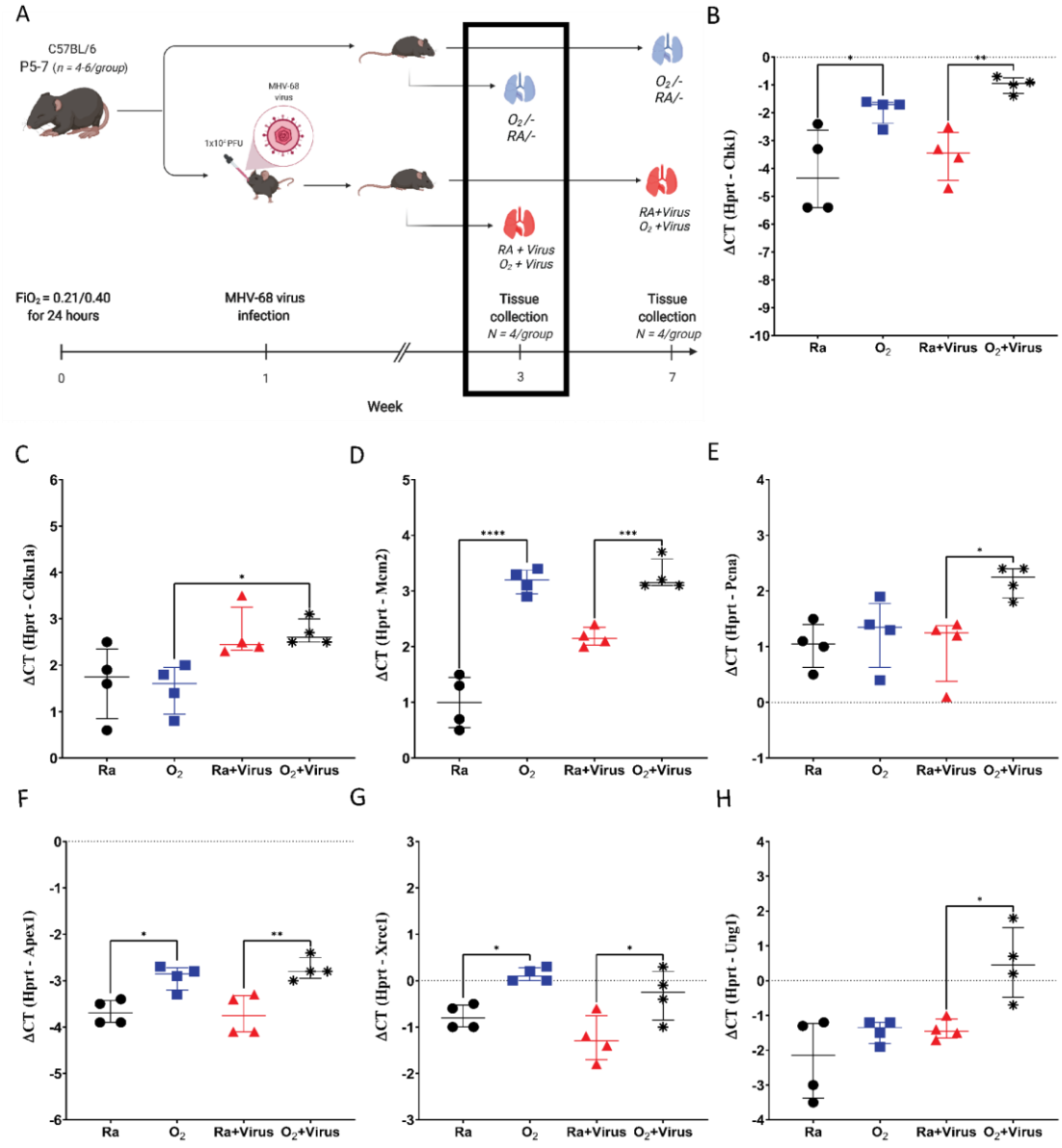

Fig 4.21: Exposure to short-term O_2 drove the upregulation of DDR and BER genes after a second hit with viral infection

Experimental design indicating the three-week time point (A). qPCR was used to quantitate the mRNA expression of Chk1 (B), Cdkn1a (C), Mcm2 (D), Pcna (E), Apex1 (F), Xrcc1 (G), and Ung1(H) in whole lung lysates from FiO_2 = 0.4-treated mice and controls harvested three weeks

after the first hit (N = 4 mice/group). Hprt was used as a reference gene. Relative expression was calculated with the delta CT method (Hprt CT value - target gene CT value). Quantification bars are represented as median with interquartile range. Statistical analysis: one-way ANOVA test with correction for multiple comparisons. *p<0.05. **p<0.01, ***p<0.001. ****p<0.0001. qPCR: quantitative polymerase chain reaction. RFU: relative fluorescence units.

In vivo experiments were performed in collaboration with Dr. Heiko Adler and Anna Dmitrieva, Ph.D. candidate

Contrary to the observed upregulation of Chk1, Apex1, Xrcca, and Ung1 at the three-week time point, mRNA expression of lungs collected from mice challenged with both hits (O_2+Virus) seven weeks after the first hit revealed a significant downregulation of Chk1 and all the BER genes evaluated i.e Apex, Xrcc1, Ung1 and Ogg1 (**Fig 4.22**). Interestingly, virus infection seemed to drive the upregulation of Chk1 in the Ra+Virus group, an effect that was not observed at the three-week time point (**Fig 4.22 B**). While Cdkn1a was downregulated in the O_2 group (one hit only), there was a significant upregulation of its mRNA expression in mouse lungs that received both hits (**Fig 4.22 C**). This effect did not seem to result from virus infection alone but from a double-hit injury mechanism. The observed changes in the regulation of Apex1 (**Fig 4.22 D**) and Xrcc1 (**Fig 4.22 E**) were aggravated by virus infection resulting in upregulation. In contrast, O_2 treatment seemed to trigger the opposite regulation, leading to downregulation of the mRNA expression that together with virus infection is not completely overcome, thus there is still a significant upregulation when comparing the O_2+virus group to the O_2 group. Moreover, there was decreased protein expression of Xrcc1 in the O_2+virus group compared to the Ra+Virus group suggesting that at least for Xrcc1, the regulation changes occur both at the transcriptional and protein levels (**Fig 4.22 H**). The observed downregulation of Ung1 in the O_2+virus group as compared to the Ra+Virus group was likely only driven by O_2 priming (**Fig 4.22 F**). Virus infection alone appeared to drive the upregulation of Ogg1. Notably, this upregulation is somewhat hindered by the O_2 priming of the lung (first hit) (**Fig 4.22 G**).

These data demonstrate that exposing the developing lung to short-term O_2 as a first hit does impact how the mechanisms that respond to DNA damage and repair are regulated in the presence of a second hit.

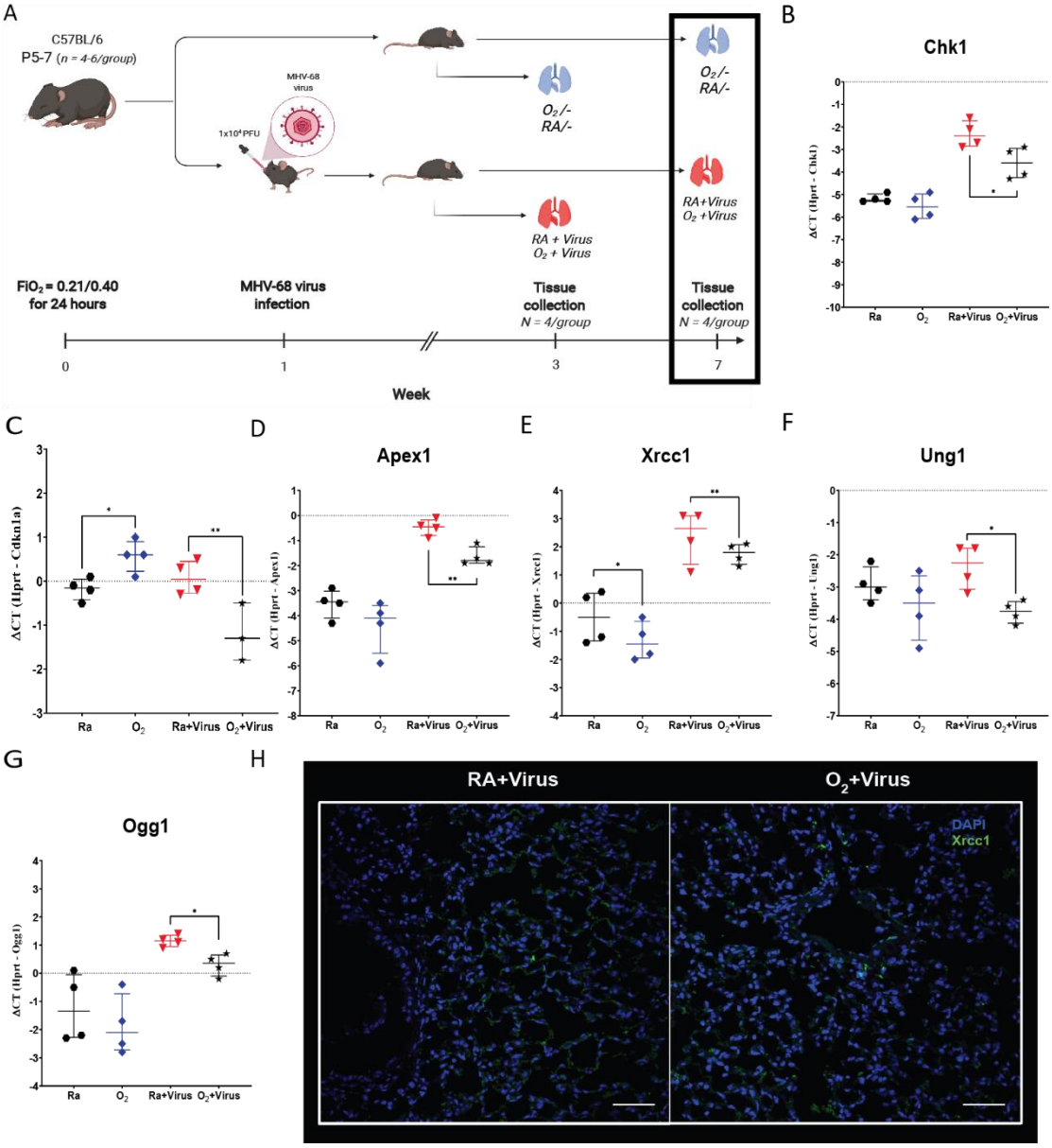

Fig 4.22: The transcriptional regulation of DDR and BER genes was altered in mice that received a second hit with virus infection seven weeks after O_2 exposure

Experimental design indicating the seven-week time point (A). qPCR was used to quantitate the mRNA expression of Chk1 (B), Cdkn1a (C), Apex1 (D), Xrcc1 (E), Ung1 (F), and Ogg1 (G) in whole lung lysates from FiO_2 = 0.4-treated mice and controls harvested seven weeks after the first hit (N = 4 mice/group). Hprt was used as a reference gene. Relative expression was calculated with the delta CT method (Hprt CT value - target gene CT value). Quantification bars are represented as median with interquartile range. Immunofluorescence staining on FFPE fixed lung tissue from mice that received virus inoculation only (Ra+virus) and mice that received both hits (O_2+virus) FFPE fixed newborn lungs (N = 1/group) harvested seven weeks after treatment revealed a modest decrease in Xrcc1 protein expression (representative image) (H). Scale bars: 50 µm. Data are expressed as RFU per 100 nuclei. Quantification bars are represented as median with interquartile range. Xrcc1 and DAPI staining were quantified in the Fiji (Image J) software.

Statistical analysis: one-way ANOVA test with correction for multiple comparisons. *<0.05. **p<0.01. qPCR: quantitative polymerase chain reaction. RFU: relative fluorescence units.

Immunofluorescence staining was performed by Dr. Motaharehsadat Heydarian, postdoctoral fellow at the Comprehensive Pneumology Center.
In vivo experiments were performed in collaboration with Dr. Heiko Adler and Anna Dmitrieva, Ph.D. candidate

Fig 4.24 summarizes the key *in vitro* and *in vivo* results previously reported.

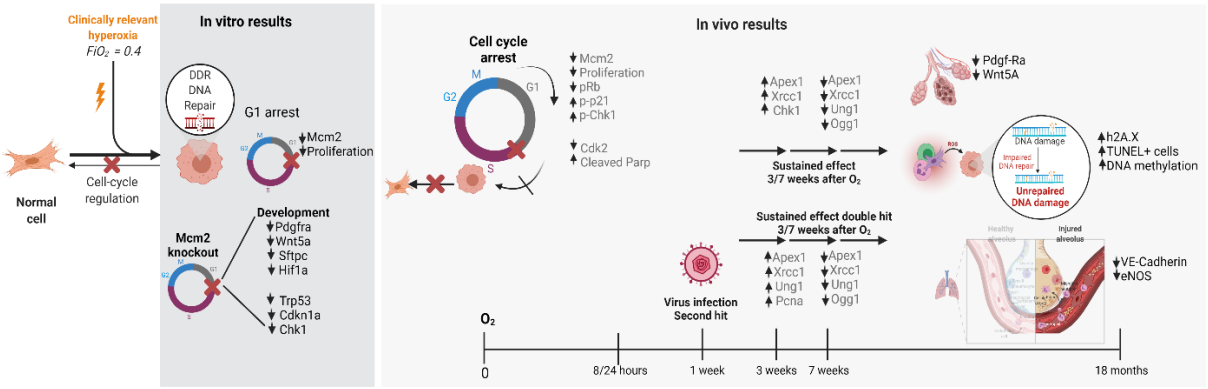

Fig 4.24: Summary of *key in vitro* and *in vivo* results.

4.2.3 Part 3: Translation of results

4.2.3.1 Plasma proteomic analysis of premature newborns

To translate our results to the clinical setting, we analyzed the proteome profile of enrolled pre-term babies from plasma samples collected during the first week of life (early samples) and at day 28 (late samples). The demographics of these patients can be seen on **Table 4.1**. In a post-hoc analysis, we investigated the correlation of Apex1, Parp, Pcna and Mdm2 with oxygen days in proteomic data derived from the OLINK platform. After controlling for gestational age, the proteomic analysis revealed that protein levels of Apex1 were significantly a moderate and significant positive correlation between the BER protein, Apex1 and days of oxygen supplementation (R= 0.48; p = 0.021). In the late samples,

this correlation was mild only. This could be due to other confounding factors like other treatments.

The statistical analysis was performed in collaboration with Dr. Alida Kindt, Division of Analytical Biosciences, Leiden Academic Centre for Drug Research (LACDR), Leiden University, Leiden, The Netherlands.

n	28
GA (weeks)	28.2 (25.1-30.6)
Birth weight (g)	1031 (650-1770)
IUGR	2 (8%)
Gender (female/male)	12/16
ANCS	25 (89.3%)
Chorioamnionitis	11 (39.3%)
Early onset infection	7 (25.0%)
RDS≥III°	7 (25.0%)
Days of mechanical ventilation	34 (0-70)
Days of O_2 supplementation	22 (0-88)
Postnatal steroids	10 (35.7%)
ROP	5 (17.9%)
IVH	2 (7.1%)
ICU days	64 (30-109)
BPD	
- None	17 (60.7%)
- Mild	7 (25.0%)
- Moderate	3 (10-7%)
- Severe	1 (3.6%)

Table 4.1: Patient demographics of premature neonates enrolled in the study

Data are presented as median and range for continuous variables or number and percent of total for categorical variables. ANCS, antenatal corticosteroids; RDS, respiratory distress syndrome; IUGR, intrauterine growth retardation; GA, gestational age; ROP, retinopathy of prematurity; IVH, intraventricular hemorrhage; ICU, intensive care unit; BPD, bronchopulmonary dysplasia. PMA: postmenstrual age. Intrauterine growth restriction: birth weight below the 10th percentile. Postnatally, severity of RDS was scored on anterior-posterior (a.-p.) chest radiographs. We defined Chorioamnionitis based on 1 or more signs of maternal and fetal infection (clinical and laboratory) or based on histologic examination as inflammatory changes of the chorionic plate. BPD was graded as mild, moderate or severe. Mild BPD was defined as: O_2 supplementation at

28 days after birth; moderate BPD was defined as: O_2 supplementation less than 30% and/or ventilator support at 36 weeks PMA; severe: O_2 supplementation less than 30% and/or ventilator support at 36 weeks PMA.

This table was adapted from Impaired BMP signaling provoked by prevalent clinical risk factors at the earliest stage of vascular injury in the preterm infant. Heydarian et.al, in review in Thorax (thoraxjnl-2021-218083)

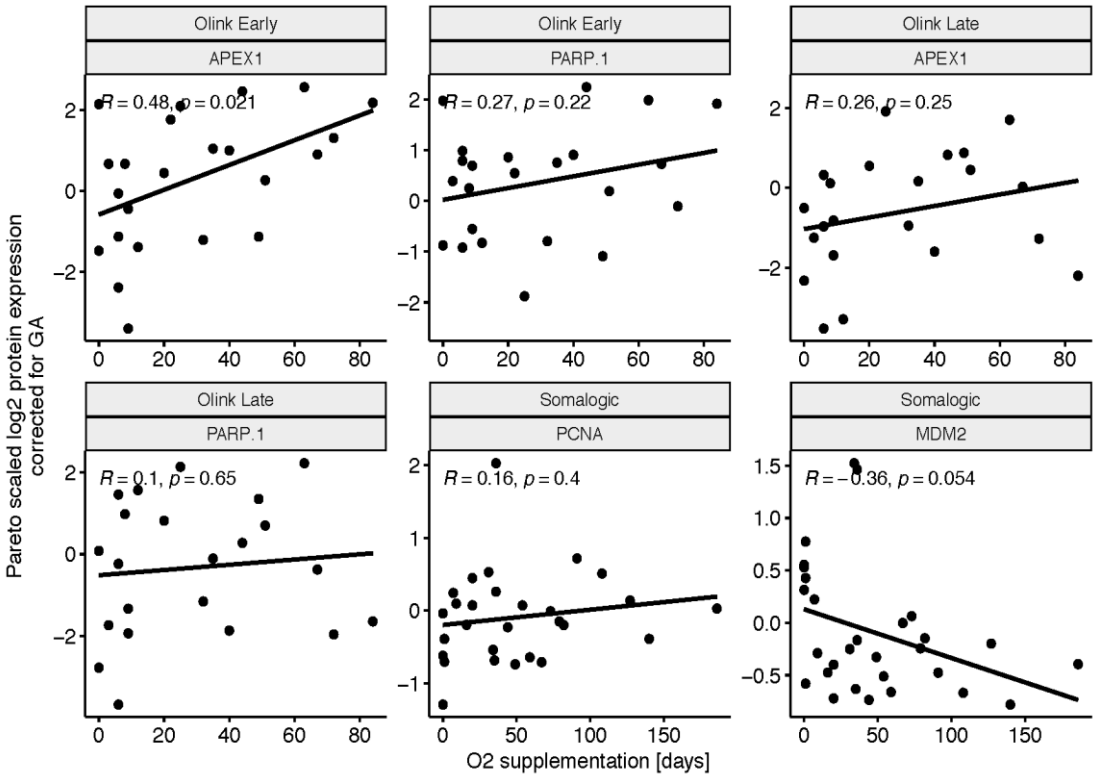

Fig 4.23: Apex1 protein levels are positively correlated with days of oxygen supplementation

Using the OLINK or Somalogic platform in plasma, protein expression of targets was measured in plasma samples collected within the first week of life (early) or on day 28th (late) from pre-term infants.

4.2.3.2 Genetic background analysis associated cell-cycle regulators with BPD development

To gain insight into a potential genetic background on cell cycle regulation in infants with and without BPD, we employed data from a genetic association study. We identified 4 SNPs within cell cycle regulation-related genes (see Methods 3.5.1.3) with an FDR≤0.05 and a minor allele frequency of 5%, all found in intronic regions of CCND2 (dbSNP: rs12299509, rs3217916), CDK1 (dbSNP:

rs2448343), and CDC25A (dbSNP: rs3731553) respectively. Only rs3217916 has been previously associated with cancer i.e., ovarian and breast cancer (PID:19258477,18174243,18281541).

Further 10 SNPs distributed across CDC25A (rs3729577, rs3731487, rs3731489, rs3731497, rs3731515, rs3731534, rs3731553), CDK1 (rs1871447, rs2448343), and CDKN1A (rs2395655) could be identified as associated with days of oxygen supplementation. All SNPs were either found in intronic regions or within the 5" UTR. Of these identified SNPs only rs2395655 *and rs2448343 (PID: 19738611)* were previously clinically indicated (Goode et al., 2009; Gravina et al., 2009; Melzer et al., 2007).

The statistical analysis was performed in collaboration with Juan Henao, PhD candidate, and Benjamin Schubert, Institute of Computational Biology, Helmholtz Zentrum, Munich.

4.2.4 Discussion

Premature neonates often require life-saving oxygen therapy. Although survival improves with oxygen supplementation, morbidity increases with higher oxygen concentration and longer exposures. The induction of lung injury by short-term postnatal hyperoxia has been suggested by clinical observations and was in part supported by experimental studies. However, underlying mechanisms of lasting effects provoked by clinically relevant oxygen levels remain poorly understood. Therefore, my studies addressed significant and functionally relevant changes in the three major lung cell types, i.e., ATII, EC, and MFB, and confirmed their lasting effects. This study presents previously unidentified immediate and sustained effects of the early postnatal exposure to clinically relevant hyperoxia concentrations (FiO_2 = 0.4). One of the main findings of this study was that treatment with O_2 (FiO_2 = 0.4) arrests the cell cycle potentially through the downregulation of the pre-replication complex, which is critical for cell cycle progression. The predominant downregulation of genes following hyperoxia exposure revealed a significant overlap between the MFB and ATII cell transcriptome pattern, partially shared by the lung EC. The significant overlap in the transcriptome profile between MFBs and ATII cells potentially indicate similar effects (and coping strategies) in response to oxidative stress.

In Mcm2 knockdown experiments *in vitro*, I established a causal link between cell-cycle arrest in G1 and changes in developmentally relevant gene expression and cell function in MFB and AT2 cells. Furthermore, Mcm2 knockdown cells presented with aberrations in DNA damage response and repair genes. These results together suggest that O_2 exposure leads to cell cycle arrest that can alter cell-cycle phase dependent gene expression. To study further the implications of cell cycle arrest induced by O_2 treatment in the developing lung, we employed several *in vivo* mouse models of short-term O_2 exposure and double-hit injury with viral infection.

In vivo, we were able to recapitulate our main *in vitro* findings. A model employing FiO_2 = 0.4 for 8 hours revealed indications of cell cycle arrest at the proteomic level in the absence of classical apoptosis. Longer O_2 treatment revealed a similar signature of cell cycle arrest, and the regulation of other critical proteins involved in the DDR such as Parp1. Moreover, 24 hours of O_2 did not result in classical apoptosis. Interestingly, 8 hours of O_2 treatment led to the upregulation of VEGFA but no other changes in developmentally relevant proteins were observed. Remarkably, studies in 18-month-old mice that received 8 hours of O_2 as newborns revealed Pdgf-Rα and VE-cadherin to be significantly downregulated while eNOS, another vascular marker, was significantly increased. These findings paint a picture of aberrant signaling that although not evident immediately after treatment, appear to be long lasting.

To study deeper the potential consequences of short-term O_2 treatment, we treated mice with O_2 for 24 hours and allow them to recover after treatment. Three and seven weeks after treatment, the lungs were harvested. We observed that at the transcriptional level, the downregulation of genes like Pdg-Rα can already be seen seven weeks after treatment. This model also revealed alterations in Wnt5a mRNA expression three and seven weeks after treatment. Remarkably, we elucidated aberrations in DDR genes i.e Chk1 and Cdkn1a, and in BER pathway genes three weeks after treatment. Several of these changes did not return to baseline by the seven-week post treatment.

Additionally, with a double-hit injury model, we delineated the changes in DNA damage response and the BER pathway that arise from O_2-lung priming. For

several of the target genes evaluated, previous treatment with O_2 modulated the response to the second-hit injury, perhaps making the lung more vulnerable.

Finally, we translated these results to the bedside by analyzing samples collected from pre-mature babies that received oxygen therapy. Remarkably, in plasma proteome analysis from blood collected during the first week of life, protein levels of Apex1, a key BER gene, were positively correlated with O_2 days mirroring our observations *in vivo*.

4.2.4.1 Unbiased approach to characterize the transcriptomic response to O_2 in three major cell types

Bronchopulmonary dysplasia (BPD) remains the main complication of prematurity and oxygen therapy is still one of the major risk factors (for review see (Niedermaier & Hilgendorff, 2015; Sucre et al., 2021)). In recent years, in clinical practice the use of oxygen concentrations ($FiO_2 < 0.5$) has become more conservative given the evidence of severe side effects like retinopathy (Askie et al., 2003). Despite this, most of the experimental models of BPD employ very high oxygen concentrations ($FiO_2 > 0.8$) for several days or weeks. Thus, our knowledge of the effects of oxygen therapy in the developing lung derive from models of severity that most likely do not reflect the clinical setting. Even though the effects of treatment with severe hyperoxia concentrations have been extensively characterized, there is still a poor understanding of the maladaptive responses that lead to BPD (Hilgendorff & O'Reilly, 2015). This lack of understanding is likely worsened by animal models that do not reflect the current clinical setting. More importantly, a real gap of knowledge remains when it comes to clinically relevant hyperoxia concentrations i.e $FiO_2 \leq 0.4$ and short and long-term effects (Hilgendorff & O'Reilly, 2015). Thus, it is critical to identify and understand the early mechanisms involved in the injury response to hyperoxia treatment in order to harness this knowledge towards therapeutics that restore normal lung function.

Here, using an unbiased approach, we characterized the response to short-term (24 hours) clinically relevant hyperoxia concentrations in three major cell types isolated from mice pups. We employed 24 hours because we were interested in investigating not only moderate concentrations of hyperoxia but also shorter

exposure times more reflective of the clinical setting. RNA-sequencing analysis revealed a 'transcriptomic storm' following O_2 treatment. When comparing the O_2-transcriptomic signature to cyclical stretch (*in vitro* model of mechanical ventilation), we confirmed this signature to be O_2- treatment specific. Moreover, our analysis revealed that alveolar epithelial cells (AT2) and myofibroblasts (MFB) presented with most differentially regulated genes. In contrast, only a few genes were significantly regulated in endothelial cells (EC). This lower regulation in EC could be due to EC cells being more adapted to changes in oxygen concentrations or that the transcriptomic changes occur at a different time point (Alhayaza et al., 2020). Another reason could be a more heterogeneous population of EC cells that were included in the study (Conway & Carmeliet, 2004). Interestingly, AT2 cells and MFBs shared over 50% of their transcriptomic response. This shared signature could be to the close interplay between AT2 cells and MFB when responding to injury (Nabhan et al., 2018). In chronic lung disease, regeneration strategies of the alveolar niche requiring epithelial-mesenchymal crosstalk are hindered (Nabhan et al., 2018; Sucre et al., 2020; Yao et al., 2021). At the same time pathologic signaling in both cell types likely further promotes lung injury and structural decay (Riccetti et al., 2022; Yao et al., 2021). Given our experimental design, a model that allows us to investigate cellular crosstalk between AT2 cells and MFB is necessary to fully understand this common signature and its implications in lung disease. Another limitation of our study is that it does not identify regulation that can be happening at the post-transcriptional level. However, this was addressed by performing protein and functional analyses in vitro and in vivo.

4.2.4.2 Cell-cycle regulation at the center of the response to clinical hyperoxia levels

The aforementioned shared response was dominated by processes involved in cell-cycle regulation, DNA damage response and DNA repair. Moreover, most of the genes shared between AT2 cells and MFB are overrepresented in cell cycle regulation and DNA damage response processes (DDR). Diving deeper into this signature, we observed that most critical checkpoint regulators were downregulated suggesting cell-cycle arrest. Notably, we also found that that several of the genes that code for the pre-replication complex (pre-RC) proteins

were significantly downregulated because of O_2 treatment. The Mcm2-7 complex makes part of the pre-RC, a protein complex that licenses replication origins and is essential to start DNA replication in S-phase (Courtot et al., 2018). We validated the downregulation of Mcm2 mRNA and protein expression in *in vitro* experiments using a human lung fibroblast cell line (IMR-90) and a murine AT2 cell line (MLE-12). These experiments revealed that after 24 hours of O_2, Mcm2 was downregulated at the protein level in IMR-90 fibroblasts. Moreover, proliferation was also significantly reduced supporting our hypothesis that O_2 leads to G1-phase cell cycle arrest (Kong et al., 2016). At the transcriptomic level, Mcm2 remained downregulated in lung fibroblasts (IMR-90) and murine AT2 cells (MLE-12) until the fourth day after O_2 cessation ('recovery period' in normoxia). Notably, when studying kidney cells exposed to O_2, Mcm2 downregulation was not a sustained effect in these cells indicating that this might not be an 'universal' response across cell types. Remarkably, Mcm2 downregulation occurred in the absence of classical apoptosis both *in vitro* and *in vivo*. Studies in neonates exposed to short-term hyperoxia at birth hinted changes to cell cycle checkpoint regulator gene expression including the downregulation of the pre-replication complex (Riccetti et al., 2022; Sucre et al., 2021). These findings, however, were obtained through exposure to high oxygen levels and accompanied by a significant increase in apoptosis (Hilgendorff & O'Reilly, 2015; Jiang et al., 2022; Kumar et al., 2020). However, both *in vitro* and *in vivo,* I demonstrated the absence of classical apoptosis pathway activation suggesting that short-term treatment with clinically relevant levels of O_2 are not harmful enough to cause apoptosis. Several studies have shown the role that ferroptosis plays in acute lung injury (Chen et al., 2020; Liu et al., 2020). Therefore, to rule out other potential mechanisms that lead to cell death, I investigated the expression of ferroptosis genes in O_2 treated and untreated cells. However, I did not find any indication that this was a potential pathway leading to cell death in this case. Furthermore, cell viability was comparable between cells treated with O_2 and room air controls strongly suggesting that the decreased proliferation was not due to cell death. With the changes to cell cycle regulation occurring in the absence of classical apoptosis pathway activation, a 'dormant' state of the affected cells likely results in long-term consequences through the accumulation of DNA damage, thereby rendering the lung vulnerable to long-term consequences and

second hits. Moreover, Mcm2-7 complex downregulation hinders cell cycle progression potentially leading to aberrant proliferation and differentiation of various lung cells, impeding the normal development of alveolus, airways and specialized cells that are required for breathing (Ge & Blow, 2010; Z. Li et al., 2020).

A recent study targeting $p16^{INK4a}$ in newborn mice exposed to 85% hyperoxia from PND3-14 showed that silencing of this checkpoint regulator improved lung regeneration potentially through its role in lipogenesis (Zysman et al., 2020). By inhibiting CDK4, $p16^{INK4a}$ modulates fibroblast differentiation into lipofibroblasts, which play a role in regeneration (Zysman et al., 2020). The hypothesis that checkpoint regulators could have other functions beyond their putative role in cell cycle regulation has been addressed in previous studies (Z. Li et al., 2020; Zysman et al., 2020). A stuy by Akagawa et al., suggested cell cycle checkpoint regulators to play roles in cytoskeletal organization, after exit from the cell-cycle (Akagawa et al., 2021). Another study found CDC2 (cell division cycle 2) to be a positive regulator of the interferon-signaling pathway, thereby playing a role in inflammation (Z. Li et al., 2020). Furthermore, my *Mcm2*- knockdown experiments revealed a link between cell-cycle arrest and the regulation of several developmentally relevant genes and cell functions. *Pdgfra*, *Hif1a, Sftpc* (in AT2 cells*)* and *Wnt5a* were significantly downregulated in Mcm2-knocout cells. Moreover, alterations in cell functions like migration and genes involved in cell function (*Acta2* and *Spp1*) were also causally linked to *Mcm2*-silencing. Thus, one can speculate that O_2-induced cell cycle arrest in the developing lung has long-lasting consequences beyond the accumulation of DNA damage. Most likely, cell cycle arrest during the critical periods of lung development in premature infants results in disturbances in cell-cycle checkpoint signaling and cell-cycle dependent gene expression. The disrupted signaling impairs critical cell functions and differentiation processes. By impairing critical cell functions and disturbing cell differentiation, the normal process of lung development cannot continue leading to long-term consequences (**Fig 4.25**). Fig 4.25 shows the potential impact that cell cycle arrest can have on cell-cycle phase dependent expression (DNA repair, plasticity) and the long-term consequences of these alterations.

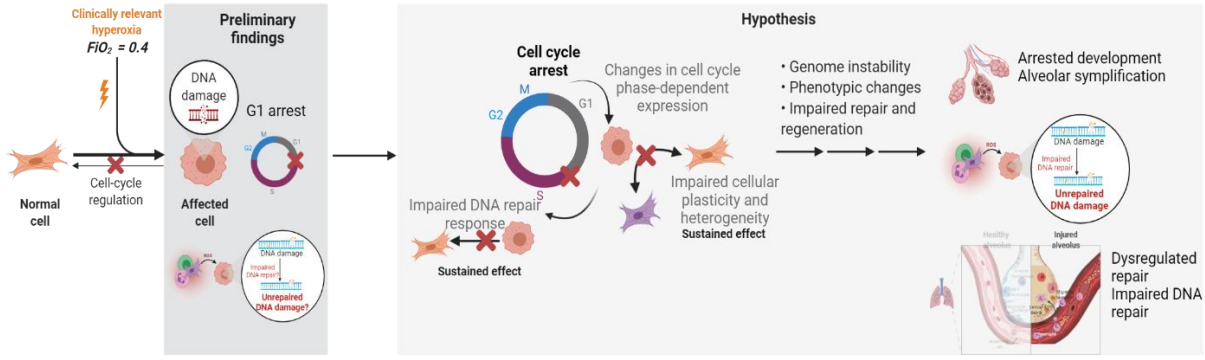

Fig 4.25: Consequences of cell-cycle dysregulation resulting from short exposure to clinically relevant hyperoxia concentrations

4.2.4.3 Consequences of short-term clinical hyperoxia levels on developmental pathways

In this thesis, I have presented data that demonstrate that short-term exposure to clinically relevant hyperoxia levels (O_2: FiO_2 = 0.4) results in aberrations in developmentally relevant proteins such as *Pdgfra*, PDGF-A, VEGFA, Wnt5a, and VE-cadherin and eNOS. The clinical implications of these results are profound given that oxygen therapy is in many cases a life-saving intervention in premature neonates. Pdgfr-α and PDGFA are necessary for alveologenesis to happen (Lau et al., 2011; Oak & Hilgendorff, 2017; Oak et al., 2017). Pdgfr-α expressing fibroblasts drive the process of secondary septation during the saccular and alveolar phase of lung development (Oak et al., 2017; Riccetti et al., 2022). Moreover, PDGFA knockout mouse models are not viable and present with severely disrupted lung development (Lau et al., 2011). In my *Mcm2*- knockdown experiments, I established a link between cell cycle arrest and decreased *Pdgfra* mRNA expression. Remarkably, *in vivo*, we showed that exposure to 8 hours of O_2 in the neonatal period led to decreased Pdgf-Rα in adult mice. Surprisingly, the downregulation in *Pdgfra* mRNA expression was already evident seven weeks after O_2 exposure. This along with the downregulation of vascular factors i.e VE-Cadherin and eNOS, and the observed histological findings of enlarged surface area three and seven weeks after exposure suggest that short exposure to clinically relevant hyperoxia levels impacts lung development. Hif1-a is the major oxygen sensing system. Contrary to what others have reported (Kirschner et al., 2022), our experiments revealed no changes in Hif1-a protein expression

8 hours after treatment or Hif1a mRNA expression three and seven weeks after O_2 exposure. This could be due to other oxygen sensing proteins playing a more important role or to post-transcriptional modifications that we did not assess.

In our *in vitro* and *in vivo* experiments, with relevance in all three major cell types, the expression of Wnt5a, another critical gene in lung development, was dysregulated at least seven weeks following 24-hour exposure to O_2 (FiO_2 = 0.4). The dysregulation of Wnt5a, a non-canonical WNT ligand, has been linked to the development of several chronic lung diseases including idiopathic pulmonary fibrosis and chronic obstructive lung disease (Baarsma et al., 2017; Liu et al., 2021; Newman et al., 2016; Vuga et al., 2009). However, little is known about the role of Wnt5a signaling in the developing lung and following injury. Recent studies have found that the lack of Wnt5a in the saccular phase decreased the differentiation of alveolar epithelial type I cells, myofibroblasts and endothelial cells, thereby blocking distal airway development (Z. Li et al., 2020). Moreover, Wnt5a signaling niches (expressed by fibroblasts) have been identified as responsible for maintaining alveolar epithelial type II (AT2) cell stemness (Nabhan et al., 2018). In contrast, a study by Sucre et al reported that Wnt5a inhibition improved alveolarization following hyperoxia exposure (Sucre et al., 2020). A study of healthy human fibroblasts and fibroblasts from patients with pulmonary fibrosis showed Wnt5a expression to be increased and associated with enhanced proliferation and resistance to apoptosis (Vuga et al., 2009). Our *in vivo* studies showed Wnt5a to be upregulated at the transcriptional level three weeks after O_2 exposure but downregulated seven weeks after. These differences in Wnt5a across disease models point to a complex signaling mechanism that highlights the essential role Wnt5a may play in lung development, injury, and repair (Nabhan et al., 2018; Riccetti et al., 2022).

4.2.4.4 Short-term clinical hyperoxia leads to aberrations in DNA damage response and repair mechanisms

By unbiased transcriptome analysis, we revealed DNA damage response (DDR) and repair processes to be enriched in all three cell types following O_2 (FiO_2 = 0.4). Furthermore, my Mcm2- knockdown experiments revealed that cell-cycle arrest leading to genotoxic stress triggers the upregulation of base excision repair

(BER) genes, Apex1 and Neil1 together with the downregulation of Cdkn1a and Trp53, DDR genes. However, when Mcm2- knockdown fibroblasts were exposed to O_2 for 24 hours, a paradoxical downregulation of these genes occurred. These results suggest that early-cell-cycle phase arrested cells cannot properly activate DNA repair genes. This is particularly relevant in the clinical setting where premature newborns receive on-and-off oxygen therapy for several days. To my knowledge, this is the first time that BER pathway dysregulation has been linked to treatment with clinically relevant O_2 concentrations. In contrast to the effects observed following severe O_2 exposure ($FiO_2 > 0.7$), the O_2 concentration used in these experiments did not trigger classical apoptosis neither *in vitro* nor *in vivo* (Jiang et al., 2022; Weng et al., 2021). Here, I showed that 24-hours of O_2 resulted in increased p-H2A.X, 8-OxoG and cleaved Parp protein expression, all three are triggered by DNA damage. As expected, this was accompanied by increases in DDR proteins, p-Chk1 and p-p21, and decreases in p-Mcm2 and Cdk2. Furthermore, three weeks after O_2 treatment, Chk1 mRNA expression was still upregulated in the O_2 group demonstrating the longevity of this response. Moreover, the expression of Cdkn1a, the gene that codes for the p21 protein, was significantly downregulated seven weeks after O_2 treatment. The downregulation of p21 has been shown to result in unscheduled entry into S-phase and inappropriate proliferation (Perucca et al., 2009). The p21 downregulation presented together with the significant downregulation in BER genes, Apex1 and Xrcc1 seven weeks after O_2 treatment. These results provide evidence that short-term treatment with O_2 results in aberrations in both DDR and repair mechanisms that persist long after treatment cessation. Providing further evidence to this argument, was the remarkable finding that adult mice exposed to O_2 for 8 hours only as neonates presented with increased DNA damage in the lung evidenced by increased p-H2A.X protein expression and a higher number of TUNEL+ cells. Moreover, in proteomic analysis of pre-term infants, there was a positive correlation between Apex1 protein levels and days of O_2 therapy demonstrating the relevance of Apex1 in the response to DNA-damage induced by O_2 therapy. Some studies have reported that newborns exposed to high concentrations of hyperoxia at birth are more likely to develop cancer in childhood (Lorente-Pozo et al., 2020). Others report that pre-term newborns show slower repair of DNA damage probably because of immature redox systems (Lorente-

Pozo et al., 2020; Lorente-Pozo et al., 2018; Vande Loock et al., 2012). Our studies quantitating DNA methylation intermediates showed a decrease of cadC in adult mice that were treated with hyperoxia as neonates. The TET (Ten-eleven translocation) enzyme system iteratively oxidize 5mC and 5hmC into other oxidized cytosines including 5-formylcytosine (5fC) and 5-carboxylcytosine (5caC). These two cytosines are recognized and excised by DNA thymine glycosylase and then repaired by the BER system with an unmodified C, leading to DNA demethylation (Lio & Rao, 2019). Therefore, an impaired TET system would not successfully oxidize fdC to cadC, which would result in lower levels of cadC, less repair and aberrant DNA demethylation. Based on all this evidence, one could speculate that O_2-dependent alterations in DDR gene expression and DNA repair negatively impacts lung development and repair. Moreover, I propose that long-term and likely epigenetic changes in the BER pathway mediate these alterations. Our study is limited by the fact that we did not measure enzymatic activity or the potential role of other DNA repair pathways. In the future, experiments that address TET enzymatic activity and methylation patterns of BER genes should be performed to establish the epigenetic signature arising from clinically relevant hyperoxia levels. To better understand the clinical relevance of these results, clinical studies in pre-term babies treated with oxygen therapy could identify important targets for epigenetic modulation.

4.2.4.5 Short-term exposure to clinically relevant hyperoxia levels primes the lung to a second hit

Former preterm infants who have normal lung function present with airway hyperreactivity and higher odds of complications after viral infection (Buczynski et al., 2013; Dylag et al., 2021). Some studies have suggested that changes in the expression of genes such as TSP-1 (important for TGF-β signaling) might be behind the increased airway hyperreactivity (Dylag et al., 2021). More evidence for this observation comes from studies in pre-term babies that examined the association between chronic oxygen therapy and the expression of SARS-CoV-2 receptors. This study found TMPRSS11D to be upregulated both at the transcriptional and protein level (Myti et al., 2020). Here, our double-hit experiments with 24 hours of FiO_2 = 0.4 followed by infection with the murine herpes virus one week later, provided evidence that even short exposures to O_2

can alter the host response to viral infection. In what seems to be an O_2-driven effect, our experiments revealed a pattern of upregulation of DDR i.e Chk1, Pcna, Mcm2 and BER genes i.e Apex1, Xrcc1 and Ung1 in double-hit mice three weeks after O2 exposure. Interestingly, by week seven, this response was dominated by downregulation of all the aforementioned genes suggesting a dysregulated compensatory response. Twisselmann et al. employed a double-hit injury model of 65% hyperoxia and lipopolysaccharide (LPS) macrophage activation. The authors found that 65% hyperoxia primed a sustained inflammatory response leading to an exaggerated pro-inflammatory response driven by Egr2 downregulation (Twisselmann et al., 2021). These studies show that hyperoxia primes the premature lung through different mechanisms that will likely result in an increased risk of complications (Collaco & McGrath-Morrow, 2021). This added to the presence of polymorphisms in cell-cycle regulatory genes (Cdkn1a, Cdk1 and Cdc25a) that we presented here, identifies a population of patients that might be at much higher risk of developing BPD (Liu et al., 2021). Identifying the mechanisms that drive the hyperoxia-priming effect would provide us with more therapeutic interventions to decrease the morbidity of pre-term infants. Moreover, these mechanisms could have an impact in diseases other than BPD where cell-priming might be beneficial (i.e., cancer).

4.2.5 Conclusions and future directions

In conclusion, the short exposure to moderate, clinically relevant levels of hyperoxia (O_2: FiO_2 = 0.4) results in cell-cycle arrest, which likely drives aberrations in developmental pathways and an increase in DNA damage and repair. The short O_2 exposure subsequently results in long-term dysregulation of DNA damage and repair pathways leading to increased DNA damage and priming of the lung to a second-hit injury. Extensive studies *in vitro* and *in vivo* models are supported by findings obtained in a genetic association study. Clinical studies are needed to further elucidate the complex interrelationship of cell cycle regulation with lung development including the identification of genetic and epigenetic changes and the involvement of immune mechanisms. The priming effects of hyperoxia need to be considered when understanding the later

response to subsequent injury hits in adulthood interfering with the process of ageing. Both, relevance in the evolution of lung disease in adulthood as well as the impact of the changes observed on the development of comorbidities need to be studied further to open new avenues for treatment strategies.

5. Appendix A:

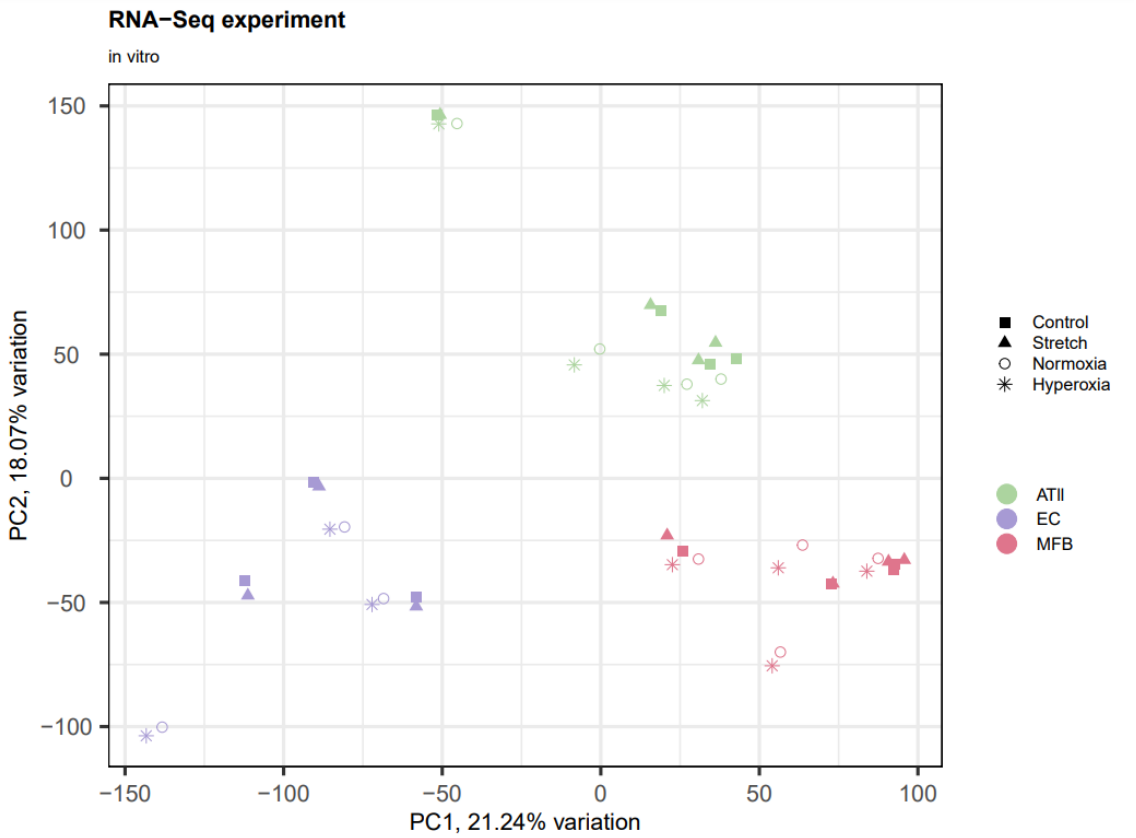

Fig A1: PCA plots from RNA-sequencing analysis showing clustering by cell-type
PCA plot showing the three lung cell types isolated clustering by cell-type but not treatment.

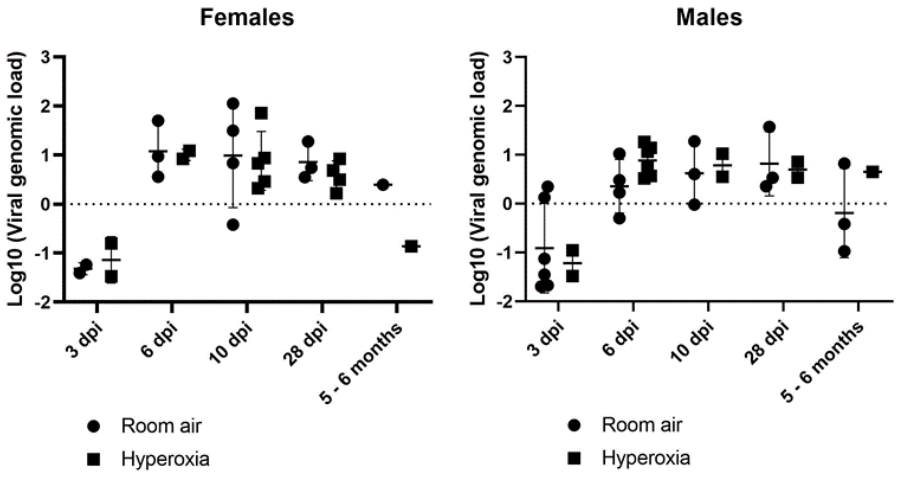

Fig A2: Infection curves in female and male mice
These graphs show the viral load in spleens collected from female and male mice 3,6,10,28 and 5-6 months post MHV-68 viral infection. By the sixth day, most of the viral particles have moved on from the lung and reached the spleen where it stays latent.

Dpi: days post infection
Hyperoxia: FiO_2 = 0.4 for 24 hours

6. Acknowledgments

I would like to thank all collaborators and people who made this work possible:

Dr. Anne Hilgendorff, Principal Investigator, for her support, mentoring and contributions to this work.

The other members of my thesis advisory committee, Prof. Dr. Juergen Behr, Prof. Dr. Thomas Gudermann, and Prof. Dr Tushar Desai.

Juan David Henao, PhD candidate and Dr. Benjamin Schubert, Institute of Computational Biology, Helmholtz Zentrum, Munich. I thank them for their computational biology analysis of the RNA-sequencing data and the genetic data.

Anna Dmitrieva, PhD candidate and Dr. Heiko Adler, Comprehensive Pneumology Center, Helmholtz Zentrum, Munich. I thank Anna dearly for her support and excellent job performing the double-hit injury model.

Xin Zhang, PhD candidate in our research group, for her support, help and intellectual input.

Valeria Vitteri, MD, PhD candidate, and Dr. Isis Fernandez, Comprehensive Pneumology Center, Helmholtz Zentrum, Munich. I thank them both for their support and assistance in performing flow cytometry analysis.

Florian Schelter, PhD candidate, Dr. Markus Mueller, and Prof. Dr. Thomas Carell, Department of Medicinal Chemistry, Ludwig Maximilian University of Munich. I thank them for their contributions regarding DNA methylation intermediates studies.

Dr. Alida Kindt. I thank her for her analysis of the proteomic data helping us translate our results to the clinical setting.

Dr. Tina Pritzke, former member in our research group, for generating the samples used for RNA-sequencing analysis.

Dr. Motarehsadat Heydarian, a postdoctoral research fellow at our group, Comprehensive Pneumology center, for performing some of the immunofluorescence staining slides presented in this work.

Dr. Prajakta Oak, a former postdoctoral fellow in our research group, for her mentoring and help.

Dr. Nona Kampari, a former member in our research group, for generating some of the samples that were used for histology analysis in this work.

Susanne Mehring, technical assistant in our group, for her support purchasing materials and reagents needed for the experiments performed in this work. Former technical assistant, Markus Koschlig, for generating some of the samples used in this work.
I also thank Daniela Dietel, Elisabeth Hennen, Anastasia Van der Berg, and all technical assistants and administrative staff at the Comprehensive Pneumology center for their help and support.

The GRK2338 Targets in Toxicology research school for providing the funding for these studies. Within the GRK2338, I thank Dr. Julia Brandt and Dr. Stefanie Resenberger for their excellent support as program coordinators, and Dr. Claudia Staab-Weijnitz for her thoughtful suggestions and help.

I thank my sister, Tania Gutierrez, for her unconditional support.
I thank Thomas Schemmer for his help, support and technical assistance.
I thank my friends, Dr. Katherine Mejia, Dr. Adriana Bruges, Dr. Leidys Gutierrez, Dr. Laura Ospina, Michael Sodamin and Dr. Gabriel Gruionu for their encouragement, advice, and unconditional support.
I thank Dr. Charles Wade, my former PI, for his training, mentoring and career advice.

7. References

Abe, S., Kurata, M., Suzuki, S., Yamamoto, K., Aisaki, K., Kanno, J., & Kitagawa, M. (2012). Minichromosome maintenance 2 bound with retroviral Gp70 is localized to cytoplasm and enhances DNA-damage-induced apoptosis. *PLoS One*, *7*(6), e40129. https://doi.org/10.1371/journal.pone.0040129

Agnez-Lima, L. F., Melo, J. T., Silva, A. E., Oliveira, A. H., Timoteo, A. R., Lima-Bessa, K. M., Martinez, G. R., Medeiros, M. H., Di Mascio, P., Galhardo, R. S., & Menck, C. F. (2012). DNA damage by singlet oxygen and cellular protective mechanisms. *Mutat Res Rev Mutat Res*, *751*(1), 15-28. https://doi.org/10.1016/j.mrrev.2011.12.005

Akagawa, R., Nabeshima, Y. I., & Kawauchi, T. (2021). Alternative Functions of Cell Cycle-Related and DNA Repair Proteins in Post-mitotic Neurons. *Front Cell Dev Biol*, *9*, 753175. https://doi.org/10.3389/fcell.2021.753175

Alhayaza, R., Haque, E., Karbasiafshar, C., Sellke, F. W., & Abid, M. R. (2020). The Relationship Between Reactive Oxygen Species and Endothelial Cell Metabolism [Review]. *Frontiers in Chemistry*, *8*. https://doi.org/10.3389/fchem.2020.592688

Andresen, J. H., & Saugstad, O. D. (2020). Oxygen metabolism and oxygenation of the newborn. *Semin Fetal Neonatal Med*, *25*(2), 101078. https://doi.org/10.1016/j.siny.2020.101078

Askie, L. M., Darlow, B. A., Finer, N., Schmidt, B., Stenson, B., Tarnow-Mordi, W., Davis, P. G., Carlo, W. A., Brocklehurst, P., Davies, L. C., Das, A., Rich, W., Gantz, M. G., Roberts, R. S., Whyte, R. K., Costantini, L., Poets, C., Asztalos, E., Battin, M., . . . Simes, R. J. (2018). Association Between Oxygen Saturation Targeting and Death or Disability in Extremely Preterm Infants in the Neonatal Oxygenation Prospective Meta-analysis Collaboration. *Jama*, *319*(21), 2190-2201. https://doi.org/10.1001/jama.2018.5725

Askie, L. M., Henderson-Smart, D. J., Irwig, L., & Simpson, J. M. (2003). Oxygen-saturation targets and outcomes in extremely preterm infants. *N Engl J Med*, *349*(10), 959-967. https://doi.org/10.1056/NEJMoa023080

Baarsma, H. A., Skronska-Wasek, W., Mutze, K., Ciolek, F., Wagner, D. E., John-Schuster, G., Heinzelmann, K., Günther, A., Bracke, K. R., Dagouassat, M., Boczkowski, J., Brusselle, G. G., Smits, R., Eickelberg, O., Yildirim, A., & Königshoff, M. (2017). Noncanonical WNT-5A signaling impairs endogenous lung repair in COPD. *J Exp Med*, *214*(1), 143-163. https://doi.org/10.1084/jem.20160675

Behnke, J., Dippel, C. M., Choi, Y., Rekers, L., Schmidt, A., Lauer, T., Dong, Y., Behnke, J., Zimmer, K. P., Bellusci, S., & Ehrhardt, H. (2021). Oxygen Toxicity to the Immature Lung-Part II: The Unmet Clinical Need for Causal Therapy. *Int J Mol Sci*, *22*(19). https://doi.org/10.3390/ijms221910694

Berger, J., & Bhandari, V. (2014). Animal models of bronchopulmonary dysplasia. The term mouse models. *American Journal of Physiology-Lung Cellular and Molecular Physiology*, *307*(12), L936-L947. https://doi.org/10.1152/ajplung.00159.2014

Berkelhamer, S. K., Kim, G. A., Radder, J. E., Wedgwood, S., Czech, L., Steinhorn, R. H., & Schumacker, P. T. (2013). Developmental differences in hyperoxia-induced oxidative stress and cellular responses in the murine lung. *Free Radic Biol Med*, *61*, 51-60. https://doi.org/10.1016/j.freeradbiomed.2013.03.003

Bik-Multanowski, M., Revhaug, C., Grabowska, A., Dobosz, A., Madetko-Talowska, A., Zasada, M., & Saugstad, O. D. (2018). Hyperoxia induces epigenetic changes in newborn mice lungs. *Free Radic Biol Med*, *121*, 51-56. https://doi.org/10.1016/j.freeradbiomed.2018.04.566

Blume, F., Kirsten, H., Ahnert, P., Chakraborty, T., Gross, A., Horn, K., Toliat, M. R., Nürnberg, P., Westenfelder, E.-M., Goepel, W., & Scholz, M. (2021). Verification of immunology-related genetic associations in BPD supports ABCA3 and five other genes. *Pediatric Research*. https://doi.org/10.1038/s41390-021-01689-y

Bochtler, M., Kolano, A., & Xu, G. L. (2017). DNA demethylation pathways: Additional players and regulators. *Bioessays*, *39*(1), 1-13. https://doi.org/10.1002/bies.201600178

Buczynski, B. W., Yee, M., Martin, K. C., Lawrence, B. P., & O'Reilly, M. A. (2013). Neonatal hyperoxia alters the host response to influenza A virus infection in adult mice through multiple pathways. *Am J Physiol Lung Cell Mol Physiol*, *305*(4), L282-290. https://doi.org/10.1152/ajplung.00112.2013

Burdak-Rothkamm, S., Rothkamm, K., & Prise, K. M. (2008). ATM acts downstream of ATR in the DNA damage response signaling of bystander cells. *Cancer research*, *68*(17), 7059-7065. https://doi.org/10.1158/0008-5472.can-08-0545

Chang, C.-W., Li, M., Xu, X., & Liu, Y. (2019). Helicase Dysfunctions in Human Diseases. In *Helicases from all domains of life* (pp. 191-210). https://doi.org/10.1016/b978-0-12-814685-9.00012-9

Chatterjee, N., & Walker, G. C. (2017). Mechanisms of DNA damage, repair, and mutagenesis. *Environ Mol Mutagen*, *58*(5), 235-263. https://doi.org/10.1002/em.22087

Chen, H., Chen, H., Liang, J., Gu, X., Zhou, J., Xie, C., Lv, X., Wang, R., Li, Q., Mao, Z., Sun, H., Zuo, G., Miao, D., & Jin, J. (2020). TGF-β1/IL-11/MEK/ERK signaling mediates senescence-associated pulmonary fibrosis in a stress-induced premature senescence model of Bmi-1 deficiency. *Exp Mol Med*, *52*(1), 130-151. https://doi.org/10.1038/s12276-019-0371-7

Choi, Y., Rekers, L., Dong, Y., Holzfurtner, L., Goetz, M. J., Shahzad, T., Zimmer, K. P., Behnke, J., Behnke, J., Bellusci, S., & Ehrhardt, H. (2021). Oxygen Toxicity to the Immature Lung-Part I: Pathomechanistic Understanding and Preclinical Perspectives. *Int J Mol Sci*, *22*(20). https://doi.org/10.3390/ijms222011006

Chou-Wei Chang, M. L., Xiaohua Xu, Yilun Liu. (2019). Helicase Dysfunctions in Human Diseases. *Helicases from all domains of life*. https://doi.org/https://doi.org/10.1016/B978-0-12-814685-9.00012-9

Colebatch, H. J. H., & Ng, C. K. Y. (1992). Estimating alveolar surface area during life. *Respiration Physiology*, *88*(1), 163-170. https://doi.org/https://doi.org/10.1016/0034-5687(92)90037-W

Collaco, J. M., & McGrath-Morrow, S. A. (2021). Bronchopulmonary dysplasia as a determinant of respiratory outcomes in adult life. *Pediatr Pulmonol*, *56*(11), 3464-3471. https://doi.org/10.1002/ppul.25301

Conway, E. M., & Carmeliet, P. (2004). The diversity of endothelial cells: a challenge for therapeutic angiogenesis. *Genome Biology*, *5*(2), 207. https://doi.org/10.1186/gb-2004-5-2-207

Courtot, L., Hoffmann, J. S., & Bergoglio, V. (2018). The Protective Role of Dormant Origins in Response to Replicative Stress. *Int J Mol Sci*, *19*(11). https://doi.org/10.3390/ijms19113569

Darlow, B. A., Graham, P. J., & Rojas-Reyes, M. X. (2016). Vitamin A supplementation to prevent mortality and short- and long-term morbidity in very low birth weight infants. *Cochrane Database Syst Rev*, *2016*(8), Cd000501. https://doi.org/10.1002/14651858.CD000501.pub4

Dash, B. C., & El-Deiry, W. S. (2005). Phosphorylation of p21 in G2/M promotes cyclin B-Cdc2 kinase activity. *Mol Cell Biol*, *25*(8), 3364-3387. https://doi.org/10.1128/mcb.25.8.3364-3387.2005

Doyle, L. W., Cheong, J. L., Ehrenkranz, R. A., & Halliday, H. L. (2017). Late (> 7 days) systemic postnatal corticosteroids for prevention of bronchopulmonary dysplasia in preterm infants. *Cochrane Database Syst Rev*, *10*(10), Cd001145. https://doi.org/10.1002/14651858.CD001145.pub4

Dylag, A. M., Haak, J., Warren, R., Yee, M., Pryhuber, G. S., & O'Reilly, M. A. (2021). Low-dose hyperoxia primes airways for fibrosis in mice after influenza A infection. *Am J Physiol Lung Cell Mol Physiol*, *321*(4), L750-l763. https://doi.org/10.1152/ajplung.00289.2020

Elective high-frequency oscillatory ventilation versus conventional ventilation for acute pulmonary dysfunction in preterm infants. (2013). *Neonatology*, *103*(1), 7-8; discussion 8-9. https://doi.org/10.1159/000338553

Ferrante, G., Carota, G., Li Volti, G., & Giuffrè, M. (2021). Biomarkers of Oxidative Stress for Neonatal Lung Disease [Mini Review]. *Frontiers in Pediatrics*, *9*. https://doi.org/10.3389/fped.2021.618867

Förster, K., Ertl-Wagner, B., Ehrhardt, H., Busen, H., Sass, S., Pomschar, A., Naehrlich, L., Schulze, A., Flemmer, A. W., Hübener, C., Eickelberg, O., Theis, F., Dietrich, O., & Hilgendorff, A. (2020). Altered relaxation times in MRI indicate bronchopulmonary dysplasia. *Thorax*, *75*(2), 184-187. https://doi.org/10.1136/thoraxjnl-2018-212384

Fraga, M. V., & Guttentag, S. (2012). Chapter 42 - Lung Development: Embryology, Growth, Maturation, and Developmental Biology. In C. A. Gleason & S. U. Devaskar (Eds.), *Avery's Diseases of the Newborn (Ninth Edition)* (pp. 571-583). W.B. Saunders. https://doi.org/https://doi.org/10.1016/B978-1-4377-0134-0.10042-3

Ge, X. Q., & Blow, J. J. (2010). Chk1 inhibits replication factory activation but allows dormant origin firing in existing factories. *J Cell Biol*, *191*(7), 1285-1297. https://doi.org/10.1083/jcb.201007074

Gilfillan, M., Bhandari, A., & Bhandari, V. (2021). Diagnosis and management of bronchopulmonary dysplasia. *BMJ*, *375*, n1974. https://doi.org/10.1136/bmj.n1974

Goode, E. L., Fridley, B. L., Vierkant, R. A., Cunningham, J. M., Phelan, C. M., Anderson, S., Rider, D. N., White, K. L., Pankratz, V. S., Song, H., Hogdall, E., Kjaer, S. K., Whittemore, A. S., DiCioccio, R., Ramus, S. J., Gayther, S. A., Schildkraut, J. M., Pharaoh, P. P., & Sellers, T. A. (2009). Candidate gene analysis using imputed genotypes: cell cycle single-nucleotide polymorphisms and ovarian cancer risk. *Cancer Epidemiol Biomarkers Prev*, *18*(3), 935-944. https://doi.org/10.1158/1055-9965.Epi-08-0860

Gravina, S., Lescai, F., Hurteau, G., Brock, G. J., Saramaki, A., Salvioli, S., Franceschi, C., & Roninson, I. B. (2009). Identification of single nucleotide polymorphisms in the p21 (CDKN1A) gene and correlations with longevity in the Italian population. *Aging (Albany NY)*, *1*(5), 470-480. https://doi.org/10.18632/aging.100041

Haddad, J. J. (2002). Oxygen-sensing mechanisms and the regulation of redox-responsive transcription factors in development and pathophysiology. *Respiratory Research*, *3*(1), 25. https://doi.org/10.1186/rr190

Hilgendorff, A., & O'Reilly, M. A. (2015). Bronchopulmonary dysplasia early changes leading to long-term consequences. *Front Med (Lausanne)*, *2*, 2. https://doi.org/10.3389/fmed.2015.00002

Hilgendorff, A., Reiss, I., Ehrhardt, H., Eickelberg, O., & Alvira, C. M. (2014). Chronic lung disease in the preterm infant. Lessons learned from animal models. *Am J Respir Cell Mol Biol*, *50*(2), 233-245. https://doi.org/10.1165/rcmb.2013-0014TR

Howie, B. N., Donnelly, P., & Marchini, J. (2009). A Flexible and Accurate Genotype Imputation Method for the Next Generation of Genome-Wide Association Studies. *PLOS Genetics*, *5*(6), e1000529. https://doi.org/10.1371/journal.pgen.1000529

Hubbi, M. E., Luo, W., Baek, J. H., & Semenza, G. L. (2011). MCM proteins are negative regulators of hypoxia-inducible factor 1. *Mol Cell*, *42*(5), 700-712. https://doi.org/10.1016/j.molcel.2011.03.029

Hurskainen, M., Mižíková, I., Cook, D. P., Andersson, N., Cyr-Depauw, C., Lesage, F., Helle, E., Renesme, L., Jankov, R. P., Heikinheimo, M., Vanderhyden, B. C., & Thébaud, B. (2021). Single cell transcriptomic analysis of murine lung development on hyperoxia-induced damage. *Nat Commun*, *12*(1), 1565. https://doi.org/10.1038/s41467-021-21865-2

Hyödynmaa, E., Korhonen, P., Ahonen, S., Luukkaala, T., & Tammela, O. (2012). Frequency and clinical correlates of radiographic patterns of bronchopulmonary dysplasia in very low birth weight infants by term age. *Eur J Pediatr*, *171*(1), 95-102. https://doi.org/10.1007/s00431-011-1486-6

Jankov, R. P., & Keith Tanswell, A. (2004). Growth factors, postnatal lung growth and bronchopulmonary dysplasia. *Paediatr Respir Rev*, *5 Suppl A*, S265-275. https://doi.org/10.1016/s1526-0542(04)90050-4

Jia, X., Wu, B., Huang, J., Fan, L., Yang, M., & Xu, W. (2021). YAP and Wnt3a independently promote AECIIs proliferation and differentiation by increasing nuclear β-catenin expression in experimental bronchopulmonary dysplasia. *Int J Mol Med*, *47*(1), 195-206. https://doi.org/10.3892/ijmm.2020.4791

Jiang, J., Wang, J., Li, C., Mo, L., & Huang, D. (2022). Hyperoxia induces alveolar epithelial cell apoptosis by regulating mitochondrial function through small mothers against decapentaplegic 3 (SMAD3) and extracellular signal-regulated kinase 1/2 (ERK1/2). *Bioengineered*, *13*(1), 242-252. https://doi.org/10.1080/21655979.2021.2012953

Keller, R. L., Eichenwald, E. C., Hibbs, A. M., Rogers, E. E., Wai, K. C., Black, D. M., Ballard, P. L., Asselin, J. M., Truog, W. E., Merrill, J. D., Mammel, M. C., Steinhorn, R. H., Ryan, R. M., Durand, D. J., Bendel, C. M., Bendel-Stenzel, E. M., Courtney, S. E., Dhanireddy, R., Hudak, M. L., . . . Ballard, R. A. (2017). The Randomized, Controlled Trial of Late Surfactant: Effects on Respiratory Outcomes at 1-Year Corrected Age. *J Pediatr*, *183*, 19-25.e12. https://doi.org/10.1016/j.jpeds.2016.12.059

Kirschner, K. M., Kelterborn, S., Stehr, H., Penzlin, J. L. T., Jacobi, C. L. J., Endesfelder, S., Sieg, M., Kruppa, J., Dame, C., & Sciesielski, L. K. (2022). Adaptation of the Oxygen Sensing System during Lung Development. *Oxid Med Cell Longev*, *2022*, 9714669. https://doi.org/10.1155/2022/9714669

Klingenberg, C., Wheeler, K. I., McCallion, N., Morley, C. J., & Davis, P. G. (2017). Volume-targeted versus pressure-limited ventilation in neonates. *Cochrane Database Syst Rev*, *10*(10), Cd003666. https://doi.org/10.1002/14651858.CD003666.pub4

Kojima, Y., Maskey, R. S., & Machida, Y. J. (2017). Cell Cycle Machinery and Its Alterations in Pancreatic Cancer. In J. P. Neoptolemos, R. Urrutia, J. Abbruzzese, & M. W. Büchler (Eds.), *Pancreatic Cancer* (pp. 1-31). Springer New York. https://doi.org/10.1007/978-1-4939-6631-8_74-1

Kong, S., Han, X., Cui, T., Zhou, C., Jiang, Y., Zhang, H., Wang, B., Wang, H., & Zhang, S. (2016). MCM2 mediates progesterone-induced endometrial stromal cell proliferation and differentiation in mice. *Endocrine*, *53*(2), 595-606. https://doi.org/10.1007/s12020-016-0894-9

Kulkarni, A., & Das, K. C. (2008). Differential roles of ATR and ATM in p53, Chk1, and histone H2AX phosphorylation in response to hyperoxia: ATR-dependent ATM activation. *Am J Physiol Lung Cell Mol Physiol*, *294*(5), L998-l1006. https://doi.org/10.1152/ajplung.00004.2008

Kumar, V. H. S., Wang, H., & Nielsen, L. (2020). Short-term perinatal oxygen exposure may impair lung development in adult mice. *Biol Res*, *53*(1), 51. https://doi.org/10.1186/s40659-020-00318-y

Kunnev, D., Rusiniak, M. E., Kudla, A., Freeland, A., Cady, G. K., & Pruitt, S. C. (2010). DNA damage response and tumorigenesis in Mcm2-deficient mice. *Oncogene*, *29*(25), 3630-3638. https://doi.org/10.1038/onc.2010.125

Lal, C. V., & Ambalavanan, N. (2015). Biomarkers, Early Diagnosis, and Clinical Predictors of Bronchopulmonary Dysplasia. *Clin Perinatol*, *42*(4), 739-754. https://doi.org/10.1016/j.clp.2015.08.004

Lau, M., Masood, A., Yi, M., Belcastro, R., Li, J., & Tanswell, A. K. (2011). Long-term failure of alveologenesis after an early short-term exposure to a PDGF-receptor antagonist. *Am J Physiol Lung Cell Mol Physiol*, *300*(4), L534-547. https://doi.org/10.1152/ajplung.00262.2010

Li, C., Smith, S. M., Peinado, N., Gao, F., Li, W., Lee, M. K., Zhou, B., Bellusci, S., Pryhuber, G. S., Ho, H. H., Borok, Z., & Minoo, P. (2020). WNT5a-ROR Signaling Is Essential for Alveologenesis. *Cells*, *9*(2). https://doi.org/10.3390/cells9020384

Li, Z., Chen, Y., Li, W., & Yan, F. (2020). Cell Division Cycle 2 Protects Neonatal Rats Against Hyperoxia-Induced Bronchopulmonary Dysplasia. *Yonsei Med J*, *61*(8), 679-688. https://doi.org/10.3349/ymj.2020.61.8.679

Lio, C.-W. J., & Rao, A. (2019). TET Enzymes and 5hmC in Adaptive and Innate Immune Systems [Review]. *Frontiers in Immunology*, *10*. https://doi.org/10.3389/fimmu.2019.00210

Liu, S., Xiao, Y., Hu, C., & Li, M. (2020). Associations between polymorphisms in genes of base excision repair pathway and lung cancer risk. *Transl Cancer Res*, *9*(4), 2780-2800. https://doi.org/10.21037/tcr.2020.02.44

Liu, T., Gonzalez De Los Santos, F., Hirsch, M., Wu, Z., & Phan, S. H. (2021). Noncanonical Wnt Signaling Promotes Myofibroblast Differentiation in Pulmonary Fibrosis. *Am J Respir Cell Mol Biol*, *65*(5), 489-499. https://doi.org/10.1165/rcmb.2020-0499OC

Lorente-Pozo, S., Parra-Llorca, A., Lara-Cantón, I., Solaz, A., García-Jiménez, J. L., Pallardó, F. V., & Vento, M. (2020). Oxygen in the neonatal period: Oxidative stress, oxygen load and epigenetic changes. *Semin Fetal Neonatal Med*, *25*(2), 101090. https://doi.org/10.1016/j.siny.2020.101090

Lorente-Pozo, S., Parra-Llorca, A., Núñez-Ramiro, A., Cernada, M., Hervás, D., Boronat, N., Sandoval, J., & Vento, M. (2018). The Oxygen Load Supplied during Delivery Room Stabilization of Preterm Infants Modifies the DNA Methylation Profile. *J Pediatr*, *202*, 70-76.e72. https://doi.org/10.1016/j.jpeds.2018.07.009

Love, M. I., Huber, W., & Anders, S. (2014). Moderated estimation of fold change and dispersion for RNA-seq data with DESeq2. *Genome Biology*, *15*(12), 550. https://doi.org/10.1186/s13059-014-0550-8

Mahfoudhi, E., Talhaoui, I., Cabagnols, X., Della Valle, V., Secardin, L., Rameau, P., Bernard, O. A., Ishchenko, A. A., Abbes, S., Vainchenker, W., Saparbaev, M., & Plo, I. (2016). TET2-mediated 5-hydroxymethylcytosine induces genetic instability and mutagenesis. *DNA Repair (Amst)*, *43*, 78-88. https://doi.org/10.1016/j.dnarep.2016.05.031

Maltepe, E., & Saugstad, O. D. (2009). Oxygen in Health and Disease: Regulation of Oxygen Homeostasis-Clinical Implications. *Pediatric Research*, *65*(3), 261-268. https://doi.org/10.1203/PDR.0b013e31818fc83f

May, C., Prendergast, M., Salman, S., Rafferty, G. F., & Greenough, A. (2009). Chest radiograph thoracic areas and lung volumes in infants developing bronchopulmonary dysplasia. *Pediatr Pulmonol*, *44*(1), 80-85. https://doi.org/10.1002/ppul.20952

Melzer, D., Frayling, T. M., Murray, A., Hurst, A. J., Harries, L. W., Song, H., Khaw, K., Luben, R., Surtees, P. G., Bandinelli, S. S., Corsi, A. M., Ferrucci, L., Guralnik, J. M., Wallace, R. B., Hattersley, A. T., & Pharoah, P. D. (2007). A common variant of the p16(INK4a) genetic region is associated with physical function in older people. *Mech Ageing Dev*, *128*(5-6), 370-377. https://doi.org/10.1016/j.mad.2007.03.005

Myti, D., Gunjak, M., Casado, F., Khaghani Raziabad, S., Nardiello, C., Vadász, I., Herold, S., Pryhuber, G., Seeger, W., & Morty, R. E. (2020). Elevated FiO(2) increases SARS-CoV-2 co-receptor expression in respiratory tract epithelium. *Am J Physiol Lung Cell Mol Physiol*, *319*(4), L670-l674. https://doi.org/10.1152/ajplung.00345.2020

Nabhan, A. N., Brownfield, D. G., Harbury, P. B., Krasnow, M. A., & Desai, T. J. (2018). Single-cell Wnt signaling niches maintain stemness of alveolar type 2 cells. *Science (New York, N.Y.)*, *359*(6380), 1118-1123. https://doi.org/10.1126/science.aam6603

Nakad, R., & Schumacher, B. (2016). DNA Damage Response and Immune Defense: Links and Mechanisms [Review]. *Frontiers in Genetics*, *7*. https://doi.org/10.3389/fgene.2016.00147

Neeley, W. L., & Essigmann, J. M. (2006). Mechanisms of formation, genotoxicity, and mutation of guanine oxidation products. *Chem Res Toxicol*, *19*(4), 491-505. https://doi.org/10.1021/tx0600043

Newman, D. R., Sills, W. S., Hanrahan, K., Ziegler, A., Tidd, K. M., Cook, E., & Sannes, P. L. (2016). Expression of WNT5A in Idiopathic Pulmonary Fibrosis and Its Control by TGF-β and WNT7B in Human Lung Fibroblasts. *J Histochem Cytochem*, *64*(2), 99-111. https://doi.org/10.1369/0022155415617988

Niedermaier, S., & Hilgendorff, A. (2015). Bronchopulmonary dysplasia - an overview about pathophysiologic concepts. *Mol Cell Pediatr*, *2*(1), 2. https://doi.org/10.1186/s40348-015-0013-7

Oak, P., & Hilgendorff, A. (2017). The BPD trio? Interaction of dysregulated PDGF, VEGF, and TGF signaling in neonatal chronic lung disease. *Mol Cell Pediatr*, *4*(1), 11. https://doi.org/10.1186/s40348-017-0076-8

Oak, P., Pritzke, T., Thiel, I., Koschlig, M., Mous, D. S., Windhorst, A., Jain, N., Eickelberg, O., Foerster, K., Schulze, A., Goepel, W., Reicherzer, T., Ehrhardt, H., Rottier, R. J., Ahnert, P., Gortner, L., Desai, T. J., & Hilgendorff, A. (2017). Attenuated PDGF signaling drives alveolar and microvascular defects in neonatal chronic lung disease. *EMBO Mol Med*, *9*(11), 1504-1520. https://doi.org/10.15252/emmm.201607308

Perez, M., Robbins, M. E., Revhaug, C., & Saugstad, O. D. (2019). Oxygen radical disease in the newborn, revisited: Oxidative stress and disease in the newborn period. *Free Radic Biol Med*, *142*, 61-72. https://doi.org/10.1016/j.freeradbiomed.2019.03.035

Perucca, P., Cazzalini, O., Madine, M., Savio, M., Laskey, R. A., Vannini, V., Prosperi, E., & Stivala, L. A. (2009). Loss of p21 CDKN1A impairs entry to quiescence and activates a DNA damage response in normal fibroblasts induced to quiescence. *Cell Cycle*, *8*(1), 105-114. https://doi.org/10.4161/cc.8.1.7507

Piersigilli, F., Lam, T. T., Vernocchi, P., Quagliariello, A., Putignani, L., Aghai, Z. H., & Bhandari, V. (2019). Identification of new biomarkers of bronchopulmonary dysplasia using metabolomics. *Metabolomics*, *15*(2), 20. https://doi.org/10.1007/s11306-019-1482-9

Pilié, P. G., Tang, C., Mills, G. B., & Yap, T. A. (2019). State-of-the-art strategies for targeting the DNA damage response in cancer. *Nature Reviews Clinical Oncology*, *16*(2), 81-104. https://doi.org/10.1038/s41571-018-0114-z

Rasmussen, K. D., & Helin, K. A.-O. Role of TET enzymes in DNA methylation, development, and cancer. (1549-5477 (Electronic)).

Raudvere, U., Kolberg, L., Kuzmin, I., Arak, T., Adler, P., Peterson, H., & Vilo, J. (2019). g:Profiler: a web server for functional enrichment analysis and conversions of gene lists (2019 update). *Nucleic Acids Res*, *47*(W1), W191-w198. https://doi.org/10.1093/nar/gkz369

Reddy, N. M., Tamatam, C. M., Aparna, A., & Reddy, S. P. (2022). Nrf2 Is Required for Optimal Alveolar-Macrophage-Mediated Apoptotic Neutrophil Clearance after Oxidant Injury. *Antioxidants (Basel)*, *11*(2). https://doi.org/10.3390/antiox11020212

Riccetti, M. R., Ushakumary, M. G., Waltamath, M., Green, J., Snowball, J., Dautel, S. E., Endale, M., Lami, B., Woods, J., Ahlfeld, S. K., & Perl, A.-K. T. (2022). Maladaptive functional changes in alveolar fibroblasts due to perinatal hyperoxia impair epithelial differentiation. *JCI Insight*. https://doi.org/10.1172/jci.insight.152404

Schittny, J. C. (2017). Development of the lung. *Cell Tissue Res*, *367*(3), 427-444. https://doi.org/10.1007/s00441-016-2545-0

Schmidt, B., Roberts, R. S., Davis, P., Doyle, L. W., Barrington, K. J., Ohlsson, A., Solimano, A., & Tin, W. (2007). Long-term effects of caffeine therapy for apnea of prematurity. *N Engl J Med*, *357*(19), 1893-1902. https://doi.org/10.1056/NEJMoa073679

Sejersted, Y., Aasland, A. L., Bjørås, M., Eide, L., & Saugstad, O. D. (2009). Accumulation of 8-oxoguanine in liver DNA during hyperoxic resuscitation of newborn mice. *Pediatr Res*, *66*(5), 533-538. https://doi.org/10.1203/PDR.0b013e3181ba1a42

Stewart, J. P., Silvia, O. J., Atkin, I. M., Hughes, D. J., Ebrahimi, B., & Adler, H. (2004). In vivo function of a gammaherpesvirus virion glycoprotein: influence on B-cell infection and mononucleosis. *J Virol*, *78*(19), 10449-10459. https://doi.org/10.1128/jvi.78.19.10449-10459.2004

Stoecklein, S., Hilgendorff, A., Li, M., Förster, K., Flemmer, A. W., Galiè, F., Wunderlich, S., Wang, D., Stein, S., Ehrhardt, H., Dietrich, O., Zou, Q., Zhou, S., Ertl-Wagner, B., & Liu, H. (2020). Variable functional connectivity architecture of the preterm human brain: Impact of developmental cortical expansion and maturation. *Proc Natl Acad Sci U S A*, *117*(2), 1201-1206. https://doi.org/10.1073/pnas.1907892117

Sucasas Alonso, A., Pértega Diaz, S., Sáez Soto, R., & Avila-Alvarez, A. (2022). Epidemiology and risk factors for bronchopulmonary dysplasia in preterm infants born at or less than 32 weeks of gestation. *An Pediatr (Engl Ed)*. https://doi.org/10.1016/j.anpede.2021.03.006

Sucre, J., Haist, L., Bolton, C. E., & Hilgendorff, A. (2021). Early Changes and Indicators Characterizing Lung Aging in Neonatal Chronic Lung Disease. *Front Med (Lausanne)*, *8*, 665152. https://doi.org/10.3389/fmed.2021.665152

Sucre, J. M. S., Vickers, K. C., Benjamin, J. T., Plosa, E. J., Jetter, C. S., Cutrone, A., Ransom, M., Anderson, Z., Sheng, Q., Fensterheim, B. A., Ambalavanan, N., Millis, B., Lee, E., Zijlstra, A., Königshoff, M., Blackwell, T. S., & Guttentag, S. H. (2020). Hyperoxia Injury in the Developing Lung Is Mediated by Mesenchymal Expression of Wnt5A. *Am J Respir Crit Care Med*, *201*(10), 1249-1262. https://doi.org/10.1164/rccm.201908-1513OC

Thébaud, B., Goss, K. N., Laughon, M., Whitsett, J. A., Abman, S. H., Steinhorn, R. H., Aschner, J. L., Davis, P. G., McGrath-Morrow, S. A., Soll, R. F., & Jobe, A. H. (2019). Bronchopulmonary dysplasia. *Nat Rev Dis Primers*, *5*(1), 78. https://doi.org/10.1038/s41572-019-0127-7

Torres-Cuevas, I., Parra-Llorca, A., Sánchez-Illana, A., Nuñez-Ramiro, A., Kuligowski, J., Cháfer-Pericás, C., Cernada, M., Escobar, J., & Vento, M. (2017). Oxygen and oxidative stress in the perinatal period. *Redox Biol*, *12*, 674-681. https://doi.org/10.1016/j.redox.2017.03.011

Tracy, M. K., & Berkelhamer, S. K. (2019). Bronchopulmonary Dysplasia and Pulmonary Outcomes of Prematurity. *Pediatr Ann*, *48*(4), e148-e153. https://doi.org/10.3928/19382359-20190325-03

Tuder, R. M., Chacon, M., Alger, L., Wang, J., Taraseviciene-Stewart, L., Kasahara, Y., Cool, C. D., Bishop, A. E., Geraci, M., Semenza, G. L., Yacoub, M., Polak, J. M., & Voelkel, N. F. (2001). Expression of angiogenesis-related molecules in plexiform lesions in severe pulmonary hypertension: evidence for a process of disordered angiogenesis. *J Pathol*, *195*(3), 367-374. https://doi.org/10.1002/path.953

Twisselmann, N., Pagel, J., Künstner, A., Weckmann, M., Hartz, A., Glaser, K., Hilgendorff, A., Göpel, W., Busch, H., Herting, E., Weinberg, J. B., & Härtel, C. (2021). Hyperoxia/Hypoxia Exposure Primes a Sustained Pro-Inflammatory Profile of Preterm Infant Macrophages Upon LPS Stimulation. *Front Immunol*, *12*, 762789. https://doi.org/10.3389/fimmu.2021.762789

Urrutia, A. A., & Aragonés, J. (2018). HIF Oxygen Sensing Pathways in Lung Biology. *Biomedicines*, *6*(2). https://doi.org/10.3390/biomedicines6020068

Vande Loock, K., Ciardelli, R., Decordier, I., Plas, G., Haumont, D., & Kirsch-Volders, M. (2012). Preterm newborns show slower repair of oxidative damage and paternal smoking associated DNA damage. *Mutagenesis*, *27*(5), 573-580. https://doi.org/10.1093/mutage/ges022

Vogel, E. R., Britt, R. D., Jr., Faksh, A., Kuipers, I., Pandya, H., Prakash, Y. S., Martin, R. J., & Pabelick, C. M. (2017). Moderate hyperoxia induces extracellular matrix remodeling by human fetal airway smooth muscle cells. *Pediatr Res*, *81*(2), 376-383. https://doi.org/10.1038/pr.2016.218

Vuga, L. J., Ben-Yehudah, A., Kovkarova-Naumovski, E., Oriss, T., Gibson, K. F., Feghali-Bostwick, C., & Kaminski, N. (2009). WNT5A is a regulator of fibroblast proliferation and resistance to apoptosis. *Am J Respir Cell Mol Biol*, *41*(5), 583-589. https://doi.org/10.1165/rcmb.2008-0201OC

Walsh, M. C., Yao, Q., Gettner, P., Hale, E., Collins, M., Hensman, A., Everette, R., Peters, N., Miller, N., Muran, G., Auten, K., Newman, N., Rowan, G., Grisby, C., Arnell, K., Miller, L., Ball, B., & McDavid, G. (2004). Impact of a physiologic definition on bronchopulmonary dysplasia rates. *Pediatrics*, *114*(5), 1305-1311. https://doi.org/10.1542/peds.2004-0204

Weber, A. R., Krawczyk, C., Robertson, A. B., Kuśnierczyk, A., Vågbø, C. B., Schuermann, D., Klungland, A., & Schär, P. (2016). Biochemical reconstitution of TET1–TDG–BER-dependent active DNA demethylation reveals a highly coordinated mechanism. *Nature Communications*, *7*(1), 10806. https://doi.org/10.1038/ncomms10806

Weng, B., Zhang, X., Chu, X., Gong, X., & Cai, C. (2021). Nrf2-Keap1-ARE-NQO1 signaling attenuates hyperoxia-induced lung cell injury by inhibiting apoptosis. *Mol Med Rep*, *23*(3). https://doi.org/10.3892/mmr.2021.11860

Willis, J., Patel, Y., Lentz, B. L., & Yan, S. (2013). APE2 is required for ATR-Chk1 checkpoint activation in response to oxidative stress. *Proc Natl Acad Sci U S A*, *110*(26), 10592-10597. https://doi.org/10.1073/pnas.1301445110

Yao, L., Zhou, Y., Li, J., Wickens, L., Conforti, F., Rattu, A., Ibrahim, F. M., Alzetani, A., Marshall, B. G., Fletcher, S. V., Hancock, D., Wallis, T., Downward, J., Ewing, R. M., Richeldi, L., Skipp, P., Davies, D. E., Jones, M. G., & Wang, Y. (2021). Bidirectional epithelial-mesenchymal crosstalk provides self-sustaining profibrotic signals in pulmonary fibrosis. *J Biol Chem*, *297*(3), 101096. https://doi.org/10.1016/j.jbc.2021.101096

You, K., Parikh, P., Khandalavala, K., Wicher, S. A., Manlove, L., Yang, B., Roesler, A., Roos, B. B., Teske, J. J., Britt, R. D., Jr., Pabelick, C. M., & Prakash, Y. S. (2019). Moderate hyperoxia induces senescence in developing human lung fibroblasts. *Am J Physiol Lung Cell Mol Physiol*, *317*(5), L525-l536. https://doi.org/10.1152/ajplung.00067.2019

Yu, L. J., Ko, V. H., Dao, D. T., Secor, J. D., Pan, A., Cho, B. S., Mitchell, P. D., Kishikawa, H., Bielenberg, D. R., & Puder, M. (2021). Investigation of the mechanisms of VEGF-mediated compensatory lung growth: the role of the VEGF heparin-binding domain. *Scientific Reports*, *11*(1), 11827. https://doi.org/10.1038/s41598-021-91127-0

Zhang, Y., & Hunter, T. (2014). Roles of Chk1 in cell biology and cancer therapy. *Int J Cancer*, *134*(5), 1013-1023. https://doi.org/10.1002/ijc.28226

Ziyatdinov, A., Vázquez-Santiago, M., Brunel, H., Martinez-Perez, A., Aschard, H., & Soria, J. M. (2018). lme4qtl: linear mixed models with flexible covariance structure for genetic studies of related individuals. *BMC Bioinformatics*, *19*(1), 68. https://doi.org/10.1186/s12859-018-2057-x

Zysman, M., Baptista, B. R., Essari, L. A., Taghizadeh, S., Thibault de Ménonville, C., Giffard, C., Issa, A., Franco-Montoya, M. L., Breau, M., Souktani, R., Aissat, A., Caeymaex, L., Lizé, M., Van Nhieu, J. T., Jung, C., Rottier, R., Cruzeiro, M. D., Adnot, S., Epaud, R., . . . Boyer, L. (2020). Targeting p16(INK4a) Promotes Lipofibroblasts and Alveolar Regeneration after Early-Life Injury. *Am J Respir Crit Care Med*, *202*(8), 1088-1104. https://doi.org/10.1164/rccm.201908-1573OC

Affidavit

Affidavit

Gonzalez Rodriguez, Erika

Surname, first name

Street

Munich, Germany

Zip code, town, country

I hereby declare, that the submitted thesis entitled:

Oxygen Therapy in Neonatal Chronic Lung Disease – Acute and Sustained Effects and their Indicators

.....

is my own work. I have only used the sources indicated and have not made unauthorised use of services of a third party. Where the work of others has been quoted or reproduced, the source is always given.

I further declare that the submitted thesis or parts thereof have not been presented as part of an examination degree to any other university.

Munich, 16.03.22

place, date

Erika Gonzalez R

Signature doctoral candidate

Confirmation of congruency

LMU LUDWIG-MAXIMILIANS-UNIVERSITÄT MÜNCHEN | Promotionsbüro Medizinische Fakultät | MMRS

Confirmation of congruency between printed and electronic version of the doctoral thesis

Gonzalez Rodriguez, Erika

Surname, first name

Street

Munich, Germany

Zip code, town, country

I hereby declare, that the submitted thesis entitled:

Oxygen Therapy in Neonatal Chronic Lung Disease – Acute and Sustained Effects and their Indicators

.....

is congruent with the printed version both in content and format.

Munich, 16.03.22

place, date

Erika Gonzalez R

Signature doctoral candidate